Rates and Mechanisms of Mineral Carbonation in Peridotite: Natural Processes and Recipes for Enhanced, in situ CO_2 Capture and Storage

Peter B. Kelemen,[1] Juerg Matter,[1] Elisabeth E. Streit,[1] John F. Rudge,[2] William B. Curry,[3] and Jerzy Blusztajn[3]

[1]Lamont Doherty Earth Observatory, Columbia University, Palisades, New York 10964; email: peterk@ldeo.columbia.edu

[2]Institute of Theoretical Geophysics, Bullard Laboratories, University of Cambridge, Cambridge, CB3 0EZ, United Kingdom

[3]Woods Hole Oceanographic Institution, Woods Hole, Massachusetts 02543

Keywords

hydrothermal alteration, ophicalcite, listwanite, retrograde metamorphism

Abstract

Near-surface reaction of CO_2-bearing fluids with silicate minerals in peridotite and basalt forms solid carbonate minerals. Such processes form abundant veins and travertine deposits, particularly in association with tectonically exposed mantle peridotite. This is important in the global carbon cycle, in weathering, and in understanding physical-chemical interaction during retrograde metamorphism. Enhancing the rate of such reactions is a proposed method for geologic CO_2 storage, and perhaps for direct capture of CO_2 from near-surface fluids. We review, synthesize, and extend inferences from a variety of sources. We include data from studies on natural peridotite carbonation processes, carbonation kinetics, feedback between permeability and volume change via reaction-driven cracking, and proposed methods for enhancing the rate of natural mineral carbonation via in situ processes ("at the outcrop") rather than ex situ processes ("at the smokestack").

1. INTRODUCTION

Mineral carbonation has been proposed as a method for safe, essentially permanent CO_2 storage (e.g., Lackner et al. 1995, Seifritz 1990). The fastest mineral carbonation rates known are for the mineral olivine. Also, among abundant rock-forming minerals, olivine has the highest molar proportion of divalent cations needed to form natural carbonate minerals such as magnesite. Rocks rich in the mineral olivine are known as peridotites. In situ mineral carbonation, which involves transport of CO_2-bearing fluids into rock reactants, is distinguished from ex situ methods, which involve transport of solid reactants to a concentrated source of CO_2 such as fossil fuel–burning power plant.

In this review, we discuss research on in situ carbonation of minerals in peridotite, expand on our papers about mineral carbonation (Kelemen & Matter 2008, Matter & Kelemen 2009), and outline opportunities for future research on this subject. Much of the emphasis is on natural rates and processes, including our own research on two natural peridotite carbonation systems, one ancient and one ongoing, whose products are exposed in the peridotite of northern Oman. In addition to the intrinsic interest of these systems for earth scientists, engineers have much to learn through understanding how natural processes achieve almost 100% carbonation of peridotite. To maximize the practical utility of this review, we limit our discussion of natural processes to pressures less than 2 kbar, corresponding to depths less than ~7 km. Kinetic data indicate that olivine combines with CO_2 to form solid carbonates more rapidly than does the mineral plagioclase, the primary constituent of basalt, so we focus on peridotite. Nonetheless, we also offer some comparative information about in situ basalt carbonation.

This review has two parts: this journal article, and an electronic supplement that contains extended discussion and annotated bibliographies on many topics. The latter is available from the **Supplemental Materials link** on the Annual Reviews home page at **http://www.annualreviews.org**. The article is written to stand on its own and contains brief summaries of essential material from the supplement. However, there is little redundancy. For interested readers, a capital S preceding section, figure, and table numbers (e.g., Section S1) indicates material in the supplement. The article and supplement contain separate reference lists that are overlapping but not identical.

2. NATURAL PERIDOTITE CARBONATION VIA HYDROTHERMAL ALTERATION AND WEATHERING

2.1. Extent of Peridotite Near Earth's Surface

To assess the size of the geochemical reservoir represented by carbonate in natural peridotites, and the potential size of the engineered CO_2 storage reservoir, it is important to consider the mass of peridotite available at and near the surface. In the electronic supplement, **Supplemental Section S1** presents a review of this topic, and a more detailed review for the United States is provided by Krevor et al. (2009). For continuity, we provide a summary here. In considering these data, it is useful to keep in mind that average hydrothermally altered peridotite from oceanic crust contains ~0.6 wt% CO_2 in carbonate minerals, at least within 200 m of the seafloor, and that complete carbonation of 1 kg of Mg-olivine (forsterite, Mg_2SiO_4) can consume up to 0.6 kg of dissolved CO_2 from fluid to produce 1.6 kg of magnesite ($MgCO_3$) and quartz (SiO_2).

In the upper 7 km of the solid Earth, peridotite is generally found in five settings, listed in order of decreasing abundance:

1. In oceanic crust and shallow mantle, especially in oceanic crust formed at slow-spreading mid-ocean ridges where 5 to 15% of the newly formed seafloor is underlain by altered, mantle peridotite (Cannat et al. 1995, Carlson 2001)

Mineral carbonation: reaction of silicate or oxide minerals with CO_2 in fluid to form solid carbonate minerals

**Olivine:** the most abundant mineral in Earth's upper mantle, $(Mg,Fe)_2SiO_4$

Magnesite: the most common magnesium carbonate mineral, $MgCO_3$, with minor Ca and Fe substitution

Peridotite: a rock composed of more than 40% olivine and less than 10% plagioclase

Plagioclase: one of the feldspar group of minerals, mainly $NaAlSi_3O_8$-$CaAl_2Si_2O_8$

Basalt: the most common form of lava on Earth, typically with 48 to 53 wt% SiO_2; when fully crystalline, common basalts are a mixture of ~60% plagioclase, 30% clinopyroxene, and 10% olivine

Quartz: a mineral composed of SiO_2

▶ Supplemental Material

2. In the forearc regions of subduction-related magmatic arcs
3. In subaerial massifs known as ophiolites, which are thrust sheets of mafic crust and shallow mantle formed at submarine spreading ridges and then thrust over continental crust via plate tectonic processes
4. In large, mafic to ultramafic, igneous intrusions
5. In peridotite massifs where tectonic processes, typically including crustal extension, have exposed the ancient, continental upper mantle

Slow-spreading mid-ocean ridges emplace $1-4 \times 10^{12}$ kg year^{-1} of peridotite in the upper 7 km of the oceanic plates, or $\sim 10^{18}$ kg of peridotite in a swath 10 km wide on either side of the slow-spreading ridges over 1 Ma. Peridotite extends beneath a shallow veneer of pelagic sediment for thousands of kilometers on either side of the slow-spreading Mid-Atlantic and Indian Ocean Ridges, corresponding to more than 10^{20} kg of material. There is no quantitative estimate of the proportion of peridotite in forearc settings, but its total mass is probably larger than the mass of peridotites in ophiolites. The Samail ophiolite, in the Sultanate of Oman and the United Arab Emirates, contains approximately 5×10^{16} kg of peridotite within 3 km of the surface (Kelemen & Matter 2008). Peridotite in ophiolites is found on all continents, with a total mass between 10^{17} and 10^{18} kg. The gigantic, igneous Bushveld layered intrusion in South Africa contains 10^{16} to 10^{17} kg of peridotite and pyroxenite, and the similar Stillwater intrusion in Montana contains almost 10^{15} kg of peridotite. Continental peridotite massifs may have a combined mass on the order of 10^{15} kg.

2.2. Simplified Metamorphic Reactions for Peridotite Carbonation

Peridotite is a rock type composed of >40% of the mineral olivine (with the gemstone name peridot). Typical residual mantle peridotite exposed on the seafloor and in ophiolites is composed of 70–85% olivine. Bands of dunite are present within the peridotite and comprise 5–15% of the mantle section in many ophiolites. Dunite contains more than 95% olivine. Carbonation of the mineral olivine occurs together with hydration via the simplified reactions

$$4Mg_2SiO_4(\text{Mg-olivine}) + 4H_2O + 2CO_2 = 2Mg_3Si_2O_5(OH)_4(\text{serpentine})$$
$$+ 2MgCO_3(\text{magnesite}), \tag{1a}$$

$$4Mg_2SiO_4 + H_2O + 5CO_2 = Mg_3Si_4O_{10}(OH)_2(\text{talc}) + 5MgCO_3, \text{ and} \tag{1b}$$

$$4Mg_2SiO_4 + 8CO_2 = 4SiO_2(\text{quartz}) + 8MgCO_3. \tag{1c}$$
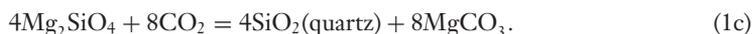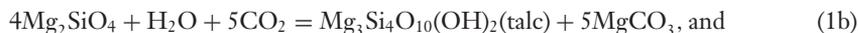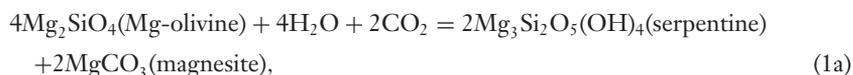
After hydration, carbonation occurs via the simplified reactions

$$4Mg_2SiO_4 + 6H_2O = 2Mg_3Si_2O_5(OH)_4 + 2Mg(OH)_2(\text{brucite}), \tag{1d}$$

$$\text{products of 1d} + 2CO_2 = 2Mg_3Si_2O_5(OH)_4 + 2MgCO_3 + 2H_2O, \tag{1e}$$

$$\text{products of 1e} + 3CO_2 = Mg_3Si_4O_{10}(OH)_2 + 5MgCO_3 + 5H_2O, \text{ and} \tag{1f}$$

$$\text{products of 1f} + 3CO_2 = 4SiO_2 + 8MgCO_3 + 6H_2O. \tag{1g}$$
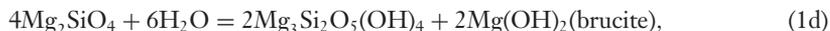
These reactions are written with no components other than H_2O and CO_2 in fluids, but of course they can take on infinite variety when other key components—such as Ca^{2+}, aqueous SiO_2, H_2, sulfur species, and O_2—are considered to be transported in fluids.

The second and third most abundant minerals in peridotite are Ca-poor pyroxene (often termed orthopyroxene or opx, with Mg-end-member enstatite, $Mg_2Si_2O_6$) and Ca-rich pyroxene (often termed clinopyroxene or cpx, with Mg-end-member diopside, $CaMgSi_2O_6$). To understand natural peridotite carbonation, it is important to add the simplified reaction:

$$4Mg_2SiO_4 + CaMgSi_2O_6 + 6H_2O + CO_2 = 3Mg_3Si_2O_5(OH)_4 + CaCO_3(calcite). \quad (1h)$$
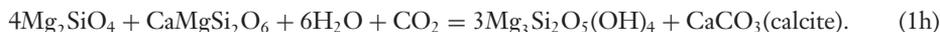
This reaction often takes place in stages; that is,

$$4Mg_2SiO_4 + CaMgSi_2O_6 + 7H_2O = 3Mg_3Si_2O_5(OH)_4 + Ca^{2+}(aq) + 2OH^-(aq) \quad (1i)$$
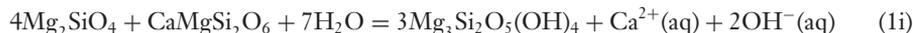
occurs in the subsurface, and then

$$Ca^{2+}(aq) + 2OH^-(aq) + CO_2(aq\ or\ gas) = CaCO_3 + H_2O \quad (1j)$$
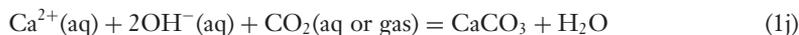
occurs when fluids modified by reaction with peridotite form travertine at or near the surface.

Mantle peridotite generally has molar Mg/(Mg + Fe), or Mg#, of ∼0.9. Iron is dissolved in silicates (e.g., $Mg_{1.8}Fe_{0.2}SiO_4$ olivine) and oxides. During hydration and carbonation, reaction products such as serpentine, talc, magnesite, dolomite, and calcite have higher Mg# values than do the olivine and pyroxene reactants (Beard et al. 2009, Evans 2008, Frost 1985, Frost & Beard 2007, Horita & Berndt 1999, Janecky & Seyfried 1986, Klein et al. 2009; Klein & Bach 2009, McCollom & Bach 2009). Excess iron is commonly taken up by hydroxides such as goethite [$FeO(OH)$] and brucite [$(Mg,Fe)(OH)_2$], by oxides such as hematite (Fe_2O_3) and magnetite (Fe_3O_4), and by metal alloys rich in Fe and Ni such as awaruite, as observed in Oman (Lorand 1987). Initial stages of reaction in rock-dominated systems often involve oxidation of iron from Fe^{2+} in silicates such as olivine to Fe^{3+} in oxides. These and other reactions lead to reduced oxygen fugacity and increased hydrogen fugacity in product fluids, e.g.,

$$6Fe_2^{2+}SiO_4 + 7H_2O = 3Fe_3^{2+}Si_2O_5(OH)_4(Fe-serpentine) + Fe_2^{3+}Fe^{2+}O_4(magnetite) + H_2(aq). \quad (1k)$$

In this way, fluids become increasingly reduced as the fluid/rock ratio decreases and eventually saturate in Fe-Ni alloys. Fluids from serpentinizing peridotites have low oxygen fugacity and enhanced levels of dissolved hydrogen and methane (Barnes & O'Neil 1969; Haggerty 1991, Kelley et al. 2005, Lang et al. 2010, Peretti et al. 1992), as observed in Oman (e.g., Neal & Stanger 1983). From the perspective of mineral carbonation, the main impacts of these redox reactions are to impart a geochemical signal (low oxygen fugacity, high fugacity of H_2) to fluids produced by hydration of peridotite at low water/rock ratios and to impart the potential for reduction of carbon species, including breakdown of carbonate minerals to form graphite and methane, e.g.,

$$MgCO_3 + 2H_2 = Mg(OH)_2(or\ aqueous\ Mg^{2+} + 2OH^-) + H_2O + C(graphite) \quad (1l)$$

and

$$MgCO_3 + 4H_2 = Mg(OH)_2 + H_2O + CH_4(methane). \quad (1m)$$
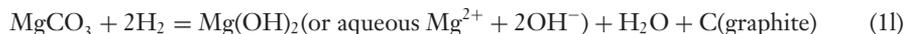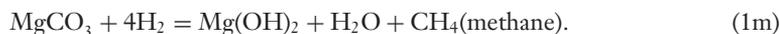
The reactions listed here and their associated mineral parageneses were explored decades ago (e.g., Evans 1977; Frost 1985; Greenwood 1967; Johannes 1969; Kerrick 1974; Skippen 1974; Trommsdorff & Evans 1977a,b). As noted by these previous workers, peridotite carbonation reactions progressively form increasingly SiO_2-rich silicates, as Mg and Ca are incorporated into carbonate minerals with increasing CO_2 contents in fluid at a given pressure and temperature (**Figure 1**). In the absence of H_2O-rich fluids, the maximum thermal stability of carbonate minerals in peridotite bulk compositions at 2 kbar are approximately 520°C for breakdown of magnesite + quartz to form opx + CO_2, and 560°C for breakdown of magnesite + opx to form olivine + CO_2 (Johannes 1969). At lower P_{CO_2}, in the presence of aqueous fluids and/or at lower total pressure, the thermal stability of carbonate minerals is reduced.
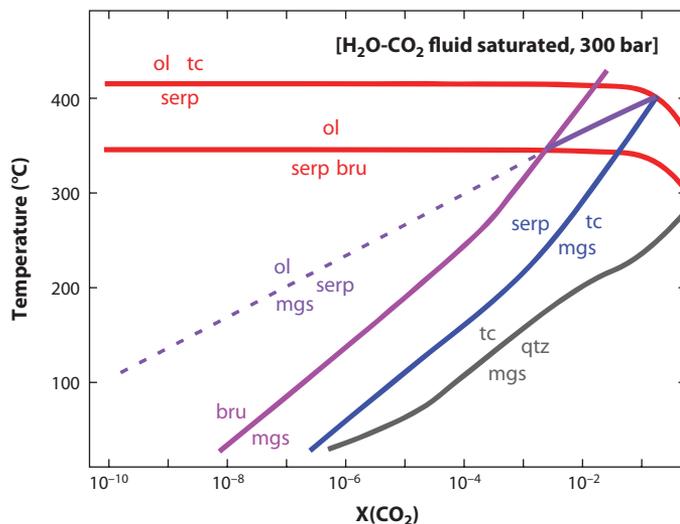
Figure 1

Schematic phase diagram for reactions involving brucite (bru), olivine (ol), the serpentine polymorph chrysotile (serp), talc (tc), quartz (qtz), and magnesite (mgs) in the system $MgO\text{-}SiO_2\text{-}H_2O\text{-}CO_2$, saturated in $H_2O\text{-}CO_2$ fluid at 300 bar, calculated using Thermocalc (Holland & Powell 1998).

2.3. Aqueous Geochemistry of Peridotite Carbonation

As originally explained by Barnes, O'Neil, and coworkers (Barnes & O'Neil 1969; Barnes et al. 1967, 1978) and quantified by Bruni, Cipolli, Marini and coworkers (Bruni et al. 2002, Cipolli et al. 2004), low-temperature reaction between surface waters and peridotite generally takes place in three steps. First, meteoric water reacts with peridotite in equilibrium with the atmosphere, increasing dissolved Mg^{++} and HCO_3^- concentrations to form $Mg\text{-}HCO_3$ waters, also known as Type I waters. Type I waters are found in shallow groundwater in peridotite massifs worldwide.

In the second step, subsurface reaction, out of equilibrium with the atmosphere, leads to precipitation of Mg-carbonates such as magnesite and dolomite, together with serpentine and clay minerals. Although Ca is a minor constituent of the peridotite, contained mainly in pyroxene minerals, it is excluded almost completely from serpentine and clay, and the concentration of Ca^{++} in resulting fluids rises even when dolomite—$CaMg(CO_3)_2$—is precipitating. Dissolution of Ca-bearing pyroxenes also leads to very high pH, as in Reaction 1i above, whereas reactions such as Reaction 1k reduce the oxygen fugacity to very low values (e.g., Barnes & O'Neil 1969, Bruni et al. 2002, Cipolli et al. 2004, Evans 2008, Frost 1985, Janecky & Seyfried 1986). Carbonate precipitation via Reactions 1a–g, together with reactions such as

$$Mg^{++} + HCO_3^- + OH^- = MgCO_3 + H_2O, \tag{2}$$
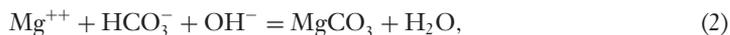
lowers the total carbon concentration in the resulting fluids to nearly zero (Barnes & O'Neil 1969, Bruni et al. 2002, Cipolli et al. 2004), producing high-pH, low-fO_2, low-carbon Ca-OH waters, sometimes termed Type II waters. These form alkaline springs that emerge from peridotite catchments worldwide.

In the third step, alkaline spring waters react with the atmosphere (or mix with shallow groundwater), precipitating calcite and lowering the pH to neutral values via reactions such as Reaction 1j.

Awaruite: an Fe-Ni alloy mineral

Paragenesis: common assemblage of rock-forming minerals, often indicative of crystallization at a particular pressure, temperature, and/or fluid composition

2.4. Observed Parageneses on Land, Especially in the Samail Ophiolite in Oman

Peridotite-hosted carbonates come in essentially three types: (*a*) partially hydrated peridotite with carbonate veins, sometimes termed ophicalite, especially in Alpine localities, (*b*) fully carbonated peridotite (magnesite or dolomite + quartz) known as listwanite (also known as listvenite, listvanite, or listwaenite), and (*c*) travertine deposited from springs in peridotite catchments. In **Supplemental Section S2**, we provide an annotated bibliography of work on these parageneses in subaerial outcrops worldwide. Here we focus on outcrops in Oman.

The Samail ophiolite in northern Oman and the eastern United Arab Emirates has been the site of classic studies of hydrothermal alteration of lower crust and upper mantle formed at an oceanic spreading ridge (e.g., Bosch et al. 2004, Gregory & Taylor 1981). Boudier et al. (2010) recently made detailed investigations of serpentinite replacement textures, and two short papers report on native metal alloys in Oman serpentinites (Leblanc et al. 1991, Lorand 1987). Dewandel et al. (2003, 2005), Weyhenmeyer et al. (2002), and Matter et al. (2006) studied the hydrology of parts of the ophiolite and peridotite alluvium.

Peridotites in Oman are generally 30–70% serpentinized, although 100% hydrated rocks (serpentinites) are found, particularly in large areas with low relief. The proportion of serpentine formed during hydrothermal circulation near a spreading ridge, versus the proportion formed during obduction versus the proportion formed during weathering, is not known. However, the qualitative observation that peridotites appear to be fresher in deep canyons than in low relief areas suggests that much of the serpentinization formed during ongoing, subaerial weathering and that its extent decreases with depth below the surface (A. Nicolas and F. Boudier, personal communication, 1990). Submillimeter-wide carbonate veins are found on almost all joint surfaces in new roadcuts, and massive magnesite veins can be seen traversing the peridotite landscape. Extensive, spectacular travertine deposits form around alkaline springs in peridotite catchments. Veins are generally composed of magnesite and/or dolomite far from travertines, and calcite and/or dolomite directly beneath travertines.

The ophiolite contains both listwanite and "normal," partially serpentinized, peridotite-hosting carbonate veins. On the basis of data in Section 2.7 and in **Supplemental Section S4**, we conclude that most of the carbonate veins form in currently active low-temperature systems—at 30°C to perhaps 60°C—that involve meteoric water. In contrast, listwanites formed in fossil high-temperature systems that reached ~200°C. Stanger and coworkers (Stanger 1985, 1986; Stanger & Neal 1994; Stanger et al. 1988) wrote several papers on the present-day peridotite alteration and seminal papers on groundwater and alkaline springs formed by peridotite alteration (Neal & Stanger 1983, 1984, 1985). Clark and coworkers (Clark & Fontes 1990, Clark et al. 1992) studied a peridotite-hosted travertine, mainly in an effort to obtain a stable isotope record of paleoclimate. There have been several studies of listwanites in Oman (Nasir et al. 2007, Stanger 1985, Wilde et al. 2002).

New [14]C "ages" for all but two of 44 peridotite-hosted travertine and carbonate vein samples from the low-temperature system are <50,000 years old (our unpublished data and Kelemen & Matter 2008). This suggests that low-temperature peridotite alteration is close to a steady state in which carbonates form in a shallow weathering horizon at approximately the same rate that this horizon is removed by erosion. In our view, there is little indication that paleoclimatic variation is recorded by stable isotope ratios in peridotite-hosted carbonates (**Supplemental Section S3**). In the subsurface, with increasing solid volume, one might expect decreasing permeability and armoring of reactive surfaces to limit the extent of reaction, yet the ^{14}C data indicate that low-temperature alkaline springs feeding travertine deposits remain active for tens of thousands of years.

Assuming that the rate of carbonate formation has been approximately constant for 50,000 years, we infer that $\sim 5 \times 10^4$ tons of peridotite-hosted carbonate form per year in Oman (**Supplemental Tables S1** and **S2**; also see Kelemen & Matter 2008). Information on the constraints and uncertainties in this rate estimate is given in **Supplemental Section S4**.

Travertine terraces form by low-temperature reaction of dissolved Ca with atmospheric CO_2, as in Reaction 1j, where alkaline spring waters exit from peridotite. Groundwater (Type I, Mg-HCO$_3$ waters) and alkaline spring water (Type II, Ca-OH waters) conform well to the compositional groups and hypotheses outlined by Barnes & O'Neil (1969) and Bruni et al. (2002). As noted in the previous section, Type I waters have high total carbon, whereas the most alkaline Type II waters have almost none, indicative of subsurface Ca-Mg carbonate precipitation. Carbonate veins in partially serpentinized peridotite have ^{14}C ages that overlap the travertine ages, and stable isotope data yield crystallization temperatures of 20–60°C for both veins and travertines, so the veins probably represent the subsurface carbonate complementary to Type II waters and travertine deposition (**Supplemental Section S4** and Kelemen & Matter 2008). Metamorphic parageneses in veined peridotites also show that they formed at <50°C, near the surface (E. Streit, P. Kelemen & J. Eiler, unpublished data).

Extensive listwanites in the Oman peridotites—billions of tons of fully carbonated peridotite—are inferred to be late Cretaceous or Paleocene on the basis of one locality in which they replace mantle peridotite, which was thrust onto the Arabian continent beginning at $\sim$96 Mya (e.g., Hacker 1994). Additionally, the listwanites are unconformably overlain by late Paleocene to Eocene conglomerate and limestone (23.44°N, 56.19°E). Preliminary stable isotope data (E. Streit, P. Kelemen & J. Eiler, unpublished data) suggest that they formed at a peak temperature of $\sim$200°C, similar to that of listwanites elsewhere (Hansen et al. 2005, Madu et al. 1990, Schandl & Naldrett 1992, Schandl & Wicks 1991). If so, they probably formed from fluids rich in CO_2 because magnesite + quartz are not stable, and they probably break down to form talc + CO_2 in the presence of H_2O-rich fluids at 200°C (**Figure 2**). All known listwanites in Oman are found within 500 m of the basal thrust, where peridotites overlie CO_2-bearing metasediments. It is likely that CO_2-rich fluids, formed by metamorphic dehydration of the underlying sediments as they were overthrust by hot peridotite, rose into the peridotite to form the listwanites.

2.5. Observed Parageneses on the Seafloor

Formation of carbonate via reaction of fluid with peridotite is occurring at and beneath the seafloor flanking slow-spreading mid-ocean ridges via submarine "weathering" as well as in more spectacular hydrothermal vent systems. In both settings, peridotite carbonation is inextricably linked with hydration. An annotated bibliography of work on these sites, and related work on phase equilibrium in these systems, is given in **Supplemental Section S5**.

Serpentine-rich mud volcanoes and associated carbonate chimneys in forearc settings attest to the importance of hydrothermal interaction with peridotite in the mantle wedge above subduction zones (Eickmann et al. 2009; Haggerty 1991; Mottl et al. 2003, 2004). This important setting for peridotite carbonation has not received sufficient attention. The Oman listwanites, formed in peridotite thrust over carbonate-bearing sediments, provide an outcrop exposure of peridotite carbonation processes in the hanging wall of a subduction zone.

Subseafloor peridotite carbonation is most spectacularly evident at the tall carbonate chimneys of the Lost City hydrothermal area, $\sim$15 km west of the Mid-Atlantic Ridge at 30°N (e.g., Früh-Green et al. 2003, Kelley et al. 2001, Ludwig et al. 2006). High-pH ($\sim$11) and low-Eh vent fluids are similar to Type II waters in alkaline springs on land. Exit fluid temperatures at Lost City are 40–75°C, higher than in subaerial Type II springs but much lower than maximum fluid
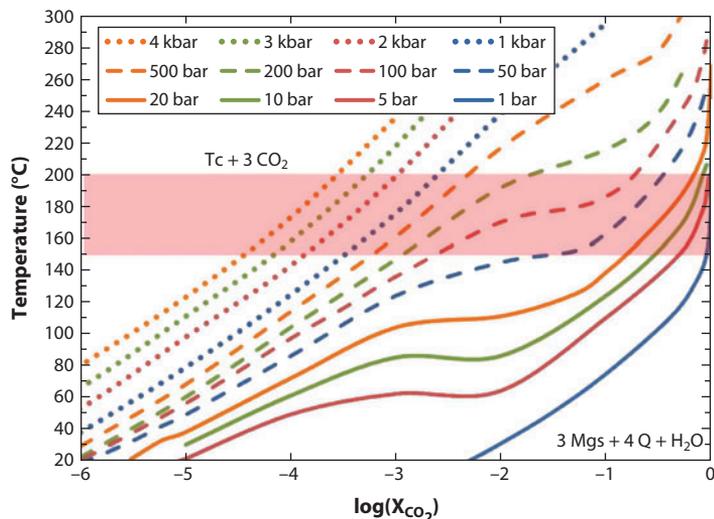
Figure 2

Mole fraction of CO_2 in H_2O-CO_2 fluid X_{CO_2} versus temperature, for the reaction talc (Tc) + CO_2 = magnesite (Mgs) + quartz (Q) + H_2O, calculated for Mg-end-members using Thermocalc (Holland & Powell 1998). At a given pressure, the assemblage magnesite + quartz at high temperature is stable only in the presence of CO_2-rich fluids. The shaded band shows the likely temperature of formation of Oman listwanites. The pressure of listwanite formation is not well constrained but was probably less than 4 kbar.

temperatures at other hydrothermal vent sites along mid-ocean ridges. An even lower-temperature (maximum 40°C), peridotite-hosted, alkaline spring forming a carbonate chimney is known just offshore from New Caledonia (Launay & Fontes 1985).

Kelley et al. (2001) suggested that, whereas other vent sites have a magmatic heat source, Lost City may be heated by exothermic hydration of peridotite (serpentinization), as proposed in general by Schuiling (1964) and Fyfe (1974). Exothermic heating via peridotite carbonation may also be important (Kelemen & Matter 2008). Experimental data coupled with thermodynamic calculations (Allen & Seyfried 2004, Seyfried et al. 2007) suggest that maximum fluid temperatures in the subsurface may have been ~200°C, with subsequent cooling to produce 40–75°C exit fluids at Lost City. Conductively cooled, diffusely venting fluids around other, higher-temperature, peridotite-hosted vent sites reach solid carbonate saturation, as in carbonate-cemented breccias around the Rainbow and Saldanha vent sites (Ribeiro Da Costa et al. 2008).

In general, diffuse interaction between seafloor peridotite and seawater at low temperature probably produces more solid carbonate than do the more spectacular features at focused hydrothermal vents, as discussed in **Supplemental Section S5**. **Figure 3** illustrates the observed concentration of CO_2 in drill holes from Ocean Drilling Program (ODP) Legs 153 and 209, at ~23°N and 15°N along the Mid-Atlantic Ridge, as a function of depth below the seafloor, extending to approximately 200 meters below seafloor (mbsf) (Casey 1997, Kelemen et al. 2004). These peridotites contain an average of 0.6 wt% CO_2 in carbonate minerals, without systematic variation with depth. Some seafloor peridotites may also contain graphite (Berndt et al. 1996).

2.6. Global Significance of Natural Peridotite Carbonation

In this section, we assess the amount of carbon in near-surface peridotite compared with the amount of carbon in the hydrosphere. There may be several sources of carbon involved.
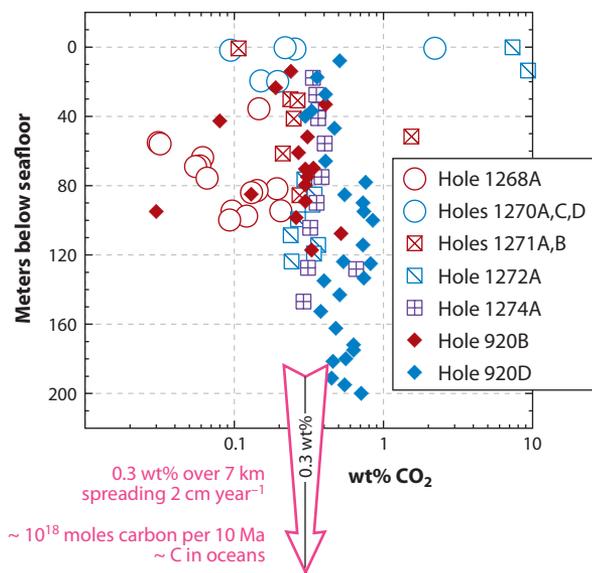
Figure 3

Concentration of carbon (expressed as wt% CO_2, although some could be in the form of graphite) versus depth (meters below seafloor) in peridotite drill core recovered on Ocean Drilling Program (ODP) Legs 153 and 209 (Casey 1997, Kelemen et al. 2004). There is no systematic variation of carbon concentration with depth, and the average concentration is 0.6 wt% CO_2. (See also Früh-Green et al. 2004, figure 8.) As described in the text, where peridotite is exposed on the seafloor at slow-spreading ridges, oceanic crust may have an average carbon concentration expressed as 0.3 wt% CO_2 extending to 7-km depth, as illustrated schematically by the pink arrow. If so, this corresponds to uptake of 10^{18} moles of carbon every 10 Ma, equivalent to the amount of carbon dissolved in the ocean.

1. The budget is dominated by carbon uptake from seawater and groundwater during hydrothermal alteration and weathering.
2. Uptake of carbon from magmatic fluids, where mafic plutons are emplaced into mantle peridotite (along slow-spreading ridges and perhaps in some subduction-related arcs), may form carbonate minerals.
3. There may be "primary" carbon in mantle peridotites, which could be preserved where uplift and erosion that expose peridotite on the surface are very slow, in regions with low heat flow.

(2) and (3) are small by comparison with (1), and are discussed in **Supplemental Section S6**.

As noted above, drill-core samples of peridotite from the Mid-Atlantic Ridge have an average CO_2 concentration of 0.6 wt% (**Figure 3**). In the 15°N area along the Mid-Atlantic Ridge, peridotite intruded by gabbroic plutons is regionally extensive on both sides of the spreading axis. Seismic data for this area suggest that gradually decreasing proportions of serpentinization extend to 6–8 km below the seafloor (figure F5 in Kelemen et al. 2004). Where peridotite is exposed on the seafloor flanking slow-spreading ridges [5–15% of the total area (Cannat et al. 1995, Carlson 2001)], assuming that the serpentinization gradient is linear and associated with carbonation, there may be ~0.3 wt% CO_2 over a 7-km depth interval. Then, for an average half-spreading rate of 0.01 m per year over a length of 60,000 km, peridotite alteration around slow-spreading ridges consumes ~10^{11} moles of carbon per year, or ~2×10^6 moles per kilometer per year. This is roughly one-tenth of the global uptake via alteration of basaltic lavas on the seafloor at fast- and slow-spreading ridges combined (Alt & Teagle 1999, Staudigel & Hart 1985). Peridotite

carbonation during 10 Ma of spreading consumes $\sim10^{18}$ moles of carbon, equivalent to the mass of carbon in the oceans. Extrapolating the estimated rate of CO_2 uptake by peridotite carbonation in Oman—5 × 10^4 tons per year or $\sim10^7$ moles per kilometer per year over the 350-km length of the Samail ophiolite—to ophiolites worldwide yields $\sim5 \times 10^9$ moles of carbon per year, which is small in comparison with peridotite carbonation beneath the seafloor.

Peridotite carbonation may be an ongoing process that continues far off axis, by analogy with carbonate formation in basaltic lavas formed at mid-ocean ridges that continues for at least 150 Ma despite their gradual burial beneath pelagic sediments (Alt & Teagle 1999, Staudigel & Hart 1985). If the carbonation process continues for hundreds of kilometers off axis, CO_2 contents in peridotites from ODP Legs 153 and 209 (close to the Mid-Atlantic Ridge) may be lower than those beneath sediments further off axis, and the total rate of CO_2 consumption via peridotite carbonation would be correspondingly higher.

⊙ Supplemental Material

2.7. Stable Isotope Data: Mineral Crystallization Thermometry

We collected preliminary, whole-rock data on oxygen and carbon isotopes in peridotite-hosted travertine and vein samples from Oman (**Figure 4** and **Supplemental Table S3**). These show two important features: (*a*) kinetic fractionation of both carbon and oxygen isotopes in travertine samples less than 1,000 years old, and (*b*) apparent equilibrium of older travertines with groundwater and spring water, recording near-surface temperatures. The kinetic fractionation seen in the young travertines (**Supplemental Section S7**) is of great interest but is tangential to the main topics of this review.

Some of our samples of calcite (travertine) and magnesite (veins) are pure enough that the oxygen isotope ratio for the whole rock is a close approximation of the ratio in the minerals.

Figure 4

Whole-rock carbon and oxygen isotope data on peridotite-hosted carbonate veins, and surficial travertine deposits associated with alkaline springs in peridotite catchments, in the ophiolite massifs of northern Oman. ^{14}C ages are in radiocarbon years before 1950. For our new data (**Supplemental Table S3**), error bars for ^{14}C ages are shown only for samples with replicate analyses because analytical precision for other samples is not an adequate reflection of the intrasample variability within our samples. (*a*) Our new data (*filled symbols*) and those of Clark & Fontes (1990; *open symbols*). For the data of Clark & Fontes (1990), analytical precision and data on replicate analyses are not given for stable isotope data, but precision is listed (and shown) for ^{14}C ages. (*b*) In addition to data from Oman (*diamonds*, as in panel *a*), outlined fields represent data from peridotite-hosted carbonate deposits in northern California (*red* and *blue*; see below), Egypt (*green*; Smith et al. 2004), the Balkans (*purple*; Fallick et al. 1991), and northwest Canada (*orange*; Wilson et al. 2009). Blue outline: "scums," "sludges," and travertines associated with Ca-OH-type alkaline springs (O'Neil & Barnes 1971); red with gray background: Ca-Mg carbonate veins (O'Neil & Barnes 1971); dashed red: hydromagnesite veins (O'Neil & Barnes 1971); filled red rectangle: magnesite veins (Barnes et al. 1973). δ^{18}O data ranging from ~20 to 25.5 are also available for travertine from the Del Puerto ophiolite (Blank et al. 2009, not shown). (*c*) In addition to data from Oman (*diamonds*, as in panel *a*), light-green rectangles show the range of data for carbonate chimneys (LCC) and calcite veins in surrounding host rocks (LCV) from the Lost City hydrothermal area along the Mid-Atlantic Ridge (Früh-Green et al. 2003). Light-green circles and oval represent calcite in veins and ophicarbonates drilled from the Iberian Margin continent-ocean transition; compositions of 36 out of 38 samples lie in oval with bold outline (Agrinier et al. 1988, 1996; Evans & Baltuck 1988; Milliken & Morgan 1996). Yellow rectangle containing black dots: aragonite in serpentinized peridotites dredged from the Mid-Atlantic Ridge (Bonatti et al. 1980). Black dashed rectangle: calcite in Ligurian and Appenine ophicalcite deposits, ranging from lower (heavy δ^{18}O) to higher metamorphic grade (light δ^{18}O; Barbieri et al. 1979). White rectangles containing diagonal black lines: (*right*) calcite in oceanic ophicarbonates affected by later Alpine regional metamorphism (Früh-Green et al. 1990); (*left*) calcite in contact-metamorphosed ophicarbonates in the Bergell aureole, Val Malenco (Abart & Pozzorini 2000, Pozzorini & Früh-Green 1996). (*d*) Oxygen isotope values versus ^{14}C ages for our data (*filled symbols*) and those of Clark & Fontes (1990) (*open symbols*, as in panel *a*), illustrating that light ratios are found only in samples that are less than a few thousand years old, and that pure calcite and pure magnesite samples record low, near-surface temperatures of equilibration with Oman groundwater and spring water. Abbreviations: SMOW, per mil deviation relative to standard mean ocean water; VPDB, per mil deviation relative to Vienna Pee Dee Belemnite.

For calcite-rich travertine with ^{14}C ages of >1,000 years and carbonate veins composed mainly of calcite, typical $\delta^{18}O$ is 23–26‰ relative to SMOW (per mil deviation relative to standard mean ocean water; see bold type in **Supplemental Table S3**). If calcite formed in equilibrium with typical Oman groundwaters and alkaline spring waters having $\delta^{18}O$ from −2‰ to 1‰ (our unpublished data and Clark et al. 1992, Matter et al. 2006 , Neal & Stanger 1985), they would record ^{16}O-^{18}O exchange at ∼23–60°C (Chacko & Deines 2008, Friedman & O'Neil 1977, O'Neil et al. 1969), approximately equivalent to the seasonal range of air temperature in Oman.

All but two veins (from near the oasis of Tuf) show systematically heavier $\delta^{18}O$ and $\delta^{13}C$ compared with that of travertine. We tentatively attribute this variability to variable proportions of carbonate and silicate minerals, all close to equilibrium with relatively similar fluid compositions. Two nearly pure magnesite veins have $\delta^{18}O$ of 35‰ to 36‰, yielding magnesite-water oxygen exchange temperatures of ∼33°C to 49°C (Chacko & Deines 2008). Less precise data for a third magnesite-rich vein yield $\delta^{18}O$ of 30‰, corresponding to 58–74°C. Of three veins with more than 60 wt% dolomite, two have $\delta^{18}O$ between 31‰ and 32‰. If these approximate the oxygen isotope
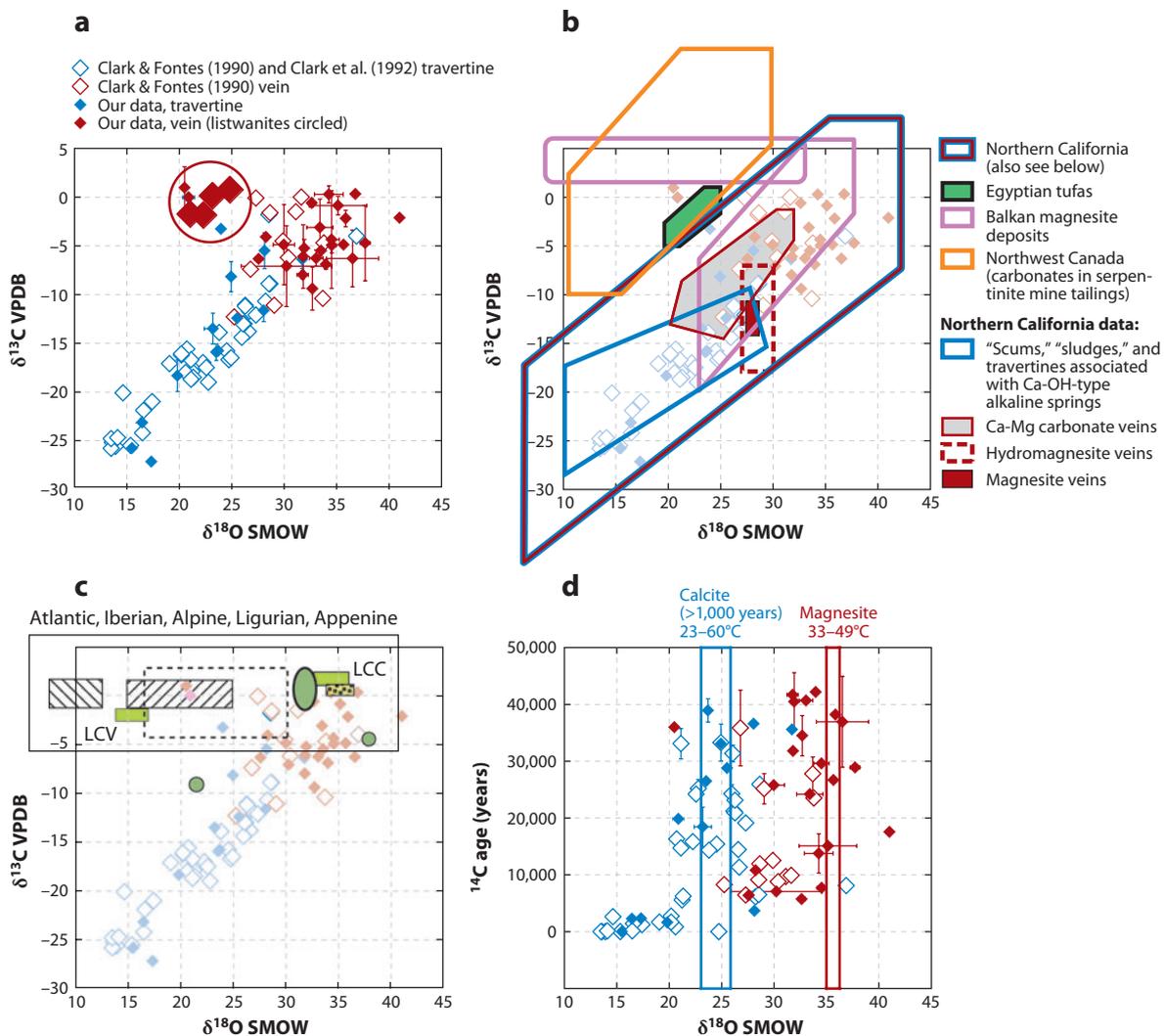
ratio in dolomite, they yield low crystallization temperatures (Tarutani et al. 1969, Vasconcelos et al. 2005) consistent with the temperatures calculated for calcite and magnesite. A third dolomite-rich sample with $\delta^{18}O$ ~41 yields an unreasonably low temperature.

The temperatures calculated here, for stable isotope exchange between peridotite-hosted carbonates and groundwater in Oman, are consistent with observed temperatures of alkaline spring waters and with temperatures of hydrogen isotope fractionation between gas and alkaline spring waters in Oman (Neal & Stanger 1983). Similarly, in the California Coast Ranges (Barnes et al. 1973, Blank et al. 2009), calcite- and dolomite-bearing travertines with $\delta^{18}O$ of 20–25‰ and magnesite veins with $\delta^{18}O$ of 27.6–28.2‰ record equilibrium with local waters at 15–40°C. All these data suggest that magnesite veins in partially carbonated peridotites and alkaline spring waters are genetically related and that they form via fluid-rock reaction at approximately the same temperature as travertine, near the surface in a shallow weathering horizon, as hypothesized by Kelemen & Matter (2008).

Supplemental Section S8 summarizes data on stable isotopes in peridotite-hosted carbonates from seafloor samples and the Alps. Unlike samples from Oman, California, Canada, and the Balkans, the Swiss and northern Italian samples have restricted $\delta^{13}C$ from approximately −4‰ to 3‰. Furthermore, they show a range of $\delta^{18}O$ that corresponds to expected depositional and metamorphic temperatures, from near 0°C for samples formed near the seafloor to more than 100°C in Alpine metamorphic rocks.

It is important to constrain the conditions of listwanite formation because complete carbonation is the goal of enhanced peridotite carbonation for CO_2 capture and storage. So far, most of our stable isotope data on Oman samples are for travertines and carbonate veins from serpentinized peridotite, not from listwanites. Furthermore, we do not know $\delta^{18}O$ in the fluids that formed listwanites. If we assume that $\delta^{18}O$ was near zero, as in Type I and II waters in Oman peridotites today, preliminary oxygen isotope data yield formation temperatures of 40–70°C for calcite and 100–150°C for magnesite. However, this assumption is highly questionable for Cretaceous, metamorphic fluids that could have been derived from isotopically heavy metasediments.

Consistent listwanite formation temperatures of 237 ± 21°C, 248 ± 12°C, and 210–240°C were determined for three localities in Canada via fluid-inclusion measurements (Hansen et al. 2005, Madu et al. 1990, Schandl & Wicks 1991). Preliminary data using the "clumped isotope" technique (Eiler 2007, Ghosh et al. 2006) show that Oman listwanites also record peak temperatures close to 200°C (E. Streit, P. Kelemen & J. Eiler, unpublished data). Inferred listwanite formation temperatures correspond well to inferred temperatures in the reaction zone beneath the Lost City hydrothermal vents (Allen & Seyfried 2004, Seyfried et al. 2007).

3. CHEMICAL KINETICS OF MINERAL CARBONATION

3.1. Experimental Dissolution and Carbonation Kinetics of Olivine, Serpentine, Plagioclase, and Basalt

In this section, we review data on the rates of dissolution and carbonation of olivine, plagioclase, and basalt, expanding on the summary by Matter & Kelemen (2009). Dissolution and carbonation of other minerals, particularly wollastonite ($CaSiO_3$) and serpentine, have been investigated in the context of CO_2 capture and storage. However, serpentine carbonation—without expensive heat treatment to ~600°C prior to reaction—is more than 10 times slower than olivine carbonation (e.g., Gerdemann et al. 2007, O'Connor et al. 2004), and wollastonite is not a common mineral.

Supplemental Section S9 provides an annotated bibliography of experimental work. For continuity, we summarize the main points here. The fastest-known olivine carbonation was observed

in unconventional studies at the U.S. Department of Energy's Albany Research Center and at Arizona State University. These studies combined olivine dissolution with carbonate precipitation, at an olivine-to-water ratio of ~1:4. Olivine in saline aqueous solutions with high bicarbonate (e.g., $NaHCO_3$, $KHCO_3$) concentrations were held in a closed reaction vessel at high P_{CO_2} (e.g., Chizmeshya et al. 2007, O'Connor et al. 2004). The fastest rates were at 185°C in aqueous solutions with 1 M NaCl and 0.64 M $NaHCO_3$ with $P_{CO_2} > 70$ bar and pH ~ 8. At high P_{CO_2}, high bicarbonate concentrations act as a catalyst, making rates 1,000 times faster than rates for the same conditions without bicarbonate and more than 10^6 times faster than rates observed and calculated at 25°C, at pH 8, and with atmospheric P_{CO_2} (**Figure 5**). Experimental olivine carbonation, together with carbonation of basaltic glass (inferred from dissolution rate data), is much faster than dissolution of basalt or minerals common in basaltic rocks.

Importantly, it seems that there are no experiments on dissolution of plagioclase or basalt with high $NaHCO_3$. If high-$NaHCO_3$ solutions catalyze rapid basalt carbonation, comparable with the effect for olivine, then basalt carbonation would be a favorable mineral carbonation method because basalt is the most common rock type in Earth's crust.

Extrapolation of chemical kinetic data on powders to natural peridotite carbonation requires knowledge of processes in porous media. The experiments of Andreani et al. (2009) on sintered olivine aggregates with a grain diameter of approximately 84 μm and a porosity of 17% achieved ~3% carbonation of olivine in 7.5 h, approximately 100 times slower than predicted for powders with a grain size of 84 μm, which is consistent with an "effective grain size" of 8.4 mm. Thus, for fractured Oman peridotite with an initial grain size of 0.001 to 0.01 m and a porosity of ~1%, we might expect an effective grain size of ~1 m.

## 3.2. Comparison of Laboratory and Natural Olivine Carbonation Rates

Kelemen & Matter (2008) fit data on the rate of olivine carbonation during the first hour of Albany Research Center experiments on 70-μm grains, and they applied this fit to reaction over periods of years at an effective grain size of ~1 m. The fit predicts that reaction at 30°C and 0.0004 bar P_{CO_2} (atmospheric P_{CO_2}) is approximately one million times slower than at 185°C and 150 bar P_{CO_2}. This prediction can be compared with natural rates. In the near-surface peridotite of Oman, we estimate CO_2 uptake of ~5×10^5 tons per year (**Supplemental Table S1** and **Section S4**). The peridotite has an exposed surface area of ~5,250 km². If olivine carbonation due to weathering takes place mainly in a horizon ~15 m thick, as inferred from ^{14}C ages and erosion rates in Oman, it corresponds to uptake of ~1 gm CO_2 per cubic meter per year (mass fraction of ~10^{-14} s^{-1}), which is approximately one million times slower than the predicted rate of 1 ton per cubic meter per year. Thus, laboratory and natural data agree surprisingly well (**Figure 5**).

In contrast, Wilson et al. (2009) infer carbonation rates of ~10^{-10} s^{-1} in serpentinite mine tailings in Canada. This rapid rate, compared with olivine carbonation in laboratory studies and in Oman, probably results from the fine-grained, fibrous nature of the serpentinite mine tailings. For additional discussion, please see **Supplemental Section S10**.

4. "PHYSICAL KINETICS" OF MINERAL CARBONATION: SELF-LIMITING REACTIVE FLOW VERSUS REACTION-DRIVEN CRACKING

4.1. Volume Changes During Natural Peridotite Hydration and Carbonation

As can be seen from the simplified reactions in Section 2.2, hydration of olivine consumes water to produce serpentine and brucite, whereas complete carbonation of olivine produces magnesite

Olivine only, pH 3 and 8

Grain size ~ 70 μm
Surface area ~ spheres

Fo91 San Carlos olivine
Prigiobbe et al. (2009)
120°C
pH 8 and pH 3

pH 8, Chizmeshya et al. (2007)
Fo91 San Carlos olivine,
carbonation
1 to 4.5 M NaHCO$_3$ or
3 to 8 M KHCO$_3$,
185°C, **P$_{CO_2}$ 150 bar**

Observed rate in Oman
peridotite **carbonation**
Upper ~15 m of peridotite
adjusted from 0.7 m to
70 μm "grain size,"
Kelemen & Matter (2008)

○ pH 8, Fo92 Twin Sisters olivine, Palandri & Kharaka (2004)

⊞ pH 8, Fo91 San Carlos olivine, Hänchen et al. (2006)

■ pH 8, Fo92 Twin Sisters olivine **carbonation**,
O'Connor et al. (2004) fit by Kelemen & Matter (2008),
1 M NaCL, 0.64 M NaHCO$_3$, **P$_{CO_2}$ 0.0004 bar**

◆ pH 8, Fo92 Twin Sisters olivine **carbonation**,
O'Connor et al. (2004) fit by Kelemen & Matter (2008),
1 M NaCL, 0.64 M NaHCO$_3$, **P$_{CO_2}$ 150 bar**

◆ pH 3, Fo92 Twin Sisters olivine, Palandri & Kharaka (2004)

Olivine, plagioclase, and basalt at pH 8

Grain size ~ 70 μm
Surface area ~ spheres

Labradorite, pH 3.2
Carroll & Knauss (2005)

● Calculated from Palandri & Kharaka (2004) for Twin Sisters olivine
[Fo92, used by O'Connor et al. (2004)] using data for Fo and Fa

◆ **Carbonation: dissolution plus
crystallization of magnesite plus quartz**
Twin Sisters, O'Connor et al. (2004) fit by Kelemen & Matter (2008)
1 M NaCl, 0.64 M NaHCO$_3$, P$_{CO_2}$ 150 bar

■ San Carlos olivine, Fo91, Hänchen et al. (2006), LiOH buffer

● Labradorite, An 50 to 70, Palandri & Kharaka (2004)

● Crystalline basalt, Schaef & McGrail (2009)

△ Basalt glass, Gislason & Oelkers (2003)
40 to 120 μm, NH$_4$Cl buffer

▲ Gislason & Oelkers (2003), experimental
range of temperature, 7 to 50°C

and quartz. These reactions, as written, consume fluid components to increase the solid volume by 33% (serpentinization) to 44% (carbonation) relative to the initial solid volume, in a manner similar to the hydration of lime, CaO, to form portlandite, $Ca(OH)_2$, with a 50% volume increase.

Many reactions in metamorphic rocks occur at conditions of constant volume [see the recent review by Putnis (2009)]. In principle, one could write hydration and carbonation reactions that conserve the solid volume, by positing that large amounts of solid material are dissolved and transported elsewhere in an open system. Obviously, most or all the Mg and Ca in peridotite-hosted carbonate veins and travertines has been extracted from peridotite. However, it is not apparent whether small proportions of Mg and Ca are extracted from large masses of rock or whether large proportions are extracted from small masses. Although there are exceptions (notably Snow & Dick 1995), most studies of peridotite alteration conclude that it is nearly isochemical for all major components except for the addition of H_2O and CO_2 (e.g., Andreani et al. 2007; Augustin et al. 2008; Coleman & Keith 1971; Evans 2008; Hansen et al. 2005; Kelemen et al. 2004, 2007; Robinson et al. 2005; Shervais et al. 2005). Experimentally, Andreani et al. (2009) demonstrated that peridotite carbonation in an open system produced an increase in the solid volume, despite dissolution and export of small amounts of Si, Mg, and Ca in the fluid.

Most of our samples from Oman—predominantly veins and travertine—are not appropriate for assessing the extent of mass transfer from the peridotite protolith. However, a few samples can be used. **Figure 6** compares typical analyses of partially hydrated peridotites from the mantle section of the Samail ophiolite (Hanghøj et al. 2010) with our new analyses of listwanites and partially carbonated peridotites. These samples have more variable Mg# than do typical Oman peridotites but approximately the same SiO_2 contents. Variable Mg#'s probably reflect extraction of small proportions of Mg and Ca that formed carbonate veins elsewhere. The volume decrease associated with Mg and Ca loss would have been less than 1% for most samples, whereas hydration and carbonation caused solid volume increases of more than 10%.

4.2. Self-Limiting Versus Self-Cracking Regimes: Force of Crystallization and Relaxation Mechanisms

Fluid-rock reactions that increase the solid volume are often self-limiting because they fill porosity, reduce permeability, and create reaction rims of solid products that act as diffusive boundary

---

Figure 5

(*Top*) Rates of olivine dissolution in aqueous fluids and of olivine carbonation in aqueous fluids with high P_{CO_2} (Chizmeshya et al. 2007, Hänchen et al. 2006, Kelemen & Matter 2008, O'Connor et al. 2004, Palandri & Kharaka 2004). Unless otherwise noted, experiments are for olivine dissolution. Although olivine dissolution can be rapid at low pH, these conditions do not favor crystallization of solid carbonate minerals. Where experimental rates were determined in units of kg m^{-2} s^{-1} or mol m^{-2} s^{-1}, they have been transformed into weight fraction per second using appropriate molecular weights, densities, and the surface areas of spheres with a diameter of 70 μm. In general, rates were calculated for reaction at pH 8. The choice of a 70-μm grain size and pH 8 was dictated by the desire to compare other data with those of O'Connor et al. (2004) and Chizmeshya et al. (2007), who did not determine surface area and/or pH dependency in their experimental studies of olivine carbonation rates. (*Bottom*) Mineral and rock dissolution rates and carbonation rates (data sources as for top panel, plus Carroll & Knauss 2005, Gislason & Oelkers 2003, Schaef & McGrail 2009). As for top panel, rates were calculated at pH 8. All data are for dissolution rates in aqueous fluid, unless the legend notes that experiments included carbonation. As for top panel, dissolution rates are rapid at low pH, but carbonate minerals are less stable in these conditions. "Fo" followed by a number refers to the molar percentage of the forsterite end-member in the mineral olivine, which is a solid solution between forsterite (Mg_2SiO_4) (Fo) and fayalite (Fe_2SiO_4) (Fa).
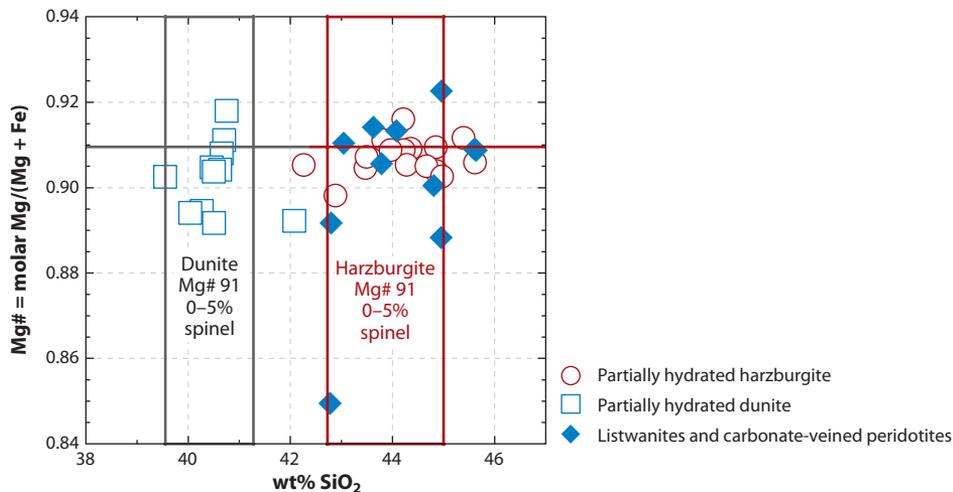
Figure 6

Bulk compositions of our listwanite and partially carbonated peridotite samples, compared with those of
typical Oman peridotites from Hanghøj et al. (2010). To filter out samples containing abundant, massive
carbonate veins, we eliminated those with more than 35 wt% $H_2O + CO_2$ ("loss on ignition") and with
molar $Ca/(Ca + Mg + Fe)$ greater than 0.1.

layers between unreacted mineral reactants and fluid (e.g., Aharonov et al. 1998, Milsch et al.
2009, Morrow et al. 2001, Tenthorey et al. 1998). Decreasing permeability with reaction progress
is commonly observed for hydration and carbonation of basalt (Alt & Teagle 1999, Bartetzko
2005, Becker & Davis 2003, Schramm et al. 2005). On shorter timescales and distance scales,
experimental dissolution and carbonation of olivine commonly show a rate decrease with time
(**Supplemental Figure S4**). This arises, at least in part, from formation of a "passivating layer"
of amorphous SiO_2 on olivine surfaces, after which reaction is limited by diffusion through this
solid layer (e.g., Chizmeshya et al. 2007).

Supplemental Material

Alternatively, precipitation of minerals in pore space can fracture rocks, maintaining perme-
ability and exposing fresh mineral surfaces. For example, salts crystallizing from water in limestone
and other building materials can fracture these materials, even while the fluid volume is decreas-
ing. [See the extensive literature on salt weathering, recently reviewed by Scherer 1999, 2004
and Steiger 2005a,b; also see the image at **http://web.mac.com/gwscherer1/SchererGroup/
Salt_Crystallization.html.**] Frost heaves and frost cracking are related phenomena (e.g., Walder
& Hallet 1985). Similarly, reaction between fluids and minerals that consume both solid and
fluid components but increase the solid volume, such as hydration of solid lime (CaO) to pro-
duce portlandite [$Ca(OH)_2$], can cause polycrystalline rocks to fracture (G.W. Scherer, personal
communication, 2009; also see the image at **http://web.mac.com/gwscherer1/SchererGroup/
Slaking_lime.html**). This process is analogous to peridotite hydration and carbonation.

Numerous studies, beginning with Correns (Correns 1949, Correns & Steinborn 1939),
demonstrated that crystal growth from a fluid in pore space, driven by surface energy and diffusion
of components in a nanofilm along the contact between a growing crystal and its host, leads to
local stresses in excess of the confining pressure, proportional to the extent of supersaturation of
the growing mineral. In the simplest formulation, the force of crystallization or crystallization
pressure is given by

$$\Delta P = RT / V_m \ln(c / c^0), \tag{3}$$

where R is the gas constant, T is the temperature in Kelvin, V_m is the molar volume of the growing crystalline phase, c is the concentration of a solute, and c^0 is the equilibrium concentration at which fluid is saturated in the growing crystalline phase. Steiger (2005a) notes that the formulation using c/c^0 is correct only for ideal solutions in which the crystal forms from a single fluid component. Given that the reaction quotient, Q, is the product of activities of reactants divided by the product of activities of products, whereas the equilibrium constant, K, is the reaction quotient for a system in equilibrium, c/c^0 should be replaced with the reaction quotient divided by the equilibrium constant. The ratio Q/K is the saturation state, Ω, so the new equation is

$$\Delta P = RT/V_m \ln(\Omega). \qquad (4)$$

Steiger (2005a) calculates overpressures of hundreds of bars to kilobars for crystallization of supersaturated NaCl in pore space. For magnesite crystallization, Ω is defined by

$$\Omega = (a_{Mg++} a_{CO3-})/K_{MgCO3}. \qquad (5)$$

Recent studies of (notoriously sluggish) magnesite crystallization kinetics (Hänchen et al. 2008, Saldi et al. 2009) found that $(a_{Mg++} a_{CO3-})/K_{MgCO3}$ can reach 100 or more at temperatures up to 120°C, yielding crystallization pressures up to 5 kbar, which is more than sufficient to fracture crustal rocks.

Because we often work with samples for which we do not know the saturation state of metamorphic fluids, the ability to estimate crystallization pressures without knowing the fluid composition would be useful. Because the standard-state free energy for a given reaction is $\Delta G^0 = -RT \ln(K)$, the free energy change for a reaction can be expressed as

$$\Delta G = -RT \ln(K) + RT \ln(Q) = RT \ln(\Omega), \qquad (6)$$

so ΔP is now given by

$$\Delta P = \Delta G/\Delta V_s, \qquad (7)$$

where ΔV_s is the solid volume change due to reaction, per mole of solid products. Equations 3–7 were developed for crystallization of a solid phase that forms entirely from solutes in fluid. For fluid-rock reactions involving dissolution of a solid reactant as well as crystallization of solid products, the volume used in the denominator of Equation 7 should probably be ΔV_s, as written, rather than the molar volume of the crystallizing phase(s).

Olivine is far from equilibrium with CO_2-rich fluids at shallow crustal conditions. If we ignore olivine dissolution kinetics for the moment, when a CO_2-rich fluid first comes into contact with olivine, there is a chemical potential driving the reaction to form magnesite + quartz, which is the free energy change of Reaction 1c. Using this free energy in Equation 7 provides an upper bound on the crystallization pressure, illustrated in **Figure 7**. In practice, slow olivine dissolution coupled with magnesite + quartz precipitation limits the saturation state, the free energy of magnesite + quartz crystallization from fluid, and the crystallization pressure to lower values. Nonetheless, these simple calculations show that there is more than enough energy, expressed as free energy/volume or pressure, to fracture rocks when olivine reacts with CO_2-rich fluids.

Reaction-driven cracking may be most likely during rapid crystallization because increasing stress in the host rock competes with slow relaxation mechanisms such as dislocation creep within growing crystals. For example, in experiments on crystallization of Na-sulfate salts in porous limestone, rapid crystallization caused fractures, whereas slow crystallization did not (Espinosa Marzal & Scherer 2008). The stress required to fracture the unconfined limestone blocks at atmospheric pressure is ~1 MPa. Salts have low viscosity (e.g., Spiers et al. 1990), and 1-MPa stresses relax in microseconds to minutes for 1–100-μm salt crystals. Thus, increasing stress due
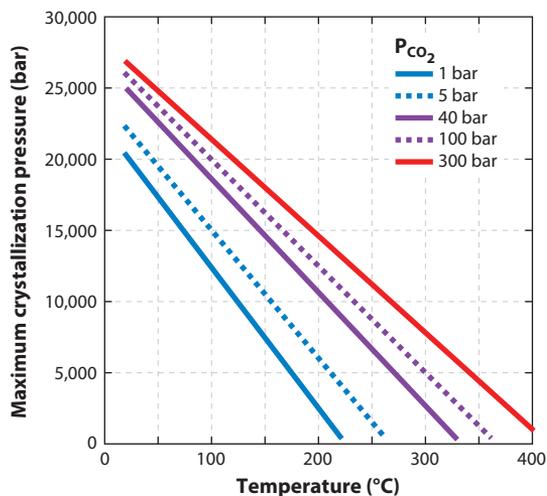
Figure 7

Maximum possible crystallization pressures, $\Delta G/\Delta V_s$, for the complete reaction of forsterite $+ CO_2 =$ magnesite $+$ quartz in the system MgO-SiO_2-CO_2, as a function of temperature and pressure, ignoring the rates of olivine dissolution and magnesite crystallization. In practice, slow olivine dissolution, coupled with magnesite $+$ quartz precipitation, limits the extent of fluid oversaturation in magnesite and quartz and thus limits crystallization pressures to lower values.

to salt crystallization in pore space had to take place in seconds to minutes to produce fracture rather than viscous flow of salt. Unfortunately, the steady-state viscosity of carbonate minerals at low temperature is not known (Liteanu & Spiers 2009), so we cannot quantify viscous relaxation times for carbonate growth in peridotite pore space.

In addition to being likely during rapid crystallization, reaction-driven cracking may also be favored when fluid flow takes place periodically, as may be common in arid areas subject to occasionally heavy rainfall. As noted by Scherer (2004), rapid evaporation of isolated fluid pockets in pore space drives increasing solute concentrations and potentially extreme supersaturation. This, in turn, could produce very high pressures of crystallization.

4.3. Reaction-Driven Cracking in Natural Olivine Hydration and Carbonation

The idea of reaction-driven cracking has been applied, qualitatively, to olivine hydration. MacDonald & Fyfe (1985) proposed that increasing solid volume during olivine hydration produces stresses that fracture surrounding rock. This was further investigated and quantified for serpentinization (e.g., Andreani et al. 2007; Evans 2004; Iyer et al. 2008; Jamtveit et al. 2008, 2009; O'Hanley 1992; Royne et al. 2009; Shervais et al. 2005), olivine carbonation (Rudge et al. 2010), and granite weathering (Fletcher et al. 2006). Evans (2004) and Jamtveit et al. (2008) emphasize textural evidence for reaction-driven cracking, in which partial serpentinization of olivine has shattered surrounding plagioclase crystals.

Conversely, peridotite hydration may reduce permeability and limit serpentinization (Cipolli et al. 2004, Lowell & Rona 2002). Martin & Fyfe (1970) observed experimental serpentinization rates decreasing with time, which they attributed to armoring of olivine surfaces with serpentine reaction products. Emmanuel & Berkowitz (2006) modeled this process. Similarly, the models of Xu et al. (2004) assumed that olivine carbonation gradually filled pore space and reduced permeability. O'Connor et al. (2004) observed a $\sim3\times$ decrease in the rate between 26% and

93% olivine carbonation (**Supplemental Figure S4**), and Chizmeshya et al. (2007) observed a "passivating," SiO_2-rich reaction rim on olivine surfaces, formed during dissolution coupled with crystallization of magnesite + quartz.

Extensive outcrops of serpentinite indicate that olivine hydration is not always self-limiting. The ubiquitous presence of dense fracture networks that host serpentine veins in partially serpentinized peridotite, with ~10-μm spacing, lends credence to the idea that serpentinization and cracking are coeval. Without the presence of serpentine "glue" along these fracture networks, the host would be a powder rather than a rock. Furthermore, it is common to observe several generations of cross-cutting serpentine veins, which indicate repeated cycles of fracturing followed by hydration. However, fracture filling by reaction products ultimately may have limited reaction progress, where we observe partially serpentinized rocks.

Similarly, the presence of extensive outcrops of listwanite demonstrates that peridotite carbonation is not always self-limiting. Listwanites have brecciated textures in outcrop and dense, hierarchical fracture networks extending to microscopic scales, filled by synkinematic carbonate and quartz veins (**Figure 8**). Outcrop scale and microscopic relationships in partially carbonated peridotites indicate coeval carbonate crystallization and fracture. Also, geochronological data
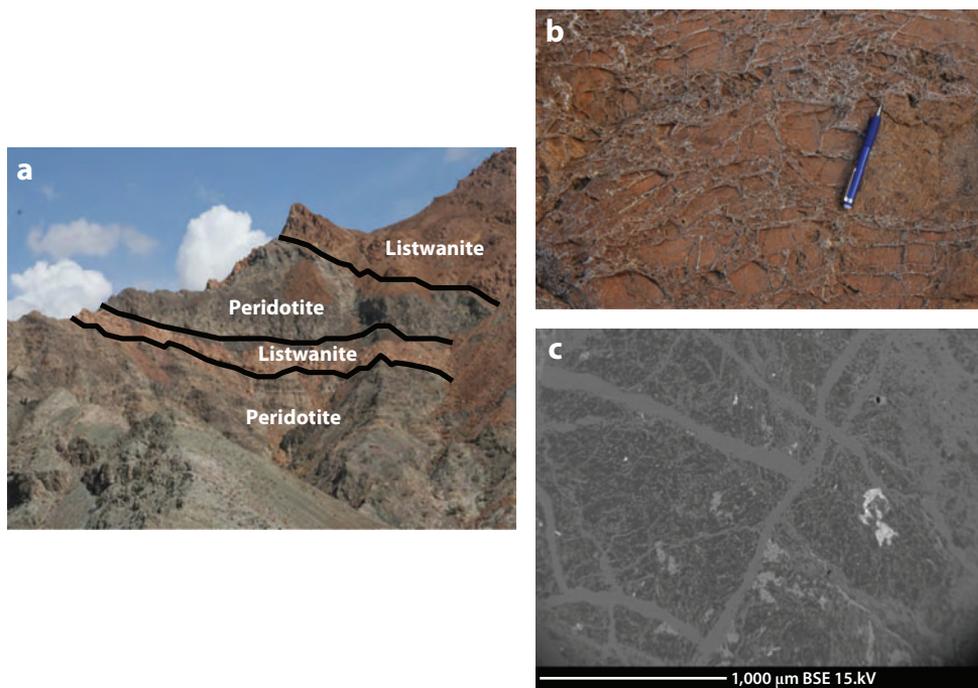

Figure 8

Outcrop and thin-section scale photographs of listwanites replacing peridotite in the ophiolite massifs of northern Oman. (*a*) Gently eastward-dipping listwanite band ~10 m in true thickness, approximately parallel to banding in partially serpentinized peridotite, and overlying, thicker band of listwanite along ridge in Oman at approximately 23.37°N, 58.19°E. This area is structurally just a few hundred meters from the basal thrust, juxtaposing peridotite with ophiolitic mélange and underlying sedimentary conglomerates in this region. [P.B. Kelemen photo, field of view (fov) 500 m.] (*b*) Typical quartz vein texture in listwanite talus block, same location. (P.B. Kelemen photo, fov 0.5 m.) (*c*) Backscattered electron (BSE) image of listwanite from same location. Dark gray indicates magnesite, light gray indicates quartz, and white indicates relict chromian spinel. (E. Streit photo, fov 0.0025 m.)

(^{14}C, U-series) show that permeability is maintained over tens of thousands of years in water-peridotite systems undergoing carbonation and serpentinization, both in Oman (Kelemen & Matter 2008) and in the Lost City hydrothermal vent field along the Mid-Atlantic Ridge (Früh-Green et al. 2003, Ludwig et al. 2006).

Carbonate veins in Oman peridotites commonly occur in three mutually perpendicular vein sets (**Figure 9** and **Supplemental Section S11**), suggesting that they formed in a nearly isotropic stress regime and not because of tectonic compression or extension. Nearly horizontal fractures roughly parallel to the paleooutcrop surface predate a second set of nearly vertical fractures perpendicular to the outcrop surface (**Figure 9**). This is consistent with models in which volume expansion in a diffusive reaction zone drives fracture parallel to the weathering surface and is followed by buckling of the detached, weathered layer and subsequent cracking perpendicular to the weathering surface (Fletcher et al. 2006, Rudge et al. 2010).

Rudge et al. (2010) predict that propagation of a cracking front associated with peridotite hydration and carbonation is a function of the reaction rate and the reactant transport velocity in pore space. On the basis of this work, we estimate that reaction at elevated temperature and P_{CO_2}, with approximately 1% initial fracture porosity and fluid flow velocities of ~0.01 m s^{-1}, can drive propagation of a cracking front at velocities of meters per day (**Figure 10**). However, the formulation of Rudge et al. (2010) is calibrated only to the average erosion rates estimated from thermochronology of samples (from lithologies other than peridotite) in the Oman mountains (Poupeau et al. 1998).

Finally, as pointed out by Cipolli et al. (2004) and Hansen et al. (2005), partial carbonation of serpentine rather than olivine, via Reactions 1e and 1f, does not involve a large change in the solid volume, yet it consumes substantial quantities of CO_2. Thus, this process might not have a large effect on porosity and permeability. However, it involves a small enthalpy change, so potential positive feedbacks due to exothermic heat production are not important. Also, serpentine carbonation—without expensive heat treatment to ~600°C prior to reaction—is more than 10 times slower than olivine carbonation under similar conditions of temperature, fluid composition, and P_{CO_2} (e.g., Gerdemann et al. 2007, O'Connor et al. 2004).

## 5. ENGINEERED, IN SITU PERIDOTITE CARBONATION FOR CO$_2$ CAPTURE AND STORAGE

Kinetic data summarized in Section 3 show conversions from olivine to magnesite + quartz (Reaction 1c) of ~50% per hour. However, even at these rapid conversion rates, the cost of ex situ olivine or serpentine carbonation—quarrying peridotite, transporting it to a concentrated source of CO$_2$ such as a fossil fuel–burning power plant, grinding it to ~70 μm in size, and reacting it with fluids at high P_{CO_2} and high temperature—may not be low enough for industrial implementation, although development work continues (Mazzotti et al. 2005).

As an alternative, Schuiling & Krijgsman (2006) proposed avoiding the cost of high-pressure, high-temperature reaction vessels via spreading fine-grained olivine powder over agricultural and forest land or along beaches. The efficacy of this method has been questioned on energetic and environmental grounds (Hangx & Spiers 2009).

Another alternative is in situ carbonation of olivine, in which CO$_2$-rich fluid is transported to areas where large volumes of peridotite are present near the surface (Cipolli et al. 2004, Guthrie et al. 2001, Hansen et al. 2005, Kelemen & Matter 2008, Kelemen et al. 2008, Marini 2007, Matter & Kelemen 2009, Schuiling 2006, Xu et al. 2004). Kelemen & Matter (2008) suggested two end-member methods for rapid, cost-effective peridotite carbonation for CO$_2$ storage:

■/— Most abundant group of planes with similar orientations
■/— Second-most abundant group of planes with similar orientations
■/— Measured planes not otherwise classified

Relative probability
<1   >2   >4   >6
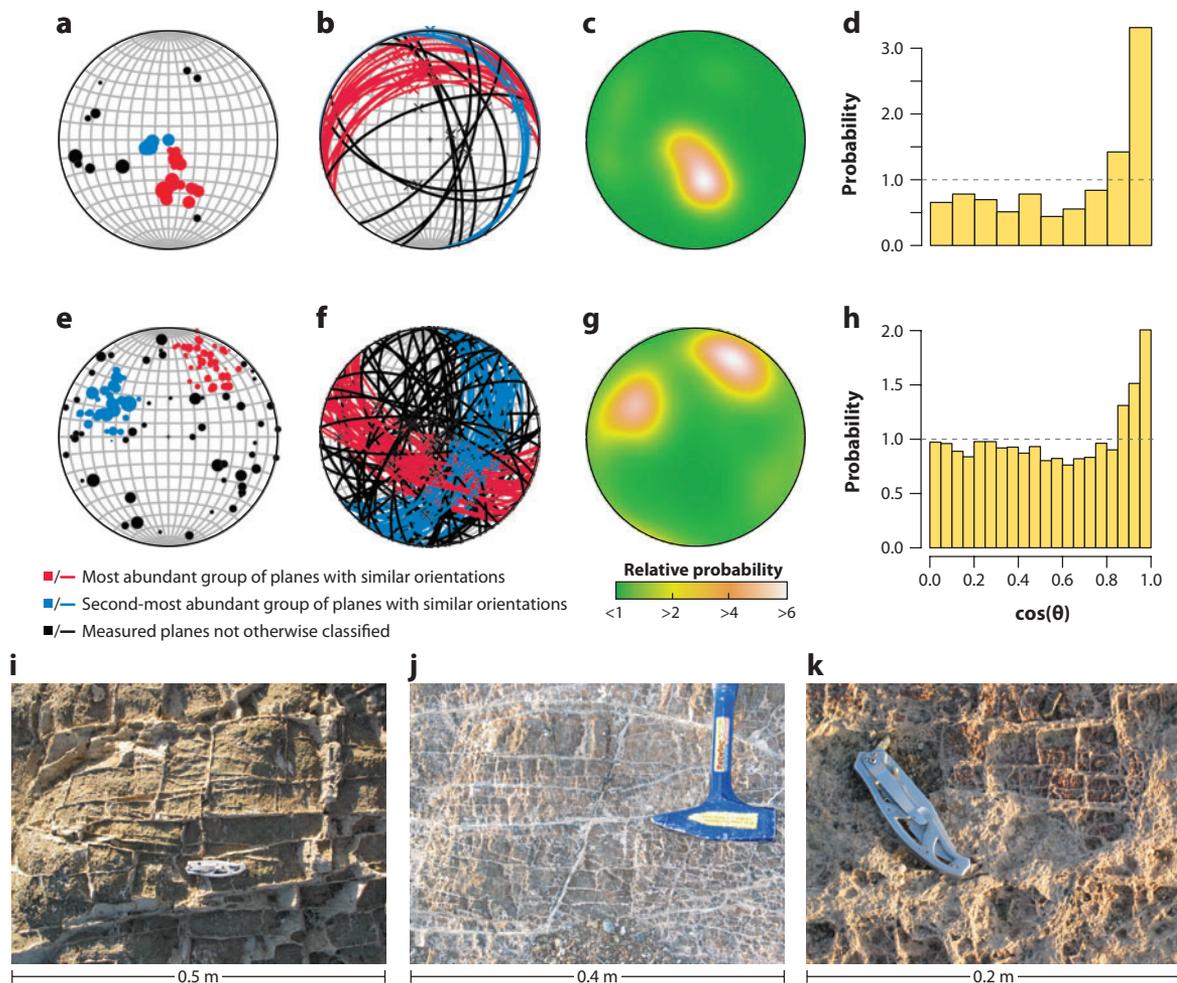
Figure 9

(*a–b*) Stereoplots and histograms: orientations of tabular carbonate veins in peridotite near a large travertine deposit in northern Oman, at approximately 21.86°N, 57.51°E. Panels *a–d* are for measurements of vein orientations measured on nearly vertical outcrop surfaces; panels *e–h* are for vein orientations measured on a nearly horizontal outcrop surface nearby. Red symbols and lines are for all planes that have poles within 25° of the density maximum. Blue symbols and lines are for all planes that have poles within the second density maximum, after the data with red symbols have been removed from the data set. (*a,e*) Poles to planes, projected on a lower-hemisphere stereonet. (*b,f*) Planes projected on a lower-hemisphere stereonet. (*c,g*) Contoured density of poles using a von Mises kernel with κ = 10, projected on a lower-hemisphere stereonet. Relative probabilities are <1 for the green region, more than 2 for the yellow region, more than 4 for the brown region, and more than 6 for the white region. (*d,h*) Histograms of intersection angles; 90° intersections are the best-represented group in both data sets. There are few intersections of steeply dipping veins with the steep outcrop surfaces of panels *a–d* and few intersections of nearly horizontal veins with the subhorizontal surfaces of panels *e–h*. If the two data sets were equal in size, one could combine them to produce a statistical representation of the three mutually orthogonal vein sets that constitute a majority of the carbonate veins in this area. (*i–k*) Outcrop-scale, hierarchical networks of carbonate veins in peridotite near a large travertine deposit in northern Oman, at approximately 21.86°N, 57.51°E (as for data in stereoplots and histograms). Photographs of nearly vertical outcrop surfaces on small canyon walls, showing progressively smaller and more closely spaced carbonate veins from left to right. Thin sections from panels *i* and *j* show sharp-sided carbonate veins in a partially serpentinized peridotite host containing little or no carbonate and 20–40% fresh olivine. In bottom half of panel *k*, peridotite is 100% replaced by carbonate. Note orthogonal vein intersections, and the fact that subhorizontal veins are larger than subvertical veins. The subhorizontal fractures that host veins formed mainly before the subvertical fractures that host veins because the steep fractures commonly terminate where they intersect with the nearly horizontal fractures.
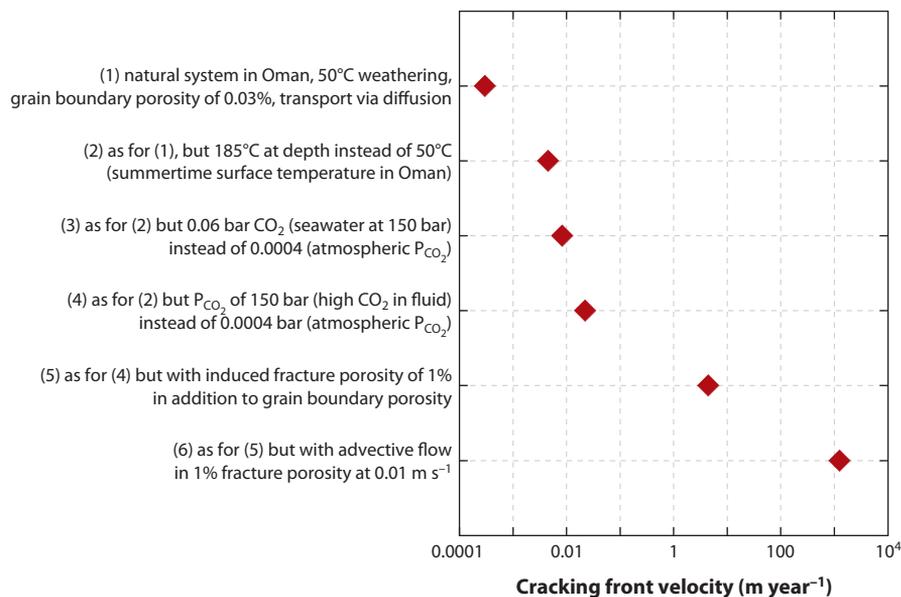
Figure 10

Rate of propagation of a reaction-driven fracture network due to increasing solid volume during peridotite carbonation, calculated using the formulation of Rudge et al. (2010).

- Method 1: A rock volume at depth is raised to the optimal temperature for olivine carbonation (~185°C), hydraulically fractured, and injected with fluids (with added $NaHCO_3$ if necessary) that are equilibrated with CO_2 at ~100 bar.
- Method 2: A high-temperature rock volume at depth is hydraulically fractured to induce thermal convection of seawater through peridotite.

5.1. Method 1: Injection of High-P_{CO_2} Aqueous Fluid into Preheated Peridotite for CO_2 Storage

Assuming that the surface-area-to-volume relationship for 70-μm particles in kinetic experiments can be approximated as it is for spheres or cubes, scaling to a grain size or crack spacing of ~0.7 m (surface area per unit volume 10^{-4} times that for 70-μm grains) yields olivine carbonation rates of ~50% per year in reaction with bicarbonate-rich aqueous solutions at 185°C and 150 bar P_{CO_2} (Kelemen & Matter 2008). Given an olivine density of ~3.3 tons per cubic meter and consumption of 0.62 tons of CO_2 per ton of olivine reactant, 50% carbonation of olivine corresponds to solidification of ~1 ton of CO_2 per cubic meter per year. At this rate, a cubic meter of olivine (~3.3 tons) would be converted to magnesite + quartz in two years, consuming two tons of CO_2. As shown by Kelemen & Matter (2008), such reaction rates are fast enough that heat evolved via the exothermic carbonation reaction offsets cooling due to injection of cold fluid and to diffusion into colder, surrounding rocks. Thus, energy may be required to raise a target rock volume to 185°C, but afterward this optimal temperature can be maintained by balancing the fluid flow rate with the exothermic heat output from carbonation and hydration reactions.

Compared with ex situ mineral carbonation, Method 1 avoids the cost of quarrying and transporting peridotite, grinding it, and reacting it with fluid at elevated temperature and P_{CO_2} in a pressure vessel. For a site used to store millions to billions of tons, the cost of initial

hydrofracture per ton of CO_2 could be small, and reaction-driven cracking might maintain permeability and reactive surface area. However, Method 1 adds the cost of preheating rock to ~185°C. An estimation of this cost is provided in **Supplemental Section S12**. If heating is done using oil, at \$80 per barrel (i.e., ~\$0.50 per kilogram of fuel), heating would cost \$8 to \$41 per ton of CO_2 stored. This would be an added cost compared with that of industrial CO_2 capture coupled with injection into subsurface pore space. If one reacting rock volume can heat an adjacent volume by diffusion, then the heating costs for that adjacent volume could be substantially smaller.

5.2. Method 2: Enhanced Convection of Seawater Through Peridotite for CO_2 Capture and Storage

Continued increases in atmospheric CO_2 [at and above predicted rates (e.g., online updates by the Global Carbon Project to Raupach et al. 2007)], together with slow progress on limiting or mitigating CO_2 emissions in the future, render it likely that atmospheric CO_2 will reach 500 ppmv or more. This may be too high to sustain an acceptable standard of living. Thus, "negative CO_2 emissions" may become necessary. Such negative emissions cannot be attained by carbon capture at fossil fuel power plants, which at best can only approach zero emissions.

Induced convection of seawater through peridotite, Method 2, offers an in situ alternative that achieves negative emissions and avoids the cost of industrial CO_2 capture and transport, as well as the cost of manufacturing or processing reagents. Use of seawater rather than purified CO_2 would also mitigate health risks associated with possible CO_2 leaks. Reaction with peridotite would remove almost all dissolved carbon from the water, as in natural hydrothermal systems (**Figure 11**). CO_2-depleted water would return to the sea surface via production wells. Once at the surface or near surface, the CO_2-depleted, slightly alkaline water would mix with ambient seawater and depress the seawater's near-surface partial pressure of CO_2. This enhanced air-sea
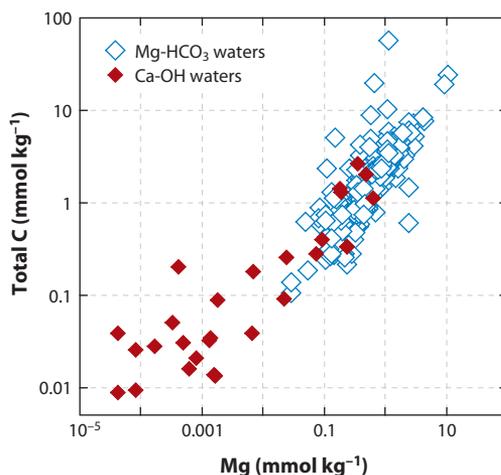
Figure 11

Mg and C concentrations in Mg-HCO$_3$ fluids (surface water, groundwater) and Ca-OH fluids (alkaline spring waters) from peridotite-hosted aquifers. Reaction progress is from upper right to lower left, as reaction between Mg-HCO$_3$ fluids and peridotite forms Mg-carbonate minerals and serpentine plus Mg- and C-depleted Ca-OH waters. Data from Barnes & O'Neil (1969), Barnes et al. (1978), Bruni et al. (2002), Launay & Fontes (1985), Matter et al. (2006), Neal & Stanger (1985), O'Neil & Barnes (1971), Weyhenmeyer (2000), and L. Marini (personal communication, 2009).

gradient of CO_2 partial pressure would draw down atmospheric CO_2, with a time constant of approximately one year (W. Broecker, personal communication, 2009).

The method is simple: Drill holes, create a network of hydraulic fractures, and induce thermal convection of seawater from the resulting holes and fracture network through peridotite and back to the sea surface, or at least to the shallow seafloor. Pumping seawater would be costly, per kilogram of CO_2 consumed, because seawater has a total carbon concentration—expressed as CO_2—of ~100 ppm by weight, so it is necessary to rely on thermal convection as much as possible. Regions with high heat flow would be ideal. Offshore drilling is approximately 10 times more costly than on land, but there are advantages to offshore CO_2 storage of any kind (e.g., Schrag 2007). Thus, it would be best to drill inclined holes from a shore-based platform into peridotite beneath adjacent, shallow seafloor. Electric power generation as a by-product seems possible because the convection cycle we invoke is essentially a geothermal power system. In fact, because it is undesirable to return geothermally heated water to the environment, use of excess heat to generate electricity might be necessary even if it is not profitable for the power generation alone.

Unlike injection of CO_2-rich fluid, CO_2 uptake via injection of seawater into peridotite would be limited by CO_2 supply to a given volume of peridotite rather than by the reaction rate, regardless of temperature, as shown in **Supplemental Section S14**. In turn, the CO_2 supply rate is limited by the permeability of fractured peridotite (**Supplemental Section S15**) or by the maximum practical flow rate in drill pipe. In the latter case, an average flow velocity of ≤ 20 m s^{-1} in a 13-inch (17-cm) pipe yields a seawater flux of ≤ 2 m^3 s^{-1}. Thus, such a system might consume up to 6,000 tons of CO_2 per year per drill hole. Maximum fluid velocities attained so far in enhanced geothermal systems that are sited in crystalline rocks are only ~0.3 m s^{-1}, with a tenfold improvement projected over the next decade (e.g., Genter et al. 2010). A flow velocity of 3.5 m s^{-1} would result in consumption of 1,000 tons of CO_2 per year per drill hole.

Although cooling due to injection of fluid would no longer be balanced by exothermic heat production, because of slower olivine carbonation rates, low fluid fluxes would yield very slow cooling of the reacting volume, and in any case the reaction rate would not limit CO_2 uptake, even at low temperature. As a result of slow reaction rates, filling of pore space and armoring of reactive surfaces might be a relatively small problem for Method 2 compared with Method 1.

Because it would involve only drilling and hydrofracture (no preheating of rock volume, no CO_2 transport, no industrial CO_2 capture, and no pumping of fluid), and because it would be combined with geothermal power generation, this process might be less costly than in situ carbonation using purified CO_2—and possibly even less costly than injection of supercritical CO_2 into underground pore space. If the net cost to engineer and maintain a system consuming ~1,000 tons of CO_2 per year for 10 years, minus the revenues from geothermal power generation, were \$100,000 to \$1 million, this would correspond to a cost of ~\$10 to \$100 per ton of CO_2. This is a total cost, for comparison with the combined cost of industrial CO_2 capture, transport, and storage. Because individual drill holes can transport only a fixed amount of water, scaling up this process simply requires more holes. Consuming one billion tons of CO_2 per year would require one million drill holes of this type, equivalent to the current number of producing oil and gas wells in the United States (**http://img36.imageshack.us/img36/9106/oilgasmaplg.jpg**).

6. FROM OBSERVATIONS TO SOLUTIONS

Enhanced, in situ carbonation of olivine in peridotite shows theoretical promise as a method of CO_2 storage and for CO_2 capture from seawater. It may be possible to capitalize on the exothermic nature of olivine carbonation to reach a positive feedback regime that maintains high temperatures

and reaction rates in selected rock volumes at depth, and to harness the large increase in solid volume to access a regime in which stress increase due to expansion forms fractures, maintaining permeability and reactive surface area for relatively long periods of time. The presence of naturally formed, fully carbonated peridotite deposits (listwanites) attests to the fact that peridotite carbonation can continue to completion. Furthermore, documented cases of ongoing peridotite carbonation demonstrate that such processes can continue for tens of thousands of years.

That said, the physical and chemical regimes required to sustain rapid reaction rates and sufficient fluid flow are not well constrained. Rapid fluid flow can cool rock volumes and thus "quench" reaction rates. Precipitation of carbonate minerals in pore space can reduce permeability and/or armor reactive surfaces. The presence of partially carbonated peridotites, typically composed of carbonate veins that cut blocks of partially hydrated, partially fresh peridotite, may provide examples of self-limiting carbonation processes.

Thus, continued research—via field studies of natural systems, laboratory experiments, and pilot experiments in drill holes—should focus on delineating the parameter ranges that define both positive and negative feedback regimes for peridotite carbonation. Reaction-driven cracking is of particular importance. At this stage, numerous approximations and extrapolations are needed to make more accurate, quantitative predictions of fracture formation or propagation rates. If a rock volume undergoing olivine carbonation enters the self-cracking regime, then the potential costs of repeated hydraulic fracture for in situ carbonation, or of grinding solid reactants for ex situ carbonation, can be avoided.

Finally, injection of seawater rather than CO_2-rich fluids avoids the cost of industrial CO_2 capture and provides a method for negative CO_2 emissions. The process may be so much less expensive than injection of CO_2-rich fluids that other drawbacks are minor.

DISCLOSURE STATEMENT

P.B. Kelemen and J. Matter have a provisional patent filing on the methods for CO_2 capture and storage via mineral carbonation that are described in their 2008 paper in the *Proceedings of the National Academy of Sciences*. Other than that, the authors are not aware of any affiliations, memberships, funding, or financial holdings that might be perceived as affecting the objectivity of this review.

LITERATURE CITED[1]

Abart R, Pozzorini D. 2000. Implications of kinetically controlled mineral-fluid exchange on the geometry of stable-isotope fronts. *Eur. J. Mineral.* 12:1069–82

Agrinier P, Cornen G, Beslier M-O. 1996. Mineralogical and oxygen isotopic features of serpentinites recovered from the ocean/continent transition in the Iberia abyssal plain. In *Proceedings of the Ocean Drilling Program*, *Scientific Results*, Vol. 149, ed. RB Whitmarsh, DS Sawyer, A Klaus, DG Masson, pp. 541–52. College Station, TX: Ocean Drill. Program

Agrinier P, Mével C, Girardeau J. 1988. Hydrothermal alteration of the peridotites cored at the ocean/continent boundary of the Iberian margin: petrologic and stable isotope evidence. In *Proceedings of the Ocean Drilling Program*, *Scientific Results*, Vol. 103, ed. G Boillot, EL Winterer, pp. 225–34. College Station, TX: Ocean Drill. Program

Aharonov E, Tenthorey E, Scholz CH. 1998. Precipitation sealing and diagenesis: 2. Theoretical analysis. *J. Geophys. Res.* 103(B10):23969–81

[1]Also see additional references in the electronic supplement. View the supplement by following the **Supplemental Materials link** on the Annual Reviews home page at **http://www.annualreviews.org**.

Allen DE, Seyfried WE Jr. 2004. Serpentinization and heat generation: constraints from Lost City and Rainbow hydrothermal systems. *Geochim. Cosmochim. Acta* 68:1347–54

Alt JC, Teagle DAH. 1999. The uptake of carbon during alteration of oceanic crust. *Geochim. Cosmochim. Acta* 63:1527–35

Andreani M, Luquot L, Gouze P, Godard M, Hoisé E, Gibert B. 2009. Experimental study of carbon sequestration reactions controlled by the percolation of CO_2-rich brine through peridotites. *Environ. Sci. Technol.* 43:1226–31

Andreani M, Mével C, Boullier A-M, Escartin J. 2007. Dynamic control on serpentine crystallization process in veins: constraints on hydration processes in oceanic peridotites. *Geochem. Geophys. Geosyst.* 8:Q02012

Augustin N, Lackschewitz KS, Kuhn T, Devey CW. 2008. Mineralogical and chemical mass changes in mafic and ultramafic rocks from the Logatchev hydrothermal field (MAR 15°N). *Mar. Geol.* 256:18–29

Barbieri M, Masi U, Tolomeo L. 1979. Stable isotope evidence for a marine origin of ophicalcites from the north-central Apennines (Italy). *Mar. Geol.* 30:193–204

Barnes I, LaMarche VC, Himmelberg G. 1967. Geochemical evidence of present-day serpentinization. *Science* 156:830–32

Barnes I, O'Neil JR. 1969. Relationship between fluids in some fresh alpine-type ultramafics and possible modern serpentinization, western United States. *Geol. Soc. Am. Bull.* 80:1947–60

Barnes I, O'Neil JR, Rapp JB, White DE. 1973. Silica-carbonate alteration of serpentine: wall rock alteration in mercury deposits of the California Coast Ranges. *Econ. Geol.* 68:388–98

Barnes I, O'Neil JR, Trescases JJ. 1978. Present-day serpentinization in New Caledonia, Oman and Yugoslavia. *Geochim. Cosmochim. Acta* 42:144–45

Bartetzko A. 2005. Effect of hydrothermal ridge flank alteration on the in situ physical properties of oceanic crust. *J. Geophys. Res.* 110:B06203

Beard JS, Frost BR, Fryer P, McCaig A, Searle R, et al. 2009. Onset and progression of serpentinization and magnetite formation in olivine-rich troctolite from IODP Hole U1309D. *J. Petrol.* 50:387–403

Becker K, Davis E. 2003. New evidence for age variation and scale effects of permeabilities of young oceanic crust from borehole thermal and pressure measurements. *Earth Planet. Sci. Lett.* 210:499–508

Berndt ME, Allen DE, Seyfried WE Jr. 1996. Reduction of CO_2 during serpentinization of olivine at 300°C and 500 bar. *Geology* 24:351–54

Blank JG, Green SJ, Blake D, Valley JW, Kita NT, et al. 2009. An alkaline spring system within the Del Puerto ophiolite (California, USA): a Mars analog site. *Planet. Space Sci.* 57:533–40

Bonatti E, Lawrence JR, Hamlyn PR, Breger D. 1980. Aragonite from deep sea ultramafic rocks. *Geochim. Cosmochim. Acta* 44:1207–14

Bosch D, Jamais M, Boudier F, Nicolas A, Dautria JM, Agrinier P. 2004. Deep and high-temperature hydrothermal circulation in the Oman ophiolite—petrological and isotopic evidence. *J. Petrol.* 45:1181–208

Boudier F, Baronnet A, Mainprice D. 2010. Serpentine mineral replacements of natural olivine and their seismic implications: oceanic lizardite versus subduction-related antigorite. *J. Petrol.* 51:495–512

Bruni J, Canepa M, Chiodini G, Cioni R, Cipolli F, et al. 2002. Irreversible water-rock mass transfer accompanying the generation of the neutral, $Mg-HCO_3$ and high-pH, Ca-OH spring waters of the Genova province, Italy. *Appl. Geochem.* 17:455–74

Cannat M, Mével C, Maïa M, Deplus C, Gente P, et al. 1995. Thin crust, ultramafic exposure and rugged faulting patterns at the Mid-Atlantic Ridge (22°–24°N). *Geology* 23:49–52

Carlson RL. 2001. The abundance of ultramafic rocks in the Atlantic ocean crust. *Geophys. J. Int.* 144:37–48

Carroll SA, Knauss KG. 2005. Dependence of labradorite dissolution kinetics on $CO_{2(aq)}$, $Al_{(aq)}$, and temperature. *Chem. Geol.* 217:213–25

Casey J. 1997. Comparison of major- and trace-element geochemistry of abyssal peridotites and mafic plutonic rocks with basalts from the MARK region of the Mid-Atlantic Ridge. In *Proceedings of the Ocean Drilling Program, Scientific Results*, Vol. 153, ed. JA Karson, M Cannat, DJ Miller, D Elthon, pp. 181–241. College Station, TX, Ocean Drill. Program

Chacko T, Deines P. 2008. Theoretical calculation of oxygen isotope fractionation factors in carbonate systems. *Geochim. Cosmochim. Acta* 72:3642–60

Chizmeshya AVG, McKelvy MJ, Squires K, Carpenter RW, Béarat H. 2007. A novel approach to mineral carbonation: enhancing carbonation while avoiding mineral pretreatment process cost. *U.S. Dep. Energy Final Rep. 924162*, Ariz. State Univ., Tempe, Ariz.

Cipolli F, Gambardella B, Marini L, Ottonello G, Zuccolini MV. 2004. Geochemistry of high-pH waters from serpentinites of the Gruppo di Voltri (Genova, Italy) and reaction path modeling of CO_2 sequestration in serpentinite aquifers. *Appl. Geochem.* 19:787–802

Clark ID, Fontes JC. 1990. Paleoclimatic reconstruction in northern Oman based on carbonates from hyper-alkaline groundwaters. *Quat. Res.* 33:320–36

Clark ID, Fontes JC, Fritz P. 1992. Stable isotope disequilibria in travertine from high pH waters: laboratory investigations and field observations from Oman. *Geochim. Cosmochim. Acta* 56:2041–50

Coleman RG, Keith TE. 1971. A chemical study of serpentinization, Burro Mountain, California. *J. Petrol.* 12:311–28

Correns CW. 1949. Growth and dissolution of crystals under linear pressure. *Discuss. Faraday Soc.* 5:267–71

Correns CW, Steinborn W. 1939. Experimente zur Messung und Erklärung der sogenannten Kristallisation-skraft. *Zeit. Krist. A* 101:117–33

Dewandel B, Boudier F, Kern H, Warsi W, Mainprice D. 2003. Seismic wave velocity and anisotropy of serpentinized peridotite in the Oman ophiolite. *Tectonophysics* 370:77–94

Dewandel B, Lachassagne P, Boudier F, Al-Hattali S, Ladouche B, et al. 2005. A conceptual hydrogeological model of ophiolite hard-rock aquifers in Oman based on a multiscale and a multidisciplinary approach. *Hydrogeol. J.* 13:708–26

Eickmann B, Bach W, Rosner M, Peckmann J. 2009. Geochemical constraints on the modes of carbonate precipitation in peridotites from the Logatchev Hydrothermal Vent Field and Gakkel Ridge. *Chem. Geol.* 268:97–106

Eiler J. 2007. "Clumped-isotope" geochemistry: the study of naturally occurring, multiply substituted iso-topologues. *Earth Planet. Sci. Lett.* 262:309–27

Emmanuel S, Berkowitz B. 2006. Suppression and stimulation of seafloor hydrothermal convection by exother-mic mineral hydration. *Earth Planet. Sci. Lett.* 243:657–68

Espinosa Marzal RM, Scherer GW. 2008. Crystallization of sodium sulfate salts in limestone. *Environ. Geol.* 56:605–21

Evans BW. 1977. Metamorphism of alpine peridotite and serpentinite. *Annu. Rev. Earth Planet. Sci.* 5:397–447

Evans BW. 2004. The serpentinite multisystem revisited: Chrysotile is metastable. *Int. Geol. Rev.* 46:479–506

Evans BW. 2008. Control of the products of serpentinization by the $Fe^{2+}Mg_{-1}$ exchange potential of olivine and orthopyroxene. *J. Petrol.* 49:1873–87

Evans CA, Baltuck M. 1988. Low-temperature alteration of peridotite, Hole 637A. In *Proceedings of the Ocean Drilling Program, Scientific Results*, Vol. 103, ed. G Boillot, EL Winterer, pp. 235–39. College Station, TX: Ocean Drill. Program

Fallick AE, Ilich M, Russell MJ. 1991. A stable isotope study of the magnesite deposits associated with the alpine-type ultramafic rocks of Yugoslavia. *Econ. Geol.* 86:847–61

Fletcher RC, Buss HL, Brantley SL. 2006. A spheroidal weathering model coupling porewater chemistry to soil thickness during steady-state denudation. *Earth Planet. Sci. Lett.* 244:444–57

Friedman I, O'Neil JR. 1977. Compilation of stable isotope fractionation factors of geochemical interest. In *USGS Prof. Pap. 440-KK, Data of Geochemistry*, ed. M Fleischer, pp. KK1–12. Reston, VA: U.S. Geol. Surv., 6th ed.

Frost BR. 1985. On the stability of sulfides, oxides, and native metals in serpentinite. *J. Petrol.* 26:31–63

Frost BR, Beard JS. 2007. On silica activity and serpentinization. *J. Petrol.* 48:1351–68

Früh-Green GL, Kelley DS, Bernasconi SM, Karson JA, Ludwig KA, et al. 2003. 30,000 years of hydrothermal activity at the Lost City vent field. *Science* 301:495–98

Früh-Green GL, Weissert H, Bernoulli D. 1990. A multiple fluid history recorded in Alpine ophiolites. *J. Geol. Soc. Lond.* 147:959–70

Früh-Green GL, Connolly JAD, Plas A, Kelley DS, Grobety B. 2004. Serpentinization of oceanic peridotites: implications for geochemical cycles and biological activity. In *The Subseafloor Biosphere at Mid-Ocean Ridges*, ed. WSD Wilcock, EF DeLong, DS Kelley, JA Baross, SC Cary, *Geophys. Monogr.* 144:119–136. Washington, DC: AGU

Fyfe WS. 1974. Heats of chemical reactions and submarine heat production. *Geophys. J. R. Astron. Soc.* 37:213–15

Genter A, Goerke X, Graff, JJ, Cuenot N, Krall G, et al. 2010. Current status of the EGS Soultz geothermal project (France). *Proc. World Geotherm. Cong.*, *Apr. 25–29*, Bali, Indones., pp. 1–6. Reykjavik: Int. Geotherm. Assoc.

Gerdemann SJ, O'Connor WK, Dahlin DC, Penner LR, Rush H. 2007. Ex situ aqueous mineral carbonation. *Environ. Sci. Technol.* 41:2587–93

Ghosh P, Adkins J, Affek H, Balta B, Guo W, et al. 2006. ^{13}C–^{18}O bonds in carbonate minerals: a new kind of paleothermometer. *Geochim. Cosmochim. Acta* 70:1439–56

Gislason SR, Oelkers EH. 2003. Mechanism, rates and consequences of basaltic glass dissolution: II. An experimental study of the dissolution rates of basaltic glass as a function of pH and temperature. *Geochim. Cosmochim. Acta* 67:3817–32

Greenwood HJ. 1967. Mineral equilibria in the system MgO-SiO_2-H_2O-CO_2. In *Researches in Geochemistry II*, ed. PH Abelson, pp. 542–47. New York: John Wiley & Sons

Gregory RT, Taylor HP. 1981. An oxygen isotope profile in a section of Cretaceous oceanic crust, Samail ophiolite, Oman: evidence for $\delta^{18}O$ buffering of the oceans by deep (>5 km) seawater-hydrothermal circulation at mid-ocean ridges. *J. Geophys. Res.* 86:2737–55

Guthrie GD, Carey JW, Bergfeld D, Byer D, Chipera S, et al. 2001. Geochemical aspects of the carbonation of magnesium silicates in an aqueous medium. *Proc. First Natl. Conf. Carbon Sequestration*, *Wash.*, *DC*, pp. 1–14. Washington, DC: U.S. Dep. Energy Natl. Energy Technol. Lab.

Hacker BR. 1994. Rapid emplacement of young oceanic lithosphere: argon geochronology of the Oman ophiolite. *Science* 265:1563–65

Haggerty JA. 1991. Evidence from fluid seeps atop serpentine seamounts in the Mariana Forearc: clues for emplacement of the seamounts and their relationship to forearc tectonics. *Mar. Geol.* 102:293–309

Hänchen M, Prigiobbe V, Baciocchi R, Mazzotti M. 2008. Precipitation in the Mg-carbonate system: effects of temperature and CO_2 pressure. *Chem. Eng. Sci.* 63:1012–28

Hänchen M, Prigiobbe V, Storti G, Seward TM, Mazzotti M. 2006. Dissolution kinetics of fosteritic olivine at 90–150°C including effects of the presence of CO_2. *Geochim. Cosmochim. Acta* 70:4403–16

Hanghøj K, Kelemen PB, Hassler D, Godard M. 2010. Composition and genesis of depleted mantle peridotites from the Wadi Tayin massif, Oman ophiolite: major and trace element geochemistry, and Os isotope and PGE systematics. *J. Petrol.* 51:206–27

Hangx SJT, Spiers CJ. 2009. Coastal spreading of olivine to control atmospheric CO_2 concentrations: a critical analysis of viability. *Int. J. Greenh. Gas Control* 3:757–67

Hansen LD, Dipple GM, Gordon TM, Kellett DA. 2005. Carbonated serpentinite (listwanite) at Atlin, British Columbia: a geological analogue to carbon dioxide sequestration. *Can. Mineral.* 43:225–39

Holland TJB, Powell R. 1998. An internally consistent thermodynamic data set for phases of petrological interest. *J. Metamorph. Geol.* 16:309–43

Horita J, Berndt ME. 1999. Abiotic methane formation and isotopic fractionation under hydrothermal conditions. *Science* 285:1055–57

Iyer K, Jamtveit B, Mathiesen J, Malthe-Sorenssen A, Feder J. 2008. Reaction-assisted hierarchical fracturing during serpentinization. *Earth Planet. Sci. Lett.* 267:503–16

Jamtveit B, Malthe-Sorenssen A, Kostenko O. 2008. Reaction enhanced permeability during retrogressive metamorphism. *Earth Planet. Sci. Lett.* 267:620–27

Jamtveit B, Putnis C, Malthe-Sorenssen A. 2009. Reaction induced fracturing during replacement processes. *Contrib. Mineral. Petrol.* 157:127–33

Janecky DR, Seyfried WE Jr. 1986. Hydrothermal serpentinization of peridotite within the oceanic crust: experimental investigations of mineralogy and major element chemistry. *Geochim. Cosmochim. Acta* 50:1357–78

Johannes W. 1969. An experimental investigation of the system MgO-SiO_2-H_2O-CO_2. *Am. J. Sci.* 267:1083–104

Kelemen PB, Kikawa E, Miller DJ, Natsue A, Bach W, et al. 2004. *Proceedings of the Ocean Drilling Program*, *Initial Reports*, Vol. 209. College Station, TX: Ocean Drill. Program

Kelemen PB, Kikawa E, Miller DJ, Party SS. 2007. Leg 209 summary: Processes in a 20-km-thick conductive boundary layer beneath the Mid-Atlantic Ridge, 14°–16°N. In *Proceedings of the Ocean Drilling Program, Scientific Results*, Vol. 209, ed. PB Kelemen, E Kikawa, DJ Miller, pp. 1–33. College Station, TX: Ocean Drill. Program

Kelemen PB, Matter JM. 2008. In situ carbonation of peridotite for CO_2 storage. *Proc. Natl. Acad. Sci. USA* 105:17295–300

Kelemen PB, Matter JM, Streit E. 2008. Field observations and theoretical studies relevant to enhanced in situ carbonation of peridotite. *Proc. Conf. Accel. Carbonation Environ. Mater. Eng., Oct. 1–3, Rome*, pp. 105–12. Rome: Sapienza Univ.

Kelley DS, Karson JA, Blackman DK, Früh-Green GL, Butterfield DA, et al. 2001. An off-axis hydrothermal vent field near the Mid-Atlantic Ridge at 30°N. *Nature* 412:145–49

Kelley DS, Karson JA, Früh-Green GL, Yoerger DR, Shank TM, et al. 2005. A serpentinite-hosted ecosystem: the Lost City hydrothermal field. *Science* 307:1428–34

Kerrick DM. 1974. Review of metamorphic mixed-volatile (H_2O-CO_2) equilibria. *Am. Mineral.* 59:729–62

Klein F, Bach W. 2009. Fe-Ni-Co-O-S phase relations in peridotite-seawater interactions. *J. Petrol.* 50:37–59

Klein F, Bach W, Jons N, McCollom T, Moskowitz B, Berquo T. 2009. Iron partitioning and hydrogen generation during serpentinization of abyssal peridotites from 15°N on the Mid-Atlantic Ridge. *Geochim. Cosmochim. Acta* 73:6868–93

Krevor SC, Graves CR, Van Gosen BS, McCafferty AE. 2009. Mapping the mineral resource base for mineral carbon-dioxide sequestration in the conterminous United States. *U.S. Geol. Surv. Digit. Data Ser. 414.* **http://pubs.usgs.gov/ds/414/**

Lackner KS, Wendt CH, Butt DP, Joyce EL, Sharp DH. 1995. Carbon dioxide disposal in carbonate minerals. *Energy* 20:1153–70

Lang SQ, Butterfield DA, Schulte MD, Kelley DS, Lilley MD. 2010. Elevated concentrations of formate, acetate and dissolved organic carbon found at the Lost City hydrothermal field. *Geochim. Cosmochim. Acta* 74:941–52

Launay J, Fontes J-C. 1985. Les sources thermales de Prony (Nouvelle-Calédonie) et leurs précipités chimiques: exemple de formation de brucite primaire. *Géol. Fr.* 1:83–100

Leblanc M, Ceuleneer G, Al Azri H, Jedwab J. 1991. Hydrothermal concentration of palladium and platinum in mantle peridotites from the Oman ophiolite. *C.R. Acad. Sci. Ser. II* 312:1007–12

Liteanu E, Spiers CJ. 2009. Influence of pore salt content on compaction creep of calcite aggregates in the presence of supercritical CO_2. *Chem. Geol.* 265:134–47

Lorand JP. 1987. A new occurrence of native iron in a serpentinized mantle peridotite—Maqsad, Sumail massif, Semail ophiolite (southern Oman). *C.R. Acad. Sci. Ser. II* 304:703–6

Lowell RP, Rona PA. 2002. Seafloor hydrothermal systems driven by the serpentinization of peridotite. *Geophys. Res. Lett.* 29(11):1531

Ludwig KA, Kelley DS, Butterfield DA, Nelson BK, Früh-Green G. 2006. Formation and evolution of carbonate chimneys at the Lost City hydrothermal field. *Geochim. Cosmochim. Acta* 70:3625–45

MacDonald AH, Fyfe WS. 1985. Rate of serpentinization in seafloor environments. *Tectonophysics* 116:123–35

Madu BE, Nesbitt BE, Muehlenbachs K. 1990. A mesothermal gold-stibnite-quartz vein occurrence in the Canadian Cordillera. *Econ. Geol.* 85:1260–68

Marini L. 2007. *Geological Sequestration of Carbon Dioxide: Thermodynamics, Kinetics, and Reaction Path Modeling*. Amsterdam: Elsevier. 470 pp.

Martin B, Fyfe WS. 1970. Some experimental and theoretical observations on kinetics of hydration reactions with particular reference to serpentinization. *Chem. Geol.* 6:185–202

Matter JM, Kelemen PB. 2009. Permanent CO_2 storage and mineral carbonation in geologic reservoirs. *Nat. Geosci.* 2:837–41

Matter JM, Waber HN, Loew S, Matter A. 2006. Recharge areas and geochemical evolution of groundwater in an alluvial aquifer system in the Sultanate of Oman. *Hydrogeol. J.* 14:203–24

Mazzotti M, Abanades JC, Allam R, Lackner KS, Meunier F, et al. 2005. Mineral carbonation and industrial uses of CO_2. In *IPCC Special Report on Carbon Dioxide Capture and Storage*, ed. B Metz, O Davidson, H de Coninck, M Loos, L Meyer, pp. 319–38. Cambridge: Cambridge Univ. Press

McCollom TM, Bach W. 2009. Thermodynamic constraints on hydrogen generation during serpentinization of ultramafic rocks. *Geochim. Cosmochim. Acta* 73:856–75

Milliken KL, Morgan JK. 1996. Chemical evidence for near-seafloor precipitation of calcite in serpentinites (Site 897) and serpentinite breccias (Site 899), Iberia abyssal plain. In *Proceedings of the Ocean Drilling Program*, *Scientific Results*, Vol. 149, ed. RB Whitmarsh, DS Sawyer, A Klaus, DG Masson, pp. 553–58. College Station, TX: Ocean Drill. Program

Milsch H, Seibt A, Spangenberg E. 2009. Long-term petrophysical investigations on geothermal reservoir rocks at simulated in situ conditions. *Transport Porous Media* 77:59–78

Morrow C, Moore D, Lockner D. 2001. Permeability reduction in granite under hydrothermal conditions. *J. Geophys. Res.* 106:30551–60

Mottl MJ, Komor SC, Fryer P, Moyer CL. 2003. Deep-slab fluids fuel extremophilic *Archaea* on a Mariana forearc serpentinite mud volcano: Ocean Drilling Program Leg 195. *Geochem. Geophys. Geosyst.* 4(11):9009

Mottl MJ, Wheat G, Fryer P, Gharib J, Martin JB. 2004. Chemistry of springs across the Mariana forearc shows progressive devolatilization of the subducting plate. *Geochim. Cosmochim. Acta* 68:4915–33

Nasir S, Al Sayigh AR, Al Harthy A, Al-Khirbash S, Al-Jaaidi O, et al. 2007. Mineralogical and geochemical characterization of listwaenite from the Semail ophiolite, Oman. *Chem. Erde Geochem.* 67:213–28

Neal C, Stanger G. 1983. Hydrogen generation from mantle source rocks in Oman. *Earth Planet. Sci. Lett.* 66:315–20

Neal C, Stanger G. 1984. Calcium and magnesium-hydroxide precipitation from alkaline groundwaters in Oman, and their significance to the process of serpentinization. *Mineral. Mag.* 48:237–41

Neal C, Stanger G. 1985. Past and present serpentinization of ultramafic rocks: an example from the Semail ophiolite nappe of northern Oman. In *The Chemistry of Weathering*, ed. JI Drever, pp. 249–75. Dordrecht, Neth.: D. Reidel

O'Connor WK, Dahlin DC, Rush GE, Gerdemann SJ, Nilsen DN. 2004. Aqueous mineral carbonation. *U.S. Dep. Energy Final Rep. DOE/ARC-TR-04-002*, U.S. Dep. Energy Albany Res. Cent., Albany

O'Hanley DS. 1992. Solution to the volume problem in serpentinization. *Geology* 20:705–8

O'Neil JR, Barnes I. 1971. ^{13}C and ^{18}O compositions in some fresh-water carbonates associated with ultramafic rocks and serpentinites: western United States. *Geochim. Cosmochim. Acta* 35:687–97

O'Neil JR, Clayton RN, Mayeda TK. 1969. Oxygen isotope fractionation in divalent metal carbonates. *J. Chem. Phys.* 51:5547–58

Palandri JL, Kharaka YK. 2004. A compilation of rate parameters of water-mineral interaction kinetics for application to geochemical modeling. *U.S. Geol. Surv. Open File Rep. 2004-1068*, U.S. Geol. Surv., Menlo Park, Calif.

Peretti A, Dubessy J, Mullis J, Frost BR, Tromsdorff V. 1992. Highly reducing conditions during Alpine metamorphism of the Malenco peridotite (Sondrio, northern Italy) indicated by mineral paragenesis and H_2 in fluid inclusions. *Contrib. Mineral. Petrol.* 112:329–40

Poupeau G, Saddiqi O, Michard A, Goffé B, Oberhänsli R. 1998. Late thermal evolution of the Oman Mountains subophiolitic windows: apatite fission-track thermochronology. *Geology* 26:1139–42

Pozzorini D, Früh-Green GL. 1996. Stable isotope systematics of the Ventina Ophicarbonate Zone, Bergell contact aureole. *Schweiz. Mineral. Petrogr. Mitt.* 76:549–64

Prigiobbe V, Costa G, Baciocchi R, Hänchen M, Mazzotti M. 2009. The effect of CO_2 and salinity on olivine dissolution kinetics at 120°C. *Chem. Eng. Sci.* 64:3510–15

Putnis A. 2009. Mineral replacement reactions. *Rev. Mineral. Geochem.* 70:87–124

Raupach MR, Marland G, Ciais P, Le Quéré C, Canadell JG, et al. 2007. Global and regional drivers of accelerating CO_2 emissions. *Proc. Natl. Acad. Sci. USA* 104:10288–93

Ribeiro Da Costa I, Barriga FJAS, Taylor RN. 2008. Late seafloor carbonate precipitation in serpentinites from the Rainbow and Saldanha sites (Mid-Atlantic Ridge). *Eur. J. Mineral.* 20:173–81

Robinson PT, Malpas J, Zhou MF, Ash C, Yang JS, Bai WJ. 2005. Geochemistry and origin of listwanites in the Sartohay and Luobnsa ophiolites, China. *Int. Geol. Rev.* 47:177–202

Royne A, Jamtveit B, Mathiesen J, Malthe-Sorenssen A. 2009. Controls on rock weathering rates by reaction-induced hierarchical fracturing. *Earth Planet. Sci. Lett.* 275:364–69

Rudge JF, Kelemen PB, Spiegelman M. 2010. A simple model of reaction-induced cracking applied to serpentinization and carbonation of peridotite. *Earth Planet. Sci. Lett.* 291:215–27

Saldi GD, Jordan G, Schott J, Oelkers EH. 2009. Magnesite growth rates as a function of temperature and saturation state. *Geochim. Cosmochim. Acta* 73:5646–57

Schaef HT, McGrail BP. 2009. Dissolution of Columbia River Basalt under mildly acidic conditions as a function of temperature: experimental results relevant to the geological sequestration of carbon dioxide. *Appl. Geochem.* 24:980–87

Schandl ES, Naldrett AJ. 1992. CO_2 metasomatism of serpentinites south of Timmins, Ontario. *Can. Mineral.* 30:93–108

Schandl ES, Wicks FJ. 1991. Carbonate and associated alteration of ultramafic and rhyolitic rocks at the Hemingway Property, Kidd Creek Volcanic Complex, Timmins, Ontario. *Econ. Geol.* 88:1615–35

Scherer GW. 1999. Crystallization in pores. *Cement Concrete Res.* 29:1347–58

Scherer GW. 2004. Stress from crystallization of salt. *Cement Concrete Res.* 34:1613–24

Schrag D. 2007. Preparing to capture carbon. *Science* 315:812–13

Schramm B, Devey C, Gillis KM, Lackschewitz K. 2005. Quantitative assessment of chemical and mineralogical changes due to progressive low-temperature alteration of East Pacific Rise basalts from 0 to 9 Ma. *Chem. Geol.* 218:281–313

Schuiling RD. 1964. Serpentinization as a possible cause of high heat-flow values in and near the oceanic ridges. *Nature* 201:807–8

Schuiling RD. 2006. Mineral sequestration of CO_2 and recovery of the heat of reaction. In *Macro-Engineering: A Challenge for the Future*, ed. V Badescu, RB Cathcart, RD Schuiling, pp. 21–29. Dordrecht, Neth.: Springer

Schuiling RD, Krijgsman P. 2006. Enhanced weathering: an effective and cheap tool to sequester CO_2. *Clim. Change* 74:349–54

Seifritz W. 1990. CO_2 disposal by means of silicates. *Nature* 345:486

Seyfried WE Jr, Foustoukos DI, Fu Q. 2007. Redox evolution and mass transfer during serpentinization: an experimental and theoretical study at 200°C, 500 bar with implications for ultramafic-hosted hydrothermal systems at Mid-Ocean Ridges. *Geochim. Cosmochim. Acta* 71:3872–86

Shervais JW, Kolesar P, Andreasen K. 2005. A field and chemical study of serpentinization, Stonyford, California: chemical flux and mass balance. *Int. Geol. Rev.* 47:1–23

Skippen G. 1974. An experimental model for low pressure metamorphism of siliceous dolomitic marble. *Am. J. Sci.* 274:487–509

Smith JR, Giegengack R, Schwarcz HP. 2004. Constraints on Pleistocene pluvial climates through stable-isotope analysis of fossil-spring tufas and associated gastropods, Kharga Oasis, Egypt. *Palaeogeogr. Palaeoclimatol. Palaeoecol.* 206:157–75

Snow JE, Dick HJB. 1995. Pervasive magnesium loss by marine weathering of peridotite. *Geochim. Cosmochim. Acta* 59:4219–35

Spiers CJ, Schutjes TM, Brzesowsky RH, Peach CJ, Liezenberg JL, Zwart HJ. 1990. Experimental determination of constitutive parameters governing creep of rocksalt by pressure solution. *Geol. Soc. Lond. Spec. Publ.* 54:215–27

Stanger G. 1985. Silicified serpentinite in the Semail nappe of Oman. *Lithos* 18:13–22

Stanger G. 1986. *The Hydrogeology of the Oman Mountains*. Durham, UK: The Open Univ.

Stanger G, Laver J, Neal C. 1988. Black carbonaceous calcite associated with serpentinite from Oman. *Mineral. Mag.* 52:403–8

Stanger G, Neal C. 1994. The occurrence and chemistry of huntite from Oman. *Chem. Geol.* 112:247–54

Staudigel H, Hart SR. 1985. Dating of ocean crust hydrothermal alteration: strontium isotope ratios from Hole 504B carbonates and a reinterpretation of Sr isotope data from Deep Sea Drilling Project Sites 105, 332, 417, and 418. *Deep Sea Drill. Proj. Initial Rep.* 83:297–303

Steiger M. 2005a. Crystal growth in porous materials: I. The crystallization pressure of large crystals. *J. Cryst. Growth* 282:455–69

Steiger M. 2005b. Crystal growth in porous materials: II. Influence of crystal size on the crystallization pressure. *J. Cryst. Growth* 282:470–81

Tarutani T, Clayton RN, Mayeda TK. 1969. The effect of polymorphism and magnesium substitution on oxygen isotope fractionation between calcium carbonates and water. *Geochim. Cosmochim. Acta* 33:987–96

Tenthorey E, Scholz CH, Aharonov E, Léger A. 1998. Precipitation sealing and diagenesis: 1. Experimental results. *J. Geophys. Res.* 103:23951–67

Trommsdorff V, Evans BW. 1977a. Antigorite-ophicarbonates: phase relations in a portion of the system CaO-MgO-SiO$_2$-H$_2$O-CO$_2$. *Contrib. Mineral. Petrol.* 60:39–56

Trommsdorff V, Evans BW. 1977b. Antigorite-ophicarbonates: contact metamorphism in Valmalenco, Italy. *Contrib. Mineral. Petrol.* 62:301–12

Vasconcelos C, McKenzie JA, Warthmann R, Bernasconi SM. 2005. Calibration of the δ^{18}O paleothermometer for dolomite precipitated in microbial cultures and natural environments. *Geology* 33:317–20

Walder J, Hallet B. 1985. A theoretical model of the fracture of rock during freezing. *Geol. Soc. Am. Bull.* 96:336–46

Weyhenmeyer CE. 2000. *Origin and evolution of groundwater in the alluvial aquifer of the eastern Batinah coastal plain, Sultanate of Oman: a hydrogeochemical approach*. PhD thesis. Univ. Bern, Switz. 202 pp.

Weyhenmeyer CE, Burns SJ, Waber HN, Macumber PG, Matter A. 2002. Isotope study of moisture sources, recharge areas, and groundwater flow paths within the eastern Batinah coastal plain, Sultanate of Oman. *Water Resour. Res.* 38:1184

Wilde A, Simpson L, Hanna S. 2002. Preliminary study of Cenozoic alteration and platinum deposition in the Oman ophiolite. *J. Virtual Explor.* 6:7–13

Wilson SA, Dipple GM, Power IM, Thom JM, Anderson RG, et al. 2009. Carbon dioxide fixation within mine wastes of ultramafic-hosted ore deposits: examples from the Clinton Creek and Cassiar chrysotile deposits, Canada. *Econ. Geol.* 104:95–112

Xu WY, Apps JA, Pruess K. 2004. Numerical simulation of CO$_2$ disposal by mineral trapping in deep aquifers. *Appl. Geochem.* 19:917–36

Contents

Indexes

Errata

An online log of corrections to *Annual Review of Earth and Planetary Sciences* articles
may be found at http://earth.annualreviews.org

Rates and Mechanisms of Mineral Carbonation in Peridotite:
Natural Processes and Recipes for Enhanced, *in situ* CO₂ Capture & Storage
Peter B. Kelemen, Jurg Matter, Lisa Streit, John Rudge, Bill Curry, and Jurek Blusztajn

SUPPLEMENT, TABLE OF CONTENTS

1 **Rates and Mechanisms of Mineral Carbonation Ultramafic Rocks:**
2 **Natural Processes and Recipes for Enhanced, *in situ* CO₂ Capture &**
3 **Storage**
4
5 Peter B. Kelemen[1], Jurg Matter[1], Elizabeth E. Streit[1], John F. Rudge[2], William B. Curry[3],
6 and Jerzy Blusztajn[3]
7
8 1: Lamont Doherty Earth Observatory, Columbia University, Palisades NY 10964, USA, peterk@LDEO.columbia.edu
9 2: Institute of Theoretical Geophysics, Bullard Laboratories, University of Cambridge, Madingley Road, Cambridge, CB3 0EZ, UK
10 3: Woods Hole Oceanographic Institution, Woods Hole MA 02543, USA

11

12 **SUPPLEMENTARY INFORMATION**

13

14 **S1. Mass of peridotite near the Earth's surface**

15

16 Slow-spreading mid-ocean ridges extend for more than 60,000 km, and produce new

17 oceanic crust and shallow mantle at a half-spreading rate of about 0.01 m/year. In some

18 places, the new crust is composed largely of partially hydrated mantle peridotite rather

19 than newly formed igneous rocks. If 5 to 15% of the seafloor at slow spreading ridges is

20 underlain by peridotite (Cannat et al., 1995; Carlson, 2001), then this corresponds to 1 to

21 4×10^{12} kg of peridotite emplaced in the upper 7 km of the oceanic plate per year, or $\sim 10^{18}$

22 kg of peridotite in a swath 10 km wide on either side of the slow spreading ridges, that is

23 produced over 1 million years. Seafloor peridotite is gradually buried by pelagic

24 sediments (including authigenic carbonates that may, in fact, arise partly via carbonate

25 precipitation due to diffuse venting of hydrothermal fluids from peridotite: Eickmann et

26 al., 2009b; Eickmann et al., 2009c; Lein et al., 2007; Ribeiro Da Costa et al., 2008).

27 Former seafloor peridotite extends beneath this shallow veneer of pelagic sediments all

28 the way to the continental shelves, i.e for distances of thousands of km on either side of

29 the slow-spreading portions of the Mid-Atlantic and Indian Ocean Ridges, corresponding

30 to more than 10^{20} kg of material in the upper 7 km of the igneous oceanic plates.

31

32 Intra-oceanic arcs form via thrusting of oceanic crust and mantle in the lower plate

33 beneath the same kind of crust and mantle in the upper plate. Most of the peridotite in the

34   overthrust plate lies at depths greater than 7 km, but tectonic processes such as

35   "subduction erosion" and imbricate thrust faulting (both involving migration of the

36   subduction zone thrust fault into the hanging wall) do bring peridotites closer to the

37   seafloor. Furthermore, diapirs of hydrated peridotite, less dense than the surrounding

38   column of less altered rock, tectonically intrude overlying crust and emerge as "mud

39   volcanoes" on the forearc seafloor. As a result of all these processes, fresh (Bloomer and

40   Fisher, 1987; Bonatti and Michael, 1989; Fisher and Engel, 1969) and altered (e.g., Alt

41   and Shanks, 2006; Fryer, 1992; Haggerty, 1991; Mottl et al., 2003; Mottl et al., 2004)

42   peridotites are fairly abundant on the seafloor in the forearc regions of intra-oceanic,

43   western Pacific arcs. So far as we know, there is no quantitative estimate of the

44   proportion of peridotite on and near the seafloor in forearc settings, but it may be safe to

45   guess that the total mass of these rocks is larger than the mass of peridotites in ophiolites.

46   It is interesting to note that Oman listwanites (Sections 2.4, 2.7, 4.1, 4.3, Figures 6 and 8)

47   formed in hanging wall peridotite thrust over carbonate-bearing metasediments, and can

48   be viewed as an outcrop exposure of carbonated peridotites formed in mantle peridotite

49   above a subduction zone.

50

51   We've estimated that the Sumail ophiolite, in the Sultanate of Oman and the United Arab

52   Emirates, contains about 5×10^{16} kg of peridotite within 3 km of the surface of the

53   subaerial outcrop area (Kelemen and Matter, 2008). Peridotite along the southeastern end

54   of the ophiolite, mainly covered by a few hundred meters of carbonate sediment,

55   continues across the coastline into the shallow seafloor beneath the Gulf of Oman, with

56   unknown extent. The Samail ophiolite is the largest in the world, but there are several

57   more (Papua New Guinea, New Caledonia, Albania) that contain more than 10^{16} kg of

58   peridotite. Smaller ophiolites are found on all continents, including Antarctica (Talarico

59   et al., 1999). In the United States, the total mass of peridotite in the many ophiolites,

60   considered together, is roughly equivalent to that in the Samail ophiolite (Krevor et al.,

61   2009). The total mass of peridotite in ophiolites worldwide is between 10^{17} and 10^{18} kg.

62

63   Peridotites and other ultramafic rocks in mafic to ultramafic, igneous intrusions generally

64   are much less abundant than in the other three settings described above. However,

65   notable exceptions include the gigantic Bushveld intrusion in South Africa, whose

66   ultramafic layers comprise on the order of 10^{16} to 10^{17} kg of peridotite and pyroxenite,

67   and the somewhat similar Stillwater intrusion in Montana, which probably contains

68   almost 10^{15} kg of peridotite.

69

70   It is hard to assess the total mass of continental peridotite massifs, but the two large

71   massifs near the southeast coast of Spain and the north coast of Morocco, Ronda and

72   Beni Boussera, have a combined mass on the order of 10^{15} kg, as does the Horoman

73   peridotite massif in Japan. Like the Samail and New Caledonia ophiolites, both the

74   Ronda and Beni Boussera peridotite massifs extend beneath the shallow seafloor, beneath

75   a thin veneer of sediments.

76

77   **S2. Observed parageneses in peridotite carbonation**

78

79   "Ophicalcite" (carbonate-bearing, partially hydrated peridotite, also called ophicarbonate)

80   is prized as ornamental stone for building facades, and has been the subject of numerous

81   petrogenetic studies (e.g., Barbieri et al., 1979; Bernoulli and Weissert, 1985; Boschi et

82   al., 2009; Driesner, 1993; Ferry, 1995; Folk and McBride, 1976; Früh-Green et al., 1990;

83   Jedrysek and Sachanbinski, 1994; Leake et al., 1975; Lemoine, 1980; Pozzorini and

84   Früh-Green, 1996; Surour and Arafa, 1997; Trommsdorff et al., 1980; Trommsdorff and

85   Evans, 1977; Weissert and Bernoulli, 1984). While some ophicalcite occurrences have

86   been interpreted as the result of sedimentary deposition of carbonate in peridotite talus or

87   conglomerates, it is apparent that others result from chemical interaction between CO_2-

88   bearing fluids and peridotite protoliths. Carbonate veins in ophicalcite deposits are

89   composed of calcite, magnesite, and/or dolomite ($CaMg(CO_3)_2$).

90

91   Direct evidence for formation conditions of some ophicalcites comes from observations

92   of on-land and near-shore, peridotite-hosted, alkaline springs that deposit travertine on

93   outcrop surfaces, carbonate veins in the subsurface, and carbonate cement in peridotite

94   conglomerates (Barnes and O'Neil, 1969, 1971; Barnes et al., 1973; Bruni et al., 2002;

95   Cipolli et al., 2004; Clark and Fontes, 1990; Cox et al., 1982; Kelemen and Matter, 2008;

96   Launay and Fontes, 1985; Neal and Shand, 2002; Neal and Stanger, 1983, 1984, 1985;

97   O'Neil and Barnes, 1971). These deposits form at ~ 20 to 50°C.

98

99   Carbonation of serpentine is also occurring in tailings piles associated with asbestos

100   mines in Canada (Power et al., 2007; Wilson et al., 2009; Wilson et al., 2006), probably

101   mainly in the summer when surface temperatures can exceed 35°C. Surficial carbonate

102   deposits forming on ultramafic rocks, with associated carbonate films on pools of water,

103   are composed of calcite, dolomite, magnesite, plus metastable, hydrous, magnesium-rich

104   carbonate minerals including nesquehonite, dypingite and hydromagnesite (recent review

105   in Wilson et al., 2009).

106

107   "Listwanite" (carbonated peridotite, containing quartz + magnesite or dolomite ± talc ±

108   chromian mica, also called listvanite, listwaenite, listvenite …) can be a source of

109   industrially important volumes of magnesite (magnesium carbonate), is sometimes

110   associated with gold and mercury deposits, and has been studied from a petrogenetic

111   point of view (e.g., Akbulut et al., 2006; Auclair et al., 1993; Barnes et al., 1973; Ece et

112   al., 2005; Halls and Zhao, 1995; Hansen et al., 2005; Naldrett, 1966; Nasir et al., 2007;

113   Robinson et al., 2005; Spiridonov, 1991; Stanger, 1985; Tsikouras et al., 2006; Ucurum,

114   2000; Wilde et al., 2002).

115

116   Abkulut et al. (2006), Nasir (2007) and Halls and Zhao (1995) provide literature reviews.

117   Hansen et al. (2005) provide the most thorough petrogenetic interpretation. Very

118   consistent formation temperatures of 237±21°C, 248±12°C and 210-240°C have been

119   determined by three groups (Hansen et al., 2005; Madu et al., 1990; Schandl and Wicks,

120   1991) for three widely separated localities in Canada based on fluid inclusion

121   measurements. While some definitions of listwanite require the presence of Cr-rich

122   muscovite (fuchsite, mariposite), we feel this requirement is unnecessary and apply the

123   term to completely carbonated peridotite consisting of Mg-rich carbonate + quartz. In

124   end-member listwanites, relict chrome spinels typically remain as a testament to the

125   mantle peridotite protolith.

126

127   **S3: Are climatic variations recorded by**

128   **stable isotope variation in peridotite-hosted travertines in Oman?**

129

130   Clark and Fontes (1990) sought – and believed they found – evidence for climatic

131   variability in their ^{14}C age versus oxygen and carbon isotope data for a single, peridotite-

132   hosted travertine locality in Oman. They attributed the light isotope ratios in some

133   samples to kinetic fractionation in arid environments (Clark et al., 1992), and the heavier

134   values to equilibrium isotope partitioning in pluvial environments.

135

136   There have indeed been fluctuations in aridity, and in stable isotope ratios in precipitation

137   in Oman, over the past 50,000 years (Burns et al., 2001; Fleitmann et al., 2007; Fleitmann

138   et al., 2003; Fuchs and Buerkert, 2008; Weyhenmeyer et al., 2000). However, we believe

139   that Figures 4 and S1 provide little if any evidence for an impact of climate variability on

140   stable isotope ratios in peridotite-hosted carbonates in Oman. Peridotite hosted travertines

141   in Oman with ^{14}C ages greater than 1000 years have comparatively restricted ranges of

142   δ^{18}O and δ^{13}C, (δ^{18}O of 20 to 30 ‰ relative to SMOW) and δ^{13}C (mostly -20 to -10 ‰

143   VPDB), while there were alternating arid and humid periods in Oman throughout the ^{14}C

144   age range of our samples.

145

146   The observed restriction of the kinetic δ^{13}C fractionation, and the large, correlated δ^{18}O

147   fractionation (Section S7), to travertines less than 1000 years old suggests that infilling of

148   porosity in travertines forms additional carbonate minerals in isotope exchange

149   equilibrium with the atmosphere and with H_2O in ground water, and perhaps

150   recrystallizes early formed carbonate minerals under conditions of isotope exchange

151   equilibrium with H_2O. Perhaps, such a process involves ground water or rainwater with

152   pH ~ 8, instead of the alkaline spring water that initially forms the travertine. This

153   process of infilling and recrystallization must not involve substantial additional uptake of

154   ^{14}C from the atmosphere, or there would be more samples with ^{14}C ages less than 1000

155   years that lack the light δ^{13}C and δ^{18}O isotope signature. In any case, this process could

156   obscure or obliterate the stable isotope record of climate change in travertines.

157

158   **S4. Contraints and uncertainties in**

159   **the estimated rate of formation of peridotite-hosted carbonates**

160   **in the Samail ophiolite, Oman**

161

162   We used two different methods to estimate potential rates of enhanced, *in situ*

163   carbonation of peridotite for CO_2 capture and storage (Kelemen and Matter, 2008). First,

164   we used our estimate of the natural rate for Oman of about 1.3 gm CO_2 per cubic

165   kilometer per year in a weathering horizon about 15 meters thick at about 30°C, together

166   with data indicating a factor of ~ 1 million enhancement in the rate at 185°C, 150 bars

167   P_{CO2}, with high bicarbonate concentrations in fluid, to obtain an estimate for the

168   enhanced uptake rate of ~ 1 ton of CO_2 per cubic meter per year (Tables S1 and S2).

169

170   A second estimate for the potential rate of CO_2 uptake comes from laboratory kinetic data

171   alone, but requires an assumption about the "grain size" or crack spacing in a rock

172   volume undergoing enhanced *in situ* mineral carbonation. Use of an "effective grain size"

173   of 1 meter yields a rate of ~ 1 ton CO_2 per cubic meter per year at optimal temperature,

174   P_{CO2} and bicarbonate concentration (Section 3.2 and Figure 5), consistent with the

175   estimate obtained via extrapolation of the natural rate. These two methods for estimating

176   the rate are somewhat independent, and are consistent, but uncertainty in the choice of

177   effective grain size makes this consistency less than completely reassuring.

178

179   For these reasons, it is important to review the constraints and uncertainties on the rate of

180   natural peridotite carbonation.

181

182   *S4.1 Geochronology*

183

184   We made order of magnitude estimates of the formation rate of carbonate veins and

185   travertine terraces in Oman based on ^{14}C ages, together with reconnaissance mapping of

186   the volume of travertine terraces and carbonate veins in peridotite (Kelemen and Matter,

187   2008). Since the ^{14}C ages yield a relatively "flat" histogram from 0 to 50,000 years, we

188   simply divided the mass of carbonates by the average age to determine an average rate of

189   carbonate deposition. Additional data gathered since 2008 confirm the age and volume

190   data used to make this estimate (Figure S2).

191

192   However, these data are subject to considerable uncertainty. The ^{14}C "ages" of our

193   samples are difficult to interpret, in detail, because of open system behavior.

194   Unconformities in travertine terraces, carbonate veins cutting across depositional strata,

195   and actively forming stalactites beneath overhanging portions of stratiform travertine

196   demonstrate that erosion and recrystallization take place after calcite is originally

197   deposited. Biological activity could consume ancient carbon and deposit "modern"

198   carbon. Evidence for kinetic fractionation of stable carbon and oxygen isotopes in

199   travertines with ^{14}C ages less than 1000 years (Section S7, and Figures 4 and S1), which

200   is absent – perhaps erased by diagenetic processes – in travertines more than 1000 years

201   old, suggests open system behavior. Formation of veins may involve similar, open-

202   system processes.

203

204   *S4.2 Travertine volume*

205

206   Our estimate of the volume of peridotite-hosted travertine in Oman (Kelemen and Matter,

207   2008) is based on mapping in the southern two blocks of exposed mantle peridotite in the

208   Samail ophiolite, extrapolated to the rest of the exposed peridotite. Many travertines are

209   partially covered by alluvial fans, and some massive travertine – now exposed by erosion

210   – formed entirely beneath alluvial fans (Kelemen and Matter, 2008). In our calculations

211   (Table S1) we assumed that the mass of buried travertine was about the same as the mass

212   of exposed travertine. In eroded canyons, we observed a horizon about 10 meters thick

213   beneath travertine terraces composed of heavily serpentinized peridotite with about 5%

214   calcite-rich veins which we considered to be effectively a part of the travertine bodies

215   themselves. From these observations, we estimate that there are about 5.4×10^7 m^3 of

216   peridotite-hosted travertine in Oman (Table S1).

217

218

219

220 *S4.3 Direct measurement of vein and listwanite abundance*

221

222 We estimated the volume of low temperature carbonate veins in peridotite in two ways

223 (Kelemen and Matter, 2008). First, we simply measured the frequency and width of

224 carbonate veins in outcrop. We studied outcrops along the walls of small canyons (wadis)

225 close to travertine deposits, and newly excavated road cuts in peridotite far from

226 travertine deposits. These reconnaissance measurements yielded about 5% carbonate

227 veins close to travertine deposits, and 1% carbonate veins far from travertine deposits.

228

229 It is noteworthy that, standing near a new road cut and looking out over a broad vista of

230 weathered peridotite outcrops on a 1 to 10,000 m scale, one can only a few, large

231 carbonate veins. However, in most new road cuts, millions of 10 micron to 10 centimeter

232 veins are visible as white coatings on joint surfaces. These veins penetrate into the

233 outcrop in three dimensions, veins in some road cuts have ^{14}C ages of tens of thousands

234 of years (Table S3 and Kelemen and Matter, 2008), and recent work on other road cuts

235 has yielded a number of samples that are "carbon dead" (E. Mervine, pers. comm.. 2010).

236 Thus, the veins exposed in road cuts have not formed as a result of excavation-related

237 processes, and instead were present at depth for thousands of years prior to excavation.

238 Surficial weathering, probably during heavy rainfall, removes the smaller veins from

239 outcrop surfaces that are exposed for many years, whereas the newly formed road cuts

240 reveal the true distribution of veins in the upper meters to tens of meters of Oman

241 peridotites.

242

243 It is not clear from these data alone how to extrapolate these data to depth below the

244 surface. In the Oman mountains near, but not within, the peridotite outcrop area,

245 thermochronology data indicate an average erosion rate of about 0.0003 meters per year

246 (Poupeau et al., 1998), and these data together with the older end of the range of ^{14}C ages

247 of our vein samples (~ 50,000 years) suggests that – although the erosion rate has surely

248 varied dramatically over time and from place to place, and the depth of carbonate vein

249 formation must also be highly variable as a result of groundwater percolation along faults

250 and joints – the veins are generally present in a horizon about 15 meters thick over the

251   exposed peridotite area of about 5250 km^2. For a vein abundance of 1%, this corresponds

252   to 0.79 billion cubic meters of carbonate, equivalent to ~ 2.4 billion tons of magnesite

253   and ~ 1.2 billion tons of CO_2.

254

255   Qualitatively, many scientists believe that massive carbonate veins are abundant in

256   peridotite exposed at the seafloor down to a depth of 10 to 50 meters, associated with

257   orange, oxidative weathering of the silicates. This may be reflected by the samples with

258   more than 1 wt% CO_2 within 50 meters of the seafloor in Figure 3. Below this depth,

259   massive carbonate veins are rare, and a more reducing environment is suggested by green

260   coloring of the serpentine and other silicates. However, Figure 3 shows that such

261   peridotites, generally without visible carbonate veins, contain an average of ~ 0.6 wt%

262   CO_2 down to at least 200 mbsf, with no systematic variation with depth.

263

264   None of the Oman samples that we have analyzed so far, for CO_2 abundance or ^{14}C, were

265   serpentinized peridotites lacking visible carbonate veins. This has been a significant

266   oversight. If CO_2 abundance in "typical" serpentinized peridotites in Oman is similar to

267   that in peridotites from the seafloor, this would constitute a reservoir comparable in size

268   to the visible carbonate veins. For example, if Oman peridotites contain an average of

269   0.05 wt% CO_2, this would correspond to ~ 1 billion tons of CO_2. This reservoir – if

270   present – was not included in our published calculations (Kelemen and Matter, 2008) on

271   CO_2 uptake via peridotite alteration in Oman.

272

273   Initially, we avoided work on the listwanites in Oman, for a variety of reasons. First,

274   because they formed in an ancient, high temperature, high CO_2 hydrothermal system, we

275   cannot sample the fluid input or output, as we can for the ongoing, low temperature

276   system. Second, many listwanite localities in Oman lie along fault contacts between

277   peridotite and metasediments, making it difficult to determine the protolith with certainty.

278

279   However, we came to realize that the listwanites constitute a crucial example of complete

280   mineral carbonation in peridotite, exactly the type of process that one would wish to

281   emulate in engineered, *in situ* CO_2 capture and storage. In our recent work on listwanites

282   in Oman, we have focused on tabular bodies enclosed entirely within peridotites,

283   containing relict chrome spinels identical to those in the peridotites, so that we can be

284   sure of the protolith. The largest of these is at least 200 meters thick, 6 km long and 2 km

285   wide, comprising about 10 billion tons of carbonated peridotite, containing about 4

286   billion tons of CO_2 in carbonate minerals. Unfortunately, as noted above, the listwanites

287   are probably Cretaceous. Due to the inherent uncertainties in geochronological data, it

288   may be impossible to obtain a meaningful range in ages for the listwanites that allows us

289   to calculate their rate of formation.

290

291   *S4.4 Indirect estimate of vein abundance using geochemical estimate of travertine/vein*

292   *ratio*

293

294   We also estimated the volume of peridotite-hosted carbonate veins indirectly, using the

295   observed amount of travertine together with inferences about the ratio of travertine versus

296   vein mass based on the composition of ground water and alkaline spring water in Oman

297   (Table S2). This requires knowledge of typical ground water and spring water

298   compositions in peridotite catchments, and understanding of the reactions that drive

299   changes in the water composition. A brief summary of the prevailing hypotheses on this

300   topic is presented in Section 2.3.

301

302   In data for waters in peridotite catchments in Liguria (northern Italy), the reduction in

303   carbon concentration in evolving fluids along the reaction path that transforms Type I to

304   Type II waters, via reaction with peridotite to form Mg-Ca carbonates and serpentine, is

305   about 500 mg HCO_3/liter, corresponding to formation of 690 to 750 mg of $MgCO_3$ or

306   $(Ca,Mg)CO_3$ per liter of Type 2 water produced. In the same region, precipitating calcite

307   on the surface to form travertine deposits from Type II waters could consume up to 60

308   mg of Ca, corresponding to the formation of up to 150 mg of $CaCO_3$ per liter of Type II

309   water consumed. Thus, in this region about five times more $MgCO_3$ and $(Ca,Mg)CO_3$ is

310   produced in subsurface veins than $CaCO_3$ precipitated on the surface. As can be seen in

311   Table S2, the same considerations yield a mass ratio of veins to travertine of about 17 for

312   northern California, and about 7 for Oman. The apparent difference between these places

313   is due largely to the maximum value of HCO_3/liter used in the calculation, which is much

314   higher in the highest concentration samples from California than in samples from other

315   places. We are not sure if this is because California differs from other places, or because

316   the end-member $Mg-HCO_3$ fluids have not been sampled in Italy and Oman.

317

318   If we use a mass ratio of calcite in travertine to magnesite in veins of 17, corresponding

319   to a factor of about 15 in volume, we obtain an estimated volume of 0.81 billion cubic

320   meters of magnesite veins in Oman, very close to the estimate of ~ 0.79 billion cubic

321   meters assuming 1% veins in a 15 m thick weathering horizon at the top of the exposed

322   peridotite area in Oman. On the other hand, if we use a mass ratio of 7, we obtain an

323   estimate of 0.33 billion cubic meters of magnesite veins in Oman. The factor of ~ 2.5

324   difference between this estimate and the one obtained for 1% veins over 15 m could

325   result from many uncertainties in the methods used to obtain both estimates.

326

327   One source of uncertainty that we have not yet mentioned is that erosion of the ~ 1 m

328   thick travertine deposits may have removed a substantial proportion of the older ones,

329   while parts of the associated ~ 15 m thick vein horizon complementary to these

330   travertines may still be exposed in outcrop. Such a relationship may be evident from the

331   slightly older average age for veins compared to travertines (Figure S2).

332

333   *S4.5 Temperature of formation of carbonate veins*

334

335   The temperature of formation of carbonate veins provides an independent check on our

336   interpretation of both ^{14}C ages and the depth of formation of the carbonate veins

337   associated with the active process forming alkaline springs and travertine in Oman today.

338   If carbonate vein formation occurred at temperatures close to the mean annual

339   temperature, then they probably formed in a shallow weathering horizon. Since the

340   weathering horizon is constantly being removed by erosion and renewed by alteration,

341   this also would indicate that the carbonate veins are young. Alternatively, if carbonate

342   veins formed at high temperature, then they must have formed at greater depths. In

343   addition, high temperature formation would suggest that some of the peridotite

344   carbonation occurred longer ago than the ^{14}C ages suggest, since high temperatures are

345   unknown in the shallow crust of Oman today, and erosion cannot have removed

346   kilometers of the Oman peridotite section in less than 50,000 years. Data discussed in

347   Section 2.7 suggest that carbonate veins in partially carbonated peridotites in Oman,

348   associated with alkaline springs and travertine deposits, formed at low temperature,

349   between about 20 and 60°C. This is consistent with the hypothesis that the veins form in

350   a shallow weathering horizon, at a rate that is roughly keeping pace with erosion.

351

352   *S4.6 Source of Ca, CO_2 and Sr in travertines and veins*

353

354   It is important to understand the source of Ca and CO_2 in peridotite-hosted carbonates in

355   Oman. The rate calculations of Kelemen and Matter (2008), elaborated upon here,

356   implicitly incorporate the assumption that the CO_2 that forms carbonates in peridotite is

357   dissolved in ground water via exchange with the atmosphere. Similarly, the "standard"

358   explanation for the formation of abundant, Ca-rich travertine, first offered by Barnes and

359   O'Neil (1969), is that Ca is dissolved from peridotites during serpentinization, while CO_2

360   is derived from the atmosphere. This requires very low integrated fluid/rock ratios, since

361   Ca is not abundant in peridotites.

362

363   Alternatively, at least in Oman, it is important to consider that some Ca and CO_2 may be

364   derived from carbonate-bearing metasediments beneath the thrust that emplaced

365   peridotite over continental shelf sediments. If this were the case, our rate calculations

366   would be overestimates of the amount of CO_2 uptake from the atmosphere during

367   peridotite alteration.

368

369   CO_2 uptake from underlying sediments, rather than from the atmosphere, may affect

370   peridotite carbonation elsewhere. Wilson et al. (2009) suggested that much of the carbon

371   in magnesium carbonate minerals within mine tailings in northern Canada was derived

372   from nearby carbonate sediments, and they propose mixing between carbonates

373   equilibrated with the atmosphere, with relatively heavy $\delta^{18}O$ and $\delta^{13}C$ values, and a

374   carbonate component from nearby sediments with lower $\delta^{18}O$ and $\delta^{13}C$ (Figure S3).

375   However, note that these authors recently presented a different, kinetic hypothesis for the

376   correlated trend of $\delta^{18}O$ versus $\delta^{13}C$ in their samples (Wilson et al., 2010), similar to the

377   one we discuss in Section S7.

378

379   Travertines in peridotite catchments, and some carbonate veins in peridotites, are

380   surprisingly rich in Ca, despite the fact that Ca is typically present at the level of one or

381   two weight percent in mantle peridotites depleted by melt extraction, as in Oman

382   (Hanghøj et al., 2010), in most ophiolite mantle sections, and in seafloor exposures of

383   peridotite. The high concentration of Ca in alkaline spring water is traditionally

384   considered to be the result of interaction of fluid with very large volumes of peridotite,

385   prior to precipitation of dolomite or calcite (e.g., Barnes and O'Neil, 1969; Bruni et al.,

386   2002) via reactions such as (1h) and (1i) in Section 2.2. The hydration products of

387   peridotite, typically serpentine and related minerals, do not have favorable lattice sites for

388   Ca, driving increased concentration of Ca in the fluid as in reaction (2). Based on this, if

389   the peridotite reactant has 1 wt% CaO, then each mass of calcite ($CaCO_3$, ~ 56 wt% CaO)

390   in travertine represents dissolution and reprecipitation of Ca from at least 56 times its

391   mass in peridotite. This is consistent with the high pH of alkaline springs, which is

392   thought to result from reaction (2). Thus, travertine-forming fluids with high Ca

393   concentrations and high pH are viewed as the products of extensive interaction with

394   peridotite, with a low integrated fluid/rock ratio. Alternatively, alteration of basaltic dikes

395   within peridotite could supply some of the Ca in veins and travertines (F. Klein, pers.

396   comm. 2010).

397

398   The hypothesis that the Ca in travertines is derived from the peridotite is supported by the

399   observation of very low oxygen fugacity (Eh) in the alkaline springs that give rise to

400   travertines in peridotite catchments, which indicates a low fluid/rock ratio. Similarly,

401   methane, hydrogen gas, and other reduced gas species are observed at alkaline springs. In

402   order to understand the significance of these observations, one needs to consider the role

403   of Fe in peridotite hydration (serpentinization). Idealized serpentinization reactions such

404   as reaction (1k) in Section 2.2, produce serpentine with lower Fe/Mg than the olivine

405   reactant (Fe-Mg solid solution symbolized with end-members here), and oxidize Fe to

406 form magnetite, reducing the oxygen fugacity of the resulting fluids in a predictable way.

407 Thus, the low oxygen fugacity of observed, travertine-forming fluids is consistent with

408 the hypothesis that fluid/rock ratios during interaction with peridotite are low in ongoing

409 weathering of peridotites in Oman.

410

411 All of our measurements of spring water temperature (unpublished data), and all but one

412 of those of Neal and Stanger (Neal and Stanger, 1985), are within a few degrees of the

413 mean annual air temperature in Oman, so there is little evidence for deep circulation of

414 fluids. Many peridotite-hosted alkaline springs and travertines are near the periphery of

415 large peridotite massifs, and not far from the basal thrust underlying the peridotite. Thus,

416 they could incorporate Ca from underlying rocks without recording substantially higher

417 temperature. However, other peridotite-hosted veins and travertines with high Ca

418 concentrations are found at relatively high altitude, in small peridotite catchments far

419 from the basal thrust. The geochemical characteristics of veins and travertines do not vary

420 with elevation or with distance to the basal thrust. These data support the hypothesis that

421 Ca in peridotite-hosted carbonates is derived from the peridotite, not from underlying

422 sediments.

423

424 Though in the end we endorse this hypothesis, other observations caused us to question

425 the simple reasoning outlined in the previous few paragraphs. We have less knowledge

426 about the formation of low temperature carbonate veins compared to the process that

427 forms alkaline springs and and travertine, and even less information about the relatively

428 high temperature process that forms listwanites. Our observations of relatively oxidized

429 hematite (Fe_2O_3) rather than magnetite (Fe_3O_4) in and near listwanites, and of sulfate

430 minerals ($CaSO_4$, $BaSO_4$) rather than sulfides in some carbonate veins, suggest that the

431 oxygen fugacity is locally high in the natural system, presumably at a relatively high

432 fluid/rock ratio. It is not clear to us how extensive this regime might be, compared to the

433 regime outlined above that has a low fluid/rock ratio.

434

435 Strontium is often used as a proxy for Ca, because the two are geochemically similar, and

436 Sr has a wide range of isotope variation. In order to evaluate the provenance of Sr in

437   carbonated peridotites in Oman, we collected preliminary Sr isotope data on a few

438   samples (Table S3), as did Weyhenmeyer (2000).

439

440   Low Sr isotope ratios (i.e., 0.703) would be indicative of a mantle source for Sr, and one

441   could infer that the source of Ca was also from mantle peridotite. However, Sr isotope

442   ratios for peridotite-hosted carbonate veins and travertines are high (mostly between

443   0.708 and 0.709) and surprisingly uniform (Figure S3). They overlap Sr isotope values

444   for partially hydrated (serpentinized) peridotites from the same massifs as our vein and

445   travertine samples (Gerbert-Gaillard, 2002), and Sr isotope values for the peridotite-

446   hosted, Lost City hydrothermal carbonate deposit along the Mid-Atlantic Ridge (Früh-

447   Green et al., 2003).

448

449   It is apparent that Sr in the peridotite hosted travertines and carbonate veins from Oman

450   (and Lost City) represents a mixture of Sr from a mantle source with Sr from a more

451   radiogenic source. The limestones underlying the peridotite thrust sheet have similar Sr

452   isotope ratios to our samples, (0.7075 to 0.7105), while the carbonate component in

453   clastic sediments intercalated with these limestones has very radiogenic Sr (all values >

454   0.715, most > 0.74, Weyhenmeyer, 2000). The Sr data on Oman samples alone could be

455   consistent with this radiogenic source being limestone, meteoric water, seawater that

456   exchanged Sr with peridotite in the past, or even dust derived from clastic sediments or

457   old continental crust quite distant from the peridotite outcrops.

458

459   Considering $\delta^{13}C$ and $^{87}Sr/^{86}Sr$ data together, and assuming that Ca, Sr and carbon were

460   derived from the same sources during the formation of peridotite hosted carbonates,

461   allows us to rule out a limestone or clastic sediment source for these elements. Oman

462   limestones that have $^{87}Sr/^{86}Sr$ similar to veins and travertines have distinctly different

463    $\delta^{13}C$, which is consistently higher than any vein or travertine sample, while Oman clastic

464   sediments with $\delta^{13}C$ in the range of veins and travertines have $^{87}Sr/^{86}Sr$ that is much

465   higher than veins and travertines.

466

467   Another key feature in the Sr isotope data is the consistent upper bound of 0.7092 for

468   partially hydrated peridotites from Oman, peridotite-hosted carbonates from Oman, and

469   the peridotite-hosted Lost City carbonates. This suggests that there is a radiogenic Sr

470   component common to all three rock types, with $^{87}Sr/^{86}Sr \sim 0.7092$. If so, this component

471   is probably derived from modern seawater via evaporation and rainfall. Lower $^{87}Sr/^{86}Sr$

472   in some samples could reflect an Sr component derived from older seawater, and/or

473   mantle Sr in the peridotite protolith.

474

475   Strikingly, all of the Oman peridotite-hosted travertines and carbonate veins, and all of

476   the leachates from partially hydrated peridotites in Oman, have Sr isotope ratios higher

477   than 0.7080*, higher than Cretaceous to Eocene seawater*. This demonstrates that much of

478   the radiogenic Sr in the peridotite-hosted carbonates, and in typical, partially hydrated

479   peridotites, was added to these rocks after the Eocene, after seafloor hydrothermal

480   activity had ceased, and after the ophiolite had already been emplaced onto the Arabian

481   subcontinent. The source of the high $^{87}Sr/^{86}Sr$ component could be from rainwater and

482   ocean-derived aerosols, in a process that is continuing today, or during marine

483   transgressions that deposited shallow marine carbonates uncomformably over the

484   peridotite (continuing intermittently until ~ 10 Ma, Al Lazki et al., 2002).

485

486   We now return to the hypothesis of Wilson et al. (2009), that magnesium carbonates in

487   mine tailings from northern British Columbia incorporated a component from nearby

488   carbonate sediments. Figures 4 and S3 show that the data of Wilson et al. (labeled NW

489   Canada in Figure 4) form a trend parallel to that of the vein and travertine data from

490   Oman, with the British Columbia data displaced to lower $\delta^{18}O$ and higher $\delta^{13}C$. Indeed,

491   the carbonate sediments near the tailings piles have $\delta^{18}O$ and $\delta^{13}C$ values similar to the

492   lighter end member in the carbonates in the tailings. However, the same relationship is

493   not observed for Oman, where the carbonate sediments have higher $\delta^{13}C$ than peridotite-

494   hosted veins and travertines, and do not lie along the trend formed by the veins and

495   travertines. Thus, the carbon, Sr and Ca in peridotite-hosted carbonates in Oman all

496   represent components derived from the peridotite itself, plus post-Eocene seawater and/or

497   meteoric water with a seawater signature. While this does not rule out a sediment source

498   for C in the Wilson et al. samples, it does indicate that their observations may have an

499   alternative explanation.

500

501   In summary, we conclude that the traditional explanation for high Ca in alkaline springs

502   in peridotite – dissolution of Ca from a large peridotite reservoir, with a low fluid/rock

503   ratio – is applicable to peridotite-hosted carbonates in Oman, consistent with the low Eh

504   of spring waters and the presence of reduced gas species at the springs. Observations of

505   oxidized phases (sulphates, hematite) must indicate that some areas of carbonate

506   deposition are open to exchange with the atmosphere, and/or that they form at a high

507   fluid/rock ratio. Fluid/rock ratios may be highly variable in the peridotite carbonation

508   system in Oman. Ca from underlying sediments probably does not play an important role

509   in forming Ca-rich veins and travertines. Sr isotopes record a mixture of mantle-derived

510   Sr with low $^{87}Sr/^{86}Sr$ and seawater or rainwater derived, radiogenic Sr. Values between

511   0.708 and 0.7092 for leached Sr from altered peridotites, and for peridotite-hosted

512   groundwater and carbonates, suggest that the radiogenic end-member is post-Eocene.

513   Finally, we predict a different set of relationships for Oman listwanites, in which

514   substantial CO_2, Ca and Sr may have been derived from underlying metasediments.

515

516   **S5. Annotated bibliography of work on**

517   **peridotite-hosted hydrothermal systems on the seafloor**

518

519   Peridotite-hosted hydrothermal systems are found along slow spreading ridges, at the

520   *Logatchev* (e.g., Eickmann et al., 2009c; Gebruk et al., 2000; Schmidt et al., 2007;

521   Sudarikov and Roumiantsev, 2000), *Rainbow* (e.g., Charlou et al., 2002; Douville et al.,

522   2002; German et al., 1996; Konn et al., 2009; Ribeiro Da Costa et al., 2008), *Lost City*

523   (e.g., Boschi et al., 2008; Boschi et al., 2006; Früh-Green et al., 2003; Kelley et al., 2001;

524   Kelley et al., 2005; Lang et al., 2010; Ludwig et al., 2006; Proskurowski et al., 2006,

525   2008), *Saldanha* (Dias and Barriga, 2006; Ribeiro Da Costa et al., 2008) and *Nibelungen*

526   (Melchert et al., 2008) vent sites along the Mid-Atlantic Ridge, as well as less well

527   known vent systems along the Arctic Gakkel and Indian Ocean Ridges (Bach et al., 2002;

528   Baker et al., 2004; Eickmann et al., 2009c; Gallant and Von Damm, 2006; Kumagai et

529   al., 2008; Ray et al., 2008, 2009). Interest in these systems has driven an unprecedented

530   and extremely useful burst of recent theoretical papers on peridotite hydration in the past

531   five years (Allen and Seyfried, 2004; Bach et al., 2004; Bach and Klein, 2009; Bach et

532   al., 2006; Beard et al., 2009; Emmanuel and Berkowitz, 2006; Evans, 2004; Evans, 2008;

533   Foustoukos et al., 2008; Foustoukos and Seyfried, 2007; Frost and Beard, 2007; Frost et

534   al., 2008; Iyer et al., 2008; Jamtveit et al., 2008; Klein et al., 2009; Klein and Bach, 2009;

535   McCollom, 2007; Mccollom and Bach, 2009; Seyfried et al., 2007; Shervais et al., 2005;

536   Silantyev et al., 2009a; Silantyev et al., 2009b).

537

538   Sub-seafloor peridotite carbonation is most spectacularly evident at the Lost City

539   hydrothermal area, ~ 15 km west of the Mid-Atlantic Ridge at 30°N (e.g., Früh-Green et

540   al., 2003; Kelley et al., 2001; Ludwig et al., 2006). This area is marked by chimneys tens

541   of meters tall, composed dominantly of aragonite ($CaCO_3$ polymorph) + brucite

542   ($Mg(OH)_2$). These huge chimneys are well known as a result of extensive footage in the

543   non-fiction IMAX movie, Aliens of the Deep, directed by James Cameron. Exit fluid

544   temperatures at Lost City are 40 to 91°C, high compared to peridotite-hosted alkaline

545   springs on land, but quite low compared to maximum fluid temperatures at other

546   hydrothermal vent sites along mid-ocean ridges. A lower temperature (maximum fluid

547   temperature measured to date is 40°C), near-shore example of spectacular submarine

548   peridotite carbonation is known in New Caledonia, where an aragonite + brucite chimney

549   more than 35 meters tall has formed above an alkaline spring in peridotite extending

550   upward from the seafloor at about 40 meters below sealevel (Launay and Fontes, 1985).

551

552   Kelley et al. (2001) suggested that low fluid temperatures at Lost City, compared to other

553   vent sites worldwide, reflect the fact that while others have a magmatic heat source, Lost

554   City may be heated by exothermic hydration of peridotite (serpentinization), as proposed

555   in general by Schuiling (1964) and Fyfe (1974). Exothermic heating via peridotite

556   carbonation may also be imporant (Kelemen and Matter, 2008). Experimental data

557   coupled with thermodynamic calculations (Allen and Seyfried, 2004; Seyfried et al.,

558   2007) suggest that maximum fluid temperatures in the sub-surface may have been ~

559   200°C, with subsequent cooling to produce 40-75°C exit fluids at Lost City. Thus, it is

560 possible that listwanites in Oman and elsewhere record conditions similar to the "reaction

561 zone" below the Lost City hydrothermal vent.

562

563 Higher temperature, peridotite-hosted hydrothermal vents with maximum fluid

564 temperatures ~ 400°C, including the well-studied Rainbow and Logatchev sites, lack

565 solid carbonate minerals because exit fluid temperatures and CO_2 contents are too high

566 and too low, respectively, for carbonate saturation. However, conductively-cooled,

567 diffusely venting fluids around such sites do reach solid carbonate saturation, as in

568 carbonate cemented breccias around the Rainbow and Saldanha vent sites (Ribeiro Da

569 Costa et al., 2008).

570

571 Diffuse interaction between seafloor peridotite and seawater at low temperature probably

572 produces more solid carbonate than the more spectacular features at focused

573 hydrothermal vents (Dias and Barriga, 2006; Eickmann et al., 2009a; Eickmann et al.,

574 2009c; Lein et al., 2007; Ribeiro Da Costa et al., 2008). Low temperatures of carbonate

575 formation (~ 0°C), and thus formation near the seafloor, are indicated by stable isotope

576 data on peridotites drilled from 0 to 70 m below seafloor (mbsf) along the Iberian

577 continental margin (Agrinier et al., 1996; Agrinier et al., 1988; Evans and Baltuck, 1988;

578 Gibson et al., 1996; Milliken and Morgan, 1996). Late carbonate veins in peridotite,

579 cross-cutting all other structural features, were also drilled off the conjugate,

580 Newfoundland continental margin, ~140 to 180 mbsf, below sediments including tectonic

581 breccias with peridotite blocks that also host carbonate veins (Müntener and Manatschal,

582 2006; Tucholke et al., 2004). Data discussed in Section 2.6 indicate that peridotite drill

583 core from Ocean Drilling Program Legs 153 and 209 contains an average carbon

584 concentration equivalent to 0.6 wt% CO_2, though most of these rocks lack visible

585 carbonate veins.

586

587

588

589

590

591   **S6. Additional information on**

592   **global significance of natural peridotite carbonation**

593

594   Primitive mid-ocean ridge basalts contain between 100 and 1500 ppm CO_2, and carry ~

595   10^{12} moles of C from the mantle toward the surface (Saal et al., 2006; Shaw et al., 2010).

596   Correlation between carbon concentrations and ^{3}He in high temperature hydrothermal

597   vent fluids suggests that most of the magmatic carbon is exsolved from crystallizing

598   basalt in the crust, and added to the hydrosphere (summaries in Resing et al., 2004; Shaw

599   et al., 2010). This observation has mainly been made for $CO_2/^3$He at intermediate- to fast-

600   spreading ridges, but extends to $CH_4/^3$He at the peridotite-hosted, high temperature

601   Rainbow hydrothermal field on the slow-spreading Mid-Atlantic Ridge (German et al.,

602   2010). However, as pointed out by Frieder Klein (pers. comm.. 2010), at slow spreading

603   ridges where mafic plutons are emplaced into peridotite, magmatic CO_2 may react with

604   surrounding peridotites to form carbonate minerals. In this case, carbon/^{3}He ratios in

605   associated hydrothermal fluids should be low, as observed at Lost City (Proskurowski et

606   al., 2008). If carbonate minerals do form via lower temperature reaction of cooling

607   magmatic fluids with peridotite, this could form substantial quantities of carbonate at

608   depths ~ 10 km in slow-spreading oceanic lithosphere. If this occurred for 10% of the

609   magmatic CO_2 at slow spreading ridges, this could consume ~ 10^{10} moles/yr, about $1/10^{th}$

610   of the rate derived in Section 2.6 for carbon uptake via seawater alteration of peridotite.

611

612   Some carbonate in near surface peridotite could have formed from "primary", mantle

613   carbon. Carbonate minerals in the adiabatically upwelling mantle beneath mid-ocean

614   ridges are consumed during melting, leading to nearly complete extraction of carbon

615   from the mantle source into basaltic magmas (e.g., Saal et al., 2006; Shaw et al., 2010).

616   However, there may be some settings – for example, during slow uplift and unroofing of

617   continental peridotite massifs – where temperatures remain low enough to retain primary

618   carbon. CO_2 concentrations in the mantle source of mid-ocean ridge basalts, prior to

619   melting, are estimated to range from 50 to 150 ppm, substantially less than the

620   concentration in altered peridotites near the seafloor (Figure 3).

621

622   **S7. Stable isotope data: Kinetic fractionation in young travertines**

623

624   Peridotite-hosted travertines in Oman with ^{14}C ages less than 1000 years show positively

625   correlated $\delta^{18}O$ and $\delta^{13}C$, with both ratios ranging over about 20 ‰ down to very light

626   values (Figures 4 and S1), as previously observed for a single Oman travertine deposit by

627   Clark and co-workers (Clark and Fontes, 1990; Clark et al., 1992). The correlation

628   between $\delta^{18}O$ and $\delta^{13}C$ has a slope of 0.96 with r^2 of 0.89 for Clark and Fontes' data, and

629   a slope of 1.33 with r^2 of 0.87 for our data. Similar, correlated $\delta^{18}O$ and $\delta^{13}C$ with a slope

630   ~ 1 are found in peridotite-hosted carbonates in California, Canada and the Balkans, and

631   in tufa deposits in southern Egypt (Figure 4), whereas travertines and carbonate

632   evaporites from other environments do not show the same magnitude or trend of

633   variation, as discussed below. On the other hand, very similar variations (slope, range of

634   data) of correlated, stable carbon and oxygen isotope ratios have been found in some

635   studies of very low temperature precipitation of carbonates from alkaline ground waters

636   in soils and tunnels (Dietzel et al., 1992; Renforth et al., 2009) and in dissolved and

637   redeposited mortar and plaster building materials (Kosednar-Legenstein et al., 2008).

638

639   The fractionation of carbon and oxygen isotopes in young travertines may be due to

640   stable isotope fractionation during diffusive CO_2 uptake from the atmosphere (Clark et

641   al., 1992; Hammer et al., 2005; O'Neil and Barnes, 1971; Power et al., 2007; Wilson et al.

642   2010), and/or to biologically mediated precipitation of carbonate minerals (e.g., Blank et

643   al., 2009; Delacour et al., 2008; Léveillé et al., 2007; Morrill et al., 2009; Power et al.,

644   2007). Van Strydonck et al. (1989), Clark et al. (1992), Kosednar-Legenstein et al. (2008)

645   and Wilson et al. (2010) have presented a persuasive combination of experimental data

646   and theoretical reasoning to support the hypothesis that carbon and oxygen isotope

647   fractionation occur via abiotic, kinetic processes in a thin film of aqueous fluid overlying

648   carbonates depositing from alkaline fluids (pH 11-12) characteristic of alkaline springs

649   forming peridotite-hosted travertines. As for kinetic stable isotope fractionation during

650   biological precipitaton of carbonate (McConnaughey, 1989a, b), Clark et al. proposed

651   that carbon isotope fractionation occurs during preferential uptake of light, ^{12}C in

652   hydroxylation of $CO_2 + OH^-$ to form HCO_3^-, an essential step in forming solid carbonate.

653   Equilibrium partitioning of oxygen isotopes causes OH⁻ to be ~ 40 ‰ lighter than H_2O in

654   aqueous fluid (Green and Taube, 1963). McConnaughy showed that such effects are

655   maximized in solutions with high pH. Clark et al. proposed that during wet periods in

656   Oman, pH of peridotite hosted springs was lower, and equilibrium isotope exchange was

657   maintained, while during arid periods kinetic fractionation of carbon isotopes, and the

658   effect of oxygen isotope fractionation between OH⁻and H_2O, were most marked.

659   However, only one of the experimental studies (Kosednar-Legenstein et al., 2008) has

660   produced correlated $^{13}C/^{12}C$ and $^{18}O/^{16}O$ variations with the slope and magnitude seen for

661   Oman and California travertines, and for carbonates in ultramafic mine tailings in

662   Canada, seen in Figure 4, and it remains unclear to us how the consistent slope close to 1

663   for variation in $\delta^{18}O$ vs $\delta^{13}C$ is produced in natural systems.

664

665   Young, peridotite-hosted travertines in California and western Canada show correlated,

666   20 ‰ variations in both $\delta^{18}O$ and $\delta^{13}C$, almost identical in slope and magnitude to those

667   we observe in Oman (Figure 4). Fallick et al. (1991) reported a ~ 12 ‰ variation in $\delta^{13}C$

668   (slope of 1.15) correlated with a ~ 10 ‰ variation in $\delta^{18}O$ for all but one of several

669   Miocene, "sedimentary" magnesite deposits in the former Yugoslavia, which are spatially

670   associated with peridotites hosting abundant magnesite veins. Similarly, Smith et al.

671   (2004) reported a weakly correlated, 7 ‰ variation in both $\delta^{18}O$ and $\delta^{13}C$ for tufas from

672   the "hyperarid" Egyptian desert. All of these data seem to be accounted for by the

673   hypothesis of Clark et al. (1992), though other explanations were offered in several of the

674   papers cited here.

675

676   In contrast, travertines and carbonate evaporites from other environments do not show the

677   same magnitude or trend of variation. Andrews (Andrews, 2006) reviewed stable isotope

678   data for tufa deposits, and found no correlation between $\delta^{18}O$ and $\delta^{13}C$, and very limited

679   ranges in variability, in all localities except that reported by Smith et al. in Egypt.

680   Correlated $\delta^{18}O$ and $\delta^{13}C$ variations, attributable to atmospheric temperature and/or

681   precipitation fluctuations, are seen at some low-temperature travertine sites (Brasier et al.,

682   2010; Liu et al., 2006; Sun and Liu, 2010), but do not exceed a few per mil. Travertines

683   associated with Mammoth Hot Springs in Yellowstone show correlated $\delta^{18}O$ and $\delta^{13}C$,

684 over 8 and 4 ‰, respectively, with a slope of about ½, attributable to cooling of

685 hydrothermal effluent (Chafetz and Guidry, 2003), while the Troll thermal springs in

686 Svalbard show correlated $\delta^{18}O$ and $\delta^{13}C$ variations with a slope of about 1 but a range of

687 only ~ 1 ‰ (Jamtveit et al., 2006). Canet et al. (2003) found a 29 ‰ variation in $\delta^{13}C$,

688 associated with a 7 ‰ variation in $\delta^{18}O$, in travertines formed around hydrothermal vents

689 on the shallow seafloor off the west coast of Mexico, and (2006) a 33 ‰ range in $\delta^{13}C$

690 with less than 1 ‰ variation in $\delta^{18}O$ associated with cold methane seeps in the Gulf of

691 Mexico, and attributed these variations to biological fractionation of carbon isotopes by

692 methanogens. Miocene magnesite evaporates in Turkey show an 8 ‰ variation in $\delta^{13}C$,

693 uncorrelated with a 2 ‰ variation in $\delta^{18}O$ (Alçiçek, 2009), while Triassic, magnesite-rich

694 evaporites in northern Italy show a very poorly correlated range of ~ 15 ‰ in both $\delta^{18}O$

695 and $\delta^{13}C$ (Lugli et al., 2002). These data, contrasting with those for peridotite hosted

696 travertine and magnesite deposits, and for carbonates formed from alkaline waters at very

697 low temperatures in soils and building materials, again seem to be consistent with the

698 hypothesis of Clark et al. (1992) that high pH, sustained by low water/rock ratios in arid

699 environments, is required to produce large, correlated variations in $\delta^{18}O$ and $\delta^{13}C$.

700

S8. Stable isotope data for
peridotite-hosted carbonates in seafloor and Alpine settings

703

704 Stable isotope data from the Lost City hydrothermal area along the Mid-Atlantic Ridge

705 (Früh-Green et al., 2003) indicate very different conditions of formation, compared to

706 data for peridotite-hosted carbonate vein and travertine samples from California and

707 Oman. Aragonite and calcite-rich chimney samples from Lost City, which might be

708 considered comparable to on-land travertine deposits, are close to oxygen isotope

709 exchange equilibration with seawater at seafloor temperature (~ -5 to 5°C for calcite with

710 $\delta^{18}O$ of 33 to 36 ‰, assuming water with $\delta^{18}O = 0$ relative to SMOW). Two calcite vein

711 samples from gabbro and serpentinized peridotite near the hydrothermal vent area may

712 have equilibrated with vent fluid ($\delta^{18}O= 0$) at 93 to 125°C, and thus at much higher

713 temperature than carbonate veins in peridotite from California or Oman, though perhaps

714   at temperatures similar to the Lost City reaction zone at depth, and to formation

715   temperatures for listwanites.

716

717   Other data for carbon and oxygen isotopes in oceanic samples of calcite and aragonite

718   veins in serpentinized peridotite, from the Mid-Atlantic Ridge and drill sites on the

719   Iberian abyssal plain, are similar to data for the Lost City carbonate chimneys, with δ^{13}C

720   (VPDB) from ~ -1 to 2 ‰, δ^{18}O (SMOW) of 30 to 35 ‰, and very low formation

721   temperatures consistent with near-seafloor crystallization (Agrinier et al., 1996; Agrinier

722   et al., 1988; Bonatti et al., 1980; Evans and Baltuck, 1988; Milliken and Morgan, 1996).

723

724   Like the Lost City samples, and unlike peridotite-hosted travertines in Oman, California,

725   Canada and the Balkans, "ophicalcites" and carbonate veins in serpentinized peridotite

726   from Switzerland and northern Italy have very restricted δ^{13}C from ~ -4 to 3 (Abart and

727   Pozzorini, 2000; Barbieri et al., 1979; Früh-Green et al., 1990; Pozzorini and Früh-Green,

728   1996). However, compared to most oceanic samples, Alpine, Ligurian and Appenine

729   ophicarbonates and veins have a larger range of δ^{18}O, ~ 5.5 to 25 ‰ relative to SMOW,

730   and relatively low δ^{18}O values compared to veins in California and Oman. We attribute

731   the relatively light δ^{18}O values at the *heavier* end of the range, compared to Oman, to the

732   fact that most of the Swiss and Italian samples contain calcite rather than dolomite and

733   magnesite, since calcite has lower δ^{18}O than magnesite at the same temperature (Chacko

734   and Deines, 2008). The lightest δ^{18}O in calcite in Swiss and Italian samples, lower than

735   20 ‰, may record metamorphic temperatures, *reset* during Alpine metamorphism.

736   However, it is also possible that some of the low δ^{18}O values in calcite, which overlap

737   those measured for carbonate veins from Lost City, reflect *formation* temperatures for

738   carbonate veins in excess of 100°C.

739

740

741

742

743

744

745   ## S9. Annotated bibliography of experimental work on
746   ## dissolution and carbonation rates in
747   ## olivine, serpentine, basalt and plagioclase

748

749   Matter and Kelemen (Matter and Kelemen, 2009) briefly reviewed kinetic data on

750   dissolution and carbonation of olivine, basalt and plagioclase. Here, we provide a more

751   complete discussion.

752

753   It is commonly assumed that mineral dissolution is the rate limiting step for reactions

754   transforming silicates to carbonates. Palandri and Kharaka (2004) summarize most of the

755   internally consistent dissolution rate data published prior to about 2003 for rock forming

756   minerals reacting with dilute aqueous solutions. More recent olivine, plagioclase and

757   basalt dissolution data include a study by Gislason and Oelkers (2003) showing that

758   basaltic glass dissolution can be much faster than dissolution of crystalline basalt, a paper

759   by Giammar et al. (2005) on olivine dissolution and carbonation, a paper by Hänchen et

760   al. (2006) on olivine dissolution at low and high P_{CO2}, a paper by Schaef and McGrail

761   (2008) on dissolution of basalt, a paper by Olsen and Rimstidt (Olsen, 2007; 2008) on the

762   effect of oxalic acid on olivine dissolution, and a paper by Prigiobbe et al. (2009) refining

763   the dependence of olivine dissolution rates on pH.

764

765   Some recent experimental studies investigated the effects of adding various salts and

766   organic ligands on the rate of serpentine and olivine dissolution in aqueous fluids.

767   Addition of NaCl, LiCl, NH_4Cl, $MgSO_4$, Na_2SO_4, KNO_3 and $Mg(NO_3)_2$ has little effect

768   on the rate of serpentine or olivine dissolution (Hänchen et al., 2006; Krevor, 2008;

769   Olsen, 2007; Prigiobbe et al., 2009). Addition of organic ligands increases the rate of

770   olivine and serpentine dissolution by up to a factor of five (Hänchen et al., 2006; Krevor,

771   2008; Olsen, 2007; Olsen and Rimstidt, 2008).

772

773   Most of the studies of olivine, plagioclase and basalt show a substantial decrease in

774   dissolution rates with increasing pH, up to about pH 8. Dissolution rate and the activity of

775   hydrogen (10^{-pH}) typically show a very systematic power law relationship. There are few

776   data for dissolution at high pH though basalt dissolution rates in one study increased from

777   pH 7 to 9 (Gislason and Oelkers, 2003), but this has not been demonstrated for olivine.

778

779   Paradoxically, however, the fastest known rates for olivine carbonation were obtained at

780   pH 8, as described below. As a result of this, and because the natural peridotite

781   carbonation system in Oman and elsewhere involves aqueous fluids with pH of 8 and

782   higher, in comparing different data sets we focus mainly on rates at pH 8 (Figure 5).

783   Because many experiments were done at or near a grain size of 70 microns, and not all

784   experimental data sets yielded quantitative relationships between grain size and reaction

785   rate, we converted data reported in terms of gm dissolved per square meter of surface

786   area per second ($gm/(m^2 s)$) to units of mass fraction per second (1/s), using the surface

787   area and volume of 70 micron spheres with a density of ~ 3000 kg per cubic meter.

788

789   All of the references listed above focus on fairly conventional dissolution rate

790   experiments, in the sense that they were done at very low solute concentration. An

791   exception is that Giammar et al. (2005) also did experiments at higher solute

792   concentration to investigate carbonate precipitation as well as olivine dissolution.

793

794   There are few conventional kinetic studies of carbonate mineral crystallization kinetics.

795   Hänchen et al. (2008) performed experiments on the kinetics of precipitation of the

796   magnesium carbonate minerals nesquehonite ($MgCO_3 \cdot 3H_2O$), hydromagnesite

797   (($MgCO_3)_4 \cdot Mg(OH)_2 \cdot 4H_2O$) and magnesite ($MgCO_3$), while Saldi et al. (2009) made

798   detailed studies of magnesite growth kinetics. Hänchen et al. report that in their

799   experiments, nesquehonite precipitated at 25°C and 1 bar P_{CO2}, hydromagnesite which

800   recrystallized to magnesite in 5 to 15 hours at 120°C and 3 bars P_{CO2}, and magnesite at

801   120°C and 100 bars P_{CO2}, in keeping with semi-quantitative results mentioned by

802   O'Connor et al. (2003) and McKelvy et al. (2004). Both nesquehonite and

803   hydromagnesite are thought to be thermodynamically metastable with respect to

804   magnesite and/or brucite plus fluid at all pressures and temperatures (Hänchen et al.,

805   2008). Nevertheless, they are observed in some surficial carbonate deposits associated

806   with peridotite in Canada and California (e.g., Blank et al., 2009; O'Neil and Barnes,

807   1971; Power et al., 2007; Wilson et al., 2009). In rock samples from Oman, we have not

808   observed nesquehonite or hydromagnesite, or any other hydrous magnesium carbonate

809   minerals, in travertines or veins. (We have not yet analyzed ephemeral films on pools at

810   alkaline springs). We interpret these field observations, together with the kinetic data of

811   Hänchen et al. (2008), to indicate that low humidity and/or high mean annual and

812   summertime temperatures in Oman, in excess of 40°C for several months, increase the

813   likelihood of direct precipitation of magnesite from fluid, and accelerate the

814   recrystallization of metastable hydrous magnesium carbonates to form magnesite.

815

816   In addition to the relatively conventional kinetic studies discussed above, there are two

817   very different experimental studies combining olivine dissolution with carbonate mineral

818   precipitation, in which olivine + H_2O + CO_2 + various salts in solutions with high

819   bicarbonate concentrations were held in a closed reaction vessel, with the system open

820   only to CO_2. These experiments were done to seek optimal conditions for olivine

821   carbonation at the Albany Research Center (ARC) of the Dept. of Energy (DOE), and at

822   Arizona State University (ASU).

823

824   The fastest rates in a substantial survey of possible conditions by ARC were at 185°C in

825   aqueous solutions with 1M NaCl and 0.64M $NaHCO_3$ at P_{CO2} of hundreds of bars. These

826   results were confirmed and extended by ASU as described below. Although short

827   published papers report some of the data resulting from these studies (Béarat et al., 2006;

828   Chen et al., 2006; Gerdemann et al., 2007; Jarvis et al., 2009), neither the ARC or ASU

829   work is well documented in the peer-reviewed literature. Instead, the best summaries are

830   available in unreviewed reports to DOE reports that can be found online (Chizmeshya et

831   al., 2007; O'Connor et al., 2004). Unfortunately, even in their report to DOE, Chizmeshya

832   et al. (2007) have figures illustrating data that are not reported in tables. Kelemen and

833   Matter (2008) fit ARC data in terms of mass fraction reacted per second as a function of

834   temperature and P_{CO2}. Figure 5 shows curves based on our fits to the ARC data.

835

836   Note that in general we fit data from experiments with a duration of one hour. While it

837   might be expected that experiments with longer run times would show dramatically

838   slower reaction rates, ARC data for experiments with run times up to 6 hours show rates

839   that decrease by less than a factor of three between 26% and 93% carbonation of olivine

840   (Figure S4). Thus, our fits to data from one hour experiments (~ 50% carbonation at

841   optimal conditions) are sufficient for order of magnitude estimates of rates over a range

842   of reaction progress and time.

843

844   Because the ARC and ASU experiments were done at high olivine:fluid ratios (typically

845   ~ 1:4), olivine was not as strongly undersaturated as in experiments using more dilute

846   solutions. For this reason, conventional wisdom might suggest that the ARC and ASU

847   experiments would have yielded slower rates of reaction compared to more conventional

848   experiments at low solute concentration. However, Figure 5 shows that in fact the ARC

849   and ASU rates were thousands of times faster than rates in conventional olivine

850   dissolution experiments at the same pH and grain size, and thousands of times faster than

851   rates in plagioclase and basalt dissolution experiments at the same pH and grain size

852   (*except* the Gislason & Oelkers (2003) experiments on basalt glass).

853

854   Why are the ARC and ASU rates so much faster than in other experiments on olivine?

855   We considered several possibilities:

856

857   (1) Perhaps ARC & ASU rates were high due to precipitation of magnesite ($MgCO_3$),

858   which could potentially buffer Mg concentration at a low value, and so enhance olivine

859   dissolution. However, Giammar et al. (2005) also did experiments involving precipitation

860   of magnesite, and the rates in these experiments were not exceptionally high compared to

861   the conventional olivine dissolution data.

862

863   (2) Perhaps ARC & ASU rates were high because of high P_{CO2}. However, both Giammar

864   et al. (2005) and Hanchen et al. (2006) investigated olivine dissolution at high P_{CO2}

865   without seeing a rate enhancement compared to comparable experiments at lower P_{CO2}.

866

867   (3) Perhaps ARC & ASU rates were high because they used a 1M NaCl solution.

868   However, Hanchen et al (2006), Krevor (2008) and Olsen (2007) found no significant

869   rate enhancement at elevated concentrations of NaCl, LiCl, and NH_4Cl, $MgSO_4$, Na_2SO_4,

870   KNO_3 and $Mg(NO_3)_2$.

871

872   (4) Most likely, the high rates in the ARC and ASU experiments were due to the 0.64M

873     $NaHCO_3$ (sodium bicarbonate) concentrations in their aqueous starting solutions.

874   Chizmeshya et al. (2007) explicitly investigated the rate dependence on concentration of

875     $NaHCO_3$, $KHCO_3$, and $RbHCO_3$, and showed that rapid olivine carbonation is due, at

876   least in part, to high bicarbonate concentrations, with 50 to 60% carbonation of < 38

877   micron olivine per hour between ~ 1.5 and 3.5M $NaHCO_3$, and 50 to 70% carbonation

878   between ~ 4.5 and 7.5M $KHCO_3$.

879

880   The ARC data – and our fit to the ARC data – do not show a rate enhancement due to

881   high $NaHCO_3$ alone. When P_{CO2} is 0.0004 bars, our fit (Figure 5) and the ARC

882   experiments themselves show olivine carbonation rates that are essentially identical to

883   rates in conventional olivine dissolution experiments at the same temperature, pressure

884   and pH. Thus, high $NaHCO_3$ concentration only increases the olivine carbonation rate in

885   combination with high P_{CO2}.

886

887   Chizmeshya et al. (2007) show that the rate enhancement due to $NaHCO_3$ is greatest for

888   relatively coarse-grained olivine samples (158% enhancement for grains < 150 microns)

889   compared to fine grained samples (35% increase for < 38 micron samples), and suggest

890   that this indicates that the presence of high bicarbonate concentrations interferes with

891   formation of a "passivating layer" of SiO_2 on dissolving olivine surfaces. In general, the

892   thickness of the passivating layer is thought to be limited by buckling, cracking and

893   spallation associated with volume change during reaction, and $NaHCO_3$ is thought to

894   enhance the processes that limit the thickness of this layer (Chizmeshya et al., 2007;

895   Jarvis et al., 2009).

896

897

898

899

900   ## S10. Natural carbonation rates in serpentine mine tailings

901

902   Wilson et al. (2009) studied carbonation of a serpentinite tailings pile associated with an

903   asbestos mine in British Columbia. They infer carbonation rates $\sim 10^{-10}$/s for the upper

904   meter of the tailings pile. This is faster than the rate obtained by O'Connor et al. (2004)

905   for low temperature carbonation of 70 micron serpentine powder without prior heat

906   treatment of the serpentine. Wilson et al. report a surface area $\sim 10^4$ m^2 per kg for the

907   serpentinite mine tailings. This is quite a large value, perhaps because the tailings include

908   tiny, fibrous particles. If the tailings were composed of spherical or cubic grains, this

909   would correspond to a grain size less than one micron, substantially smaller than in the

910   experiments by O'Connor et al. (2004). As noted by Wilson et al., milling of ore

911   produces very fine grained tailings favorable for mineral carbonation, which may explain

912   why the natural rates of low temperature serpentine carbonation are much faster than the

913   laboratory rates in the same temperature interval.

914

915   ## S11. Fracture and vein distribution in partially carbonated peridotite

916

917   The spatial frequency and orientation of fracture networks in partially serpentinized

918   and/or carbonated peridotite are almost unknown. Logs of fracture and vein frequency in

919   core from Ocean Drilling Project holes in peridotite are available (e.g., Kelemen et al.,

920   2004), but poor core recovery, particularly in the most fractured parts of a peridotite

921   formation, renders these of limited value. Jamtveit and co-workers (Iyer et al., 2008;

922   Jamtveit et al., 2008) have studied small scale fracture networks, in plagioclase within

923   olivine + plagioclase igneous rocks ("troctolites") and in partially serpentinized

924   peridotite.

925

926   We collected data on the width and orientation of veins exposed in small, newly eroded

927   canyons (Figure 9) and along newly created road cuts in Oman. Most outcrops and even

928   road cuts are parallel to one set of veins, so there are few measurable intersections of that

929   vein set with the parallel outcrop surface. Thus, data for several surfaces must be

930   combined. Our data confirm a qualitative impression, and the observations and models of

931   Iyer et al. (2008), that carbonate veins in many outcrops have three mutually orthogonal,

932   preferred orientations. This may result from fracture formation involving isotropic,

933   internally generated stress due to solid volume increase during peridotite hydration and

934   carbonation. However, observation of two or three mutually orthogonal joint sets is

935   common, for example in quarries (Bloomfield, 1996; Rouleau and Gale, 1985). Fletcher

936   et al. (2006) and Iyer et al. (2008) show that this is a relatively predictable consequence

937   of reaction along a planar front, or uniaxial tensile stress. So for example exfoliation of

938   granite proceeds via fracture parallel to the outcrop surface (least compressive stress)

939   followed by buckling of the exfoliated sheets, and cracking perpendicular to the outcrop

940   surface (e.g., review and figures compiled by Pollard and Aydin, 1988).

941

942   Some of our data – for measurements taken along newly eroded, vertical canyon walls –

943   show a set of nearly horizontal fractures roughly parallel to the paleo-outcrop surface,

944   and a second set of nearly vertical fractures perpendicular to the outcrop surface. The

945   steep set of fractures terminates at the horizontal fracture set, while the horizontal set of

946   veins continues uninterrupted through these intersections, indicating that the steep set

947   formed later (Figure 9). This is consistent with models (Fletcher et al., 2006; Rudge et al.,

948   2010) in which volume expansion in a diffusive reaction zone drives fracture parallel to

949   the weathering surface, followed by buckling of the detached, weathered layer, and

950   subsequent cracking perpendicular to the weathering surface.

951

952   ## S12. Cost of heating a sub-surface rock volume

953   ## for engineered, *in situ* mineral carbonation

954

955   To raise the temperature of a sub-surface rock volume by 100°C requires 90 kJ/kg

956   peridotite with heat capacity 900 J/kgK. Since complete carbonation consumes 0.62 kg

957   CO_2/kg peridotite, this is ~ 145 kJ/kg CO_2 consumed. *If the combination of heating of*

958   *water, heat transfer to peridotite, and peridotite carbonation are 5 to 20% efficient*, this

959   requires ~ 3000 to 700 kJ/kg of CO_2 consumed. Burning fossil fuel produces 32,000 to

960   54,000 kJ per kilogram of fuel consumed, or ~ 9000 to 15,000 kJ per kg CO_2 produced.

961   For these parameters, the energy penalty for heating a subsurface rock volume, to store an

962   initial mass of CO_2 (plus the additional CO_2 produced for heating), is ~ 6 to 30%. If

963   heating is done using oil, at \$80 per barrel, i.e. ~ \$0.50 per kilogram of fuel, heating

964   would cost \$8 to \$41 per ton of initial CO_2 stored.

965

966   **S14: Comparison of reaction rate to supply rate**

967   **during thermal convection of seawater through peridotite**

968

969   Seawater at 150 bars has P_{CO2} ~ 0.06 bars. According to the parameterization of Kelemen

970   and Matter (2008), the rate of natural olivine carbonation at 185°C and 0.06 bars P_{CO2}

971   (with added $NaHCO_3$ if necessary) is about ~ 1/50 of the rate at 150 bars P_{CO2}, or ~ 1%

972   per year. At 0.06 bars P_{CO2} and 25°C, the rate is predicted to be ~ 2×10^{-6} per year. This is

973   larger than the practical supply rate, as we show in the next two paragraphs.

974

975   The CO_2 supply rate is limited by the concentration of CO_2 in seawater and the fluid flux.

976   In turn, the fluid flux is limited by porous flow rates proportional to the pressure gradient

977   driving fluid flow and the permeability of the rock, or on the maximum practical flow

978   through drill holes, whichever is smaller. If one assumes that hydraulic fracture can

979   create an arbitrarily large surface area for injecting fluid into porous peridotite, flow in

980   drill pipes may often be the limiting factor. For an average flow velocity of 20 m/s or

981   less, and 13" (17 cm) pipe, the fluid flux is ≤ 2 m^3/s, delivering ≤ 6000 tons of CO_2 per

982   year. Maximum fluid velocities attained so far in enhanced geothermal systems that are

983   sited in crystalline rocks are only ~ 0.3 m/s, with a tenfold improvement projected over

984   the next decade (e.g., Genter et al., 2010). A flow velocity of 3.5 m/s would result in

985   consumption of 1000 tons of CO_2 per year per drill hole.

986

987   The Darcy flux (product of velocity and porosity) for aqueous fluid with a viscosity of

988   10^{-3} Pa s leaving the larger cracks within a hydraulic fracture network and passing into

989   peridotite with porosity of 1% and permeability of 10^{-13} m^2 (Section S15 of this electronic

990   supplement, below), driven by a pressure gradient of 100 kg/m^3 * 10 m/s^2, or 1000 Pa/m,

991   would be 10^{-7} m/s. The fluid velocity would be 10^{-5} m/s in pore space. To accommodate

992   ≤ 2 m^3/s of fluid flow from the drill pipe via porous flow into peridotite at a Darcy flux of

993   10^{-7} m/s, the area of the network of larger fractures from which the fluid flows into

994   peridotite must be $\leq 2 \cdot 10^{7}$ m^{2}. The fluid would then pass by porous flow through $\sim 2 \cdot 10^{13}$

995   kg of peridotite in a year. If the ≤ 6000 tons of CO_2 in the fluid is consumed, this

996   corresponds to an uptake rate $\leq 3 \cdot 10^{-7}$ per year, less than the olivine carbonation reaction

997   rate at 0.06 bars P_{CO2} and 25°C, $\sim 2 \cdot 10^{-6}$ per year as derived in the first paragraph of this

998   section. Thus, the CO_2 uptake rate in thermal convection of seawater through peridotite

999   will be supply limited, and not limited by the olivine carbonation rate.

1000

1001   ## S15. Porosity and permeability in peridotite (and basalt)

1002

1003   Proposed methods for enhanced, *in situ* peridotite (or basalt) carbonation involve flow of

1004   either CO_2 rich fluids or seawater through a fracture network with sufficiently high

1005   permeability to allow appreciable flux via injection or via thermal convection. Also, the

1006   fracture network must have sufficiently high surface area to allow rapid reaction. It

1007   probably would be necessary to create additional fracture porosity via "hydraulic

1008   fracture" from boreholes. However, between fractures, flow and reactive surface area will

1009   depend on pre-existing structures and – perhaps – on cracking driven by volume changes

1010   during mineral hydration and carbonation (Section 4). For these reasons, it is important to

1011   understand natural porosity and permeability in peridotites near the Earth's surface.

1012

1013   For comparison, we begin with a review of data on basaltic permeability. Basaltic lava

1014   flows and shallow intrusions of basalt ("dolerite", "diabase") often have high

1015   permeability caused by lava emplacement processes and formation of large fractures

1016   during cooling and contraction (e.g., Alt and Teagle, 1999; Bartetzko, 2005; Becker and

1017   Davis, 2003; Fisher, 1998; Fisher and Becker, 2000; Fisher et al., 1997; Schramm et al.,

1018   2005). McGrail et al. (2006) showed that interbedded layers of brecciated and vesicular

1019   basalt within dense low-permeability units of the Columbia River Basalt Group may have

1020   the regional extent, permeability and porosity to support large volume CO_2 storage.

1021   Estimated capacities for storage of supercritical CO_2 in pore space in the Columbia River

1022   Basalt range between 36-148 billion tons (McGrail et al., 2006). Goldberg et al. (2008)

1023   and Goldberg and Slagle (2009) estimated potential storage capacities for several deep-

1024   sea basalt aquifers, including 500-2500 billion tons of CO_2 in the Juan de Fuca Ridge

1025   region, and 1000-5500 billion tons in the Caribbean flood basalt provinces. Low

1026   permeability marine sediments overlying basalt act as stratigraphic traps. Similarly, basalt

1027   aquifers on land may be confined by low-permeability sedimentary interbeds and

1028   paleosoils. Nonetheless, one can anticipate that a substantial problem with injecting CO_2

1029   into basalt for long term storage in pore space would be its generally high porosity and

1030   permeability.

1031

1032   In comparison with basalt, ultramafic rocks such as mantle peridotite have lower porosity

1033   and permeability, dominated by fissures in the weathered upper ~50 m and by fractures in

1034   the deeper subsurface (e.g., Dewandel et al., 2005), though data are scarce. Permeability

1035   is likely to be scale-dependent due to fracture size/frequency distributions. Peridotite may

1036   have a permeability similar to other crystalline rocks in the upper crust, ranging from 10^{-13}

1037   to 10^{-10} for 1% fracture porosity, based on large scale measurements at shallow depths

1038   (e.g., Wu et al., 2006), or 10^{-17} to 10^{-14} m^2 based on smaller scale measurements at greater

1039   depths (review in Manning and Ingebritsen, 1999). One study of catchment-scale

1040   groundwater flow estimated the permeability of the fissured weathering horizon in mantle

1041   peridotite in Oman to be ~10^{-14} m^2 (Dewandel et al., 2005). Peridotite fracture

1042   permeability can probably be enhanced by hydraulic fracture, as in "hot dry rock"

1043   geothermal reservoirs in other types of crystalline rocks (Audigane et al., 2002; Dorbath

1044   et al., 2009; Ito, 2003; Phillips et al., 2002). As for petroleum reservoirs in fractured

1045   rocks, fractured ultramafic rocks could be excellent CO_2 storage reservoirs as long as

1046 CO_2 is mainly stored as solid carbonate minerals, and/or fractured networks are overlain

1047   by a low permeability cap.

1048

1049   ## S16. Comparison of peridotite versus basalt carbonation

1050

1051   In this section, we briefly discuss the potential for *in situ* basalt carbonation, for

1052   comparison with the methods for peridotite carbonation discussed above. Olivine

1053   carbonation rates are the fastest known for abundant, rock-forming minerals. Futhermore,

1054   there are natural examples of abundant, present-day carbonate formation in peridotites at

1055   near-surface conditions in a variety of geological settings, and widespread of fully

1056   carbonated peridotite (listwanite) occurrences comprising 10^{10} to 10^{11} tons worldwide,

1057   whereas we are not aware of any examples of fully carbonated basalt. For these reasons,

1058   we have focused our research on *in situ* peridotite carbonation. However, as discussed in

1059   Sections 3 and S9, the fastest olivine carbonation rates were measured under conditions

1060   that have not been explored for other, common rock forming minerals. The most common

1061   rock type in the Earth's crust is basalt, a type of lava that forms the upper 1 to 2 km of

1062   igneous oceanic crust worldwide (about 70% of the surface of the solid Earth), and is

1063   present as large "flood basalt provinces" onland.

1064

1065   Basalt, when fully crystalline, is composed of ~ 10% olivine, with another ~ 30%

1066 $(Ca,Mg,Fe)_2Si_2O_6$ pyroxenes, and ~ 60% plagioclase (a solid solution typically

1067   containing ~ 60% $CaAl_2Si_2O_8$ and 40% $NaAlSi_3O_8$ when present in basalt). Because

1068   basalt contains more SiO_2 and Al_2O_3 than peridotite, divalent cations that readily form

1069   carbonate minerals (Mg, Ca, …) have concentrations in basalt that are approximately

1070   25% of concentrations in peridotite. However, if basalt mineral carbonation rates were

1071   comparable to olivine carbonation rates, or if basalt formations were found to contain

1072   large volumes of glass (with a much higher reaction rate than crystalline basalt Gislason

1073   and Oelkers, 2003), the high abundance of basalt compared to peridotite, and the high

1074   porosity of some basalt lava flows, would render basalt as attractive as, or more attractive

1075   than, peridotite for *in situ* mineral carbonation.

1076

1077   **Captions for supplementary tables**

1078

1079   **Table S1:** Parameters for estimating uptake of CO_2 via natural peridotite carbonation in

1080   the ophiolite massifs of northern Oman. Data from Kelemen and Matter (2008) and our

1081   unpublished work.

1082

1083   **Table S2:** Parameters for estimating the relative mass of sub-surface veins in peridotite,

1084   versus surficial travertine deposits associated with alkaline springs in peridotite

1085   catchments. Data sources: Liguria (Cipolli et al., 2004) and L. Marini, pers. comm., 2008.

1086   California (Barnes et al., 1967; Barnes and O'Neil, 1969). Oman (our unpublished data

1087   and Dewandel et al., 2005; Matter, 2001; Neal and Stanger, 1985).

1088

1089   **Table S3:** Preliminary, whole rock oxygen isotope data for travertine and carbonate vein

1090   samples from peridotite in the ophiolite massifs of northern Oman. Calcite-rich travertine

1091   samples, for which whole-rock isotope ratios approximate the isotope composition of

1092   calcite, are marked by rows in bold font), as are magnesite-rich samples.

1093

Captions for supplementary figures

1095

1096   **Figure S1:** Plots of $\delta^{13}C$ and $\delta^{18}O$ vs ^{14}C age, for data from Table S3. Correlated

1097   variation of $\delta^{13}C$ and $\delta^{18}O$ (Figure 4) is present only in samples with ^{14}C age less than

1098   1000 years. See Section S7 for discussion.

1099

1100   **Figure S2:** Updated ^{14}C age histogram including the data reported by Kelemen and

1101   Matter (2008), which is also in Table S3, and additional data for analogous, additional

1102   samples with sample preparation and ^{14}C analyses performed in the same manner (but for

1103   samples lacking $\delta^{18}O$ or $^{87}Sr/^{86}Sr$ measurements). These additional data are available

1104   from the authors upon request.

1105

1106   **Figure S3:** A. Oxygen and carbon isotope compositions for our data (Table S3),

1107   compared to magnesium carbonate minerals in serpentine mine tailings from British

1108   Columbia (Wilson et al., 2009), sediments beneath the Oman peridotite (Weyhenmeyer,

1109   2000), and sediments beneath the British Columbia mine tailings (Wilson et al., 2009).

1110   Sediments in British Columbia are a possible source for the low $\delta^{18}O$, low $\delta^{13}C$

1111   component in the mine tailings carbonates, but sediments in Oman are not a likely end

1112   member for peridotite-hosted carbonate veins and travertines in Oman. B & C. Sr isotope

1113   compositions for our samples (Table S3) compared to samples of partially hydrated

1114   peridotites from the same massifs as our samples (Gerbert-Gaillard, 2002), sediments

1115   beneath the Oman peridotite (Weyhenmeyer, 2000), groundwater and alkaline spring

1116   waters from the Oman peridotite (Weyhenmeyer, 2000), and carbonate deposits from the

1117   Lost City hydrothermal deposit on the Mid-Atlantic Ridge (Früh-Green et al., 2003). See

1118   text for discussion.

1119

1120   **Figure S4:** Our fit to the data of O'Connor et al. (2004) on the extent of olivine

1121   carbonation as a function of time, for experiments at 185°C, 150 bars P_{CO2}, in aqueous

1122   fluid with 1M NaCl and 0.64M $NaHCO_3$.

1123
1124   **References cited in this supplement**
1125

1126   Abart, R., and Pozzorini, D., 2000, Implications of kinetically controlled mineral-fluid exchange
1127   on the geometry of stable-isotope fornts: Eur. J. Mineral., v. 12, p. 1069-1082.
1128   Agrinier, P., Cornen, G., and Beslier, M.-O., 1996, Mineralogical and oxygen isotopic features of
1129   serpentinites recovered from the ocean/continent transition in the Iberia abyssal plain, in
1130   Whitmarsh, R.B., Sawyer, D.S., Klaus, A., and Masson, D.G., eds., Proceedings of the Ocean
1131   Drilling Program, Scientific Results 149: College Station, TX, ODP, p. 541-552.
1132   Agrinier, P., Mevel, C., and Girardeau, J., 1988, Hydrothermal alteration of the peridotites cored
1133   at the ocean/continent boundary of the Iberian margin: Petrologic and stable isotope evidence,
1134   in Boillot, G., Winterer, E.L., and al., e., eds., Proceedings of the Ocean Drilling Program,
1135   Scientific Results 103: College Station, TX, ODP, p. 225-234.
1136   Akbulut, M., Piskin, O., and Karayigit, A.I., 2006, The genesis of the carbonatized and silicified
1137   ultramafics known as listvenites: A case study from the Mihaliccik region (Eskisehir), NW
1138   Turkey: Geol. J., v. 41, p. 557-580.
1139   Al Lazki, A.I., Seber, D., Sandvol, E., and Barazangi, M., 2002, A crustal transect across the
1140   Oman Mountains on the eastern margin of Arabia: GeoArabia, v. 7, p. 47-78.
1141   Alçiçek, H., 2009, Late Miocene nonmarine sedimentation and formation of magnesites in the
1142   Acigöl Basin, southwestern Anatolia, Turkey: Sedimentary Geol., v. 219, p. 115-135.
1143   Allen, D.E., and Seyfried, W.E., 2004, Serpentinization and heat generation: Constraints from
1144   Lost City and Rainbow hydrothermal systems: Geochim. Cosmochim. Acta, v. 68, p. 1347-
1145   1354.
1146   Alt, J.C., and Shanks, W.C., 2006, Stable isotope compositions of serpentinite seamounts in the
1147   Mariana forearc: Serpentinization processes, fluid sources and sulfur metasomatism: Earth
1148   and Planetary Science Letters, v. 242, p. 272-285.
1149   Alt, J.C., and Teagle, D.A.H., 1999, The uptake of carbon during alteration of oceanic crust:
1150   Geochim. Cosmochim. Acta, v. 63, p. 1527-1535.
1151   Andrews, J.E., 2006, Paleoclimatic records from stable isotopes in riverine tufas: Synthesis and
1152   review: Earth Sci. Rev., v. 75, p. 85-104.
1153   Auclair, M., Gauthier, M., Trottier, J., Jébrak, M., and Chartrand, F., 1993, Mineralogy,
1154   geochemistry, and paragenesis of the Eastern Metals serpentinite-associated Ni-Cu-Zn
1155   deposit, Quebec Appalachians: Econ. Geol., v. 88, p. 123-138.
1156   Audigane, P., Royer, J.-J., and Kaieda, H., 2002, Permeability characterization of the Soultz and
1157   Ogachi large-scale reservoir using induced microseismicity: Geophysics, v. 67, p. 204-211.
1158   Bach, W., Banerjee, N.R., Dick, H.J.B., and Baker, E.T., 2002, Discovery of ancient and active
1159   hydrothermal systems along the ultra-slow spreading Southwest Indian Ridge 10 degrees-16
1160   degrees E: Geochemistry Geophysics Geosystems, v. 3.

1161   Bach, W., Garrido, C.J., Paulick, H., Harvey, J., and Rosner, M., 2004, Seawater-peridotite
1162   interactions: First insights from ODP Leg 209, MAR 15 degrees N: Geochemistry
1163   Geophysics Geosystems, v. 5.
1164   Bach, W., and Klein, F., 2009, The petrology of seafloor rodingites: Insights from geochemical
1165   reaction path modeling: Lithos, v. 112, p. 103-117.
1166   Bach, W., Paulick, H., Garrido, C.J., Ildefonse, B., Meurer, W.P., and Humphris, S.E., 2006,
1167   Unraveling the sequence of serpentinization reactions: petrography, mineral chemistry, and
1168   petrophysics of serpentinites from MAR 15 degrees N (ODP Leg 209, Site 1274):
1169   Geophysical Research Letters, v. 33.
1170   Baker, E.T., Edmonds, H.N., Michael, P.J., Bach, W., Dick, H.J.B., Snow, J.E., Walker, S.L.,
1171   Banerjee, N.R., and Langmuir, C.H., 2004, Hydrothermal venting in magma deserts: The
1172   ultraslow-spreading Gakkel and Southwest Indian Ridges: Geochemistry Geophysics
1173   Geosystems, v. 5.
1174   Barbieri, M., Masi, U., and Tolomeo, L., 1979, Stable isotope evidence for a marine origin of
1175   ophicalcites from the north-central Apennines (Italy): Marine Geology, v. 30, p. 193-204.
1176   Barnes, I., LaMarche, V.C., and Himmelberg, G., 1967, Geochemical evidence of present-day
1177   serpentinization: Science, v. 156, p. 830-832.
1178   Barnes, I., and O'Neil, J.R., 1969, Relationship between fluids in some fresh alpine-type
1179   ultramafics and possible modern serpentinization, western United States: GSA Bull., v. 80, p.
1180   1947-1960.
1181   —, 1971, Calcium-magnesium carbonate solid solutions from Holocene conglomerate cements
1182   and travertines in Coast Range of California: Geochim. Cosmochim. Acta, v. 35, p. 699-&.
1183   Barnes, I., O'Neil, J.R., Rapp, J.B., and White, D.E., 1973, Silica-carbonate alteration of
1184   serpentine: Wall rock alteration in Mercury deposits of the California Coast-Ranges: Econ.
1185   Geol., v. 68, p. 388-398.
1186   Bartetzko, A., 2005, Effect of hydrothermal ridge flank alteration on the in situ physical
1187   properties of oceanic crust: J. Geophys. Res., v. 110, p. doi:10.1029/2004JB003228.
1188   Béarat, H., McKelvy, M.J., Chizmeshya, A.V.G., Gormley, D., Nunez, R., Carpenter, R.W.,
1189   Squires, K., and Wolf, G.H., 2006, Carbon sequestration via aqueous olivine mineral
1190   carbonation: Role of passivating layer formation: Environ. Sci. Technol., v. 40, p. 4802-4808.
1191   Beard, J.S., Frost, B.R., Fryer, P., McCaig, A., Searle, R., Ildefonse, B., Zinin, P., and Sharma,
1192   S.K., 2009, Onset and Progression of Serpentinization and Magnetite Formation in Olivine-
1193   rich Troctolite from IODP Hole U1309D: J. Petrol., v. 50, p. 387-403.
1194   Becker, K., and Davis, E., 2003, New evidence for age variation and scale effects
1195   ofpermeabilities of young oceanic crust from borehole thermal and pressure measurements:
1196   Earth Planet. Sci. Lett., v. 210, p. 499-508.
1197   Bernoulli, D., and Weissert, H., 1985, Sedimentary Fabrics in Alpine Ophicalcites, South Pennine
1198   Arosa Zone, Switzerland: Geology, v. 13, p. 755-758.
1199   Blank, J.G., Green, S.J., Blake, D., Valley, J.W., Kita, N.T., Treiman, A., and Dobson, P.F.,
1200   2009, An alkaline spring system within the Del Puerto ophiolite (California, USA): A Mars
1201   analog site: Planet. Space Sci., v. 57, p. 533-540.
1202   Bloomer, S.H., and Fisher, R.L., 1987, Petrology and geochemistry of igneous rocks from the
1203   Tonga trench: A non-accreting plate boundary: J. Geol., v. 95, p. 469-495.
1204   Bloomfield, J., 1996, Characterization of hydrologically significant fracture distributions in the
1205   Chalk: An example from the Upper Chalk of southern England: J. Hydrol., v. 184, p. 355-
1206   379.
1207   Bonatti, E., Lawrence, J.R., Hamlyn, P.R., and Breger, D., 1980, Aragonite from deep sea
1208   ultramafic rocks: Geochim. Cosmochim. Acta, v. 44, p. 1207-1214.
1209   Bonatti, E., and Michael, P., 1989, Mantle peridotites from continental rifts to ocean basins to
1210   subduction zones: Earth Planet. Sci. Lett., v. 91, p. 297-311.

1211   Boschi, C., Dini, A., Dallai, L., Ruggieri, G., and Gianelli, G., 2009, Enhanced CO2-mineral
1212   sequestration by cyclic hydraulic fracturing and Si-rich fluid infiltration into serpentinites at
1213   Malentrata (Tuscany, Italy): Chem. Geol., v. 265, p. 209-226.
1214   Boschi, C., Dini, A., Früh-Green, G.L., and Kelley, D.S., 2008, Isotopic and element exchange
1215   during serpentinization and metasomatism at the Atlantis Massif (MAR 30 N): Insights from
1216   B and Sr isotope data: Geochim. Cosmochim. Acta, v. 72, p. 1801-1823.
1217   Boschi, C., Fruh-Green, G.L., Delacour, A., Karson, J.A., and Kelley, D.S., 2006, Mass transfer
1218   and fluid flow during detachment faulting and development of an oceanic core complex,
1219   Atlantis Massif (MAR 30 degrees N): Geochemistry Geophysics Geosystems, v. 7.
1220   Brasier, A.T., Andrews, J.E., Marca-Bell, A.D., and Dennis, P.F., 2010, Depositional continuity
1221   of seasonally laminated tufas: Implications for d18O based palaeotemperatures: Global
1222   Planet. Change, v. 71, p. 160-167.
1223   Bruni, J., Canepa, M., Chiodini, G., Cioni, R., Cipolli, F., Longinelli, A., Marini, L., Ottonello,
1224   G., and Zuccolini, M.V., 2002, Irreversible water-rock mass transfer accompanying the
1225   generation of the neutral, Mg-HCO3 and high-pH, Ca-OH spring waters of the Genova
1226   province, Italy: Applied Geochem., v. 17, p. 455-474.
1227   Burns, S.J., Fleitmann, D., Matter, A., Neff, U., and Mangini, A., 2001, Speleothem evidence
1228   from Oman for continental pluvial events during interglacial periods: Geology, v. 29, p. 623-
1229   626.
1230   Canet, C., Prol-Ledesma, R.M., Escobar-Briones, E., Morterna-Gutiérrez, C., Lozano-Santa Cruz,
1231   R., Linares, C., Cienfuegos, E., and Morales-Puente, P., 2006, Mineralogical and
1232   geochemical characterization of hydrocarbon seep sediments from the Gulf of Mexico:
1233   Marine Petrol. Geol, v. 23, p. 605-619.
1234   Canet, C., Prol-Ledesma, R.M., Melgarejo, J.-C., and Reyes, A., 2003, Methane-related
1235   carbonates formed at submarine hydrothermal springs: A new setting for microbially-derived
1236   carbonates?: Marine Geology, v. 199, p. 245-261.
1237   Cannat, M., Mével, C., Maïa, M., Deplus, C., P. Gente, Agrinier, P., Belarouchi, A., Dubuisson,
1238   G., Humler, E., and Reynolds, J.R., 1995, Thin crust, ultramafic exposure and rugged faulting
1239   patterns at the Mid-Atlantic Ridge (22°-24°N): Geology, v. 23, p. 49-52.
1240   Carlson, R.L., 2001, The abundance of ultramafic rocks in the Atlantic ocean crust: Geophys. J.
1241   Int., v. 144, p. 37-48.
1242   Chacko, T., and Deines, P., 2008, Theoretical calculation of oxygen isotope fractionation factors
1243   in carbonate systems: Geochim. Cosmochim. Acta, v. 72, p. 3642-3660.
1244   Chafetz, H.S., and Guidry, S.A., 2003, Deposition and diagenesis of Mammoth Hot Springs
1245   travertine, Yellowstone National Park, Wyoming, U.S.A.: Can. J. Earth Sci., v. 40, p. 1515-
1246   1529.
1247   Charlou, J.L., Donval, J.P., Fouquet, Y., Jean-Baptiste, P., and Holm, N., 2002, Geochemistry of
1248   high H-2 and CH4 vent fluids issuing from ultramafic rocks at the Rainbow hydrothermal
1249   field (36 degrees 14 ' N, MAR): Chemical Geology, v. 191, p. 345-359.
1250   Chen, S.Y., O'Connor, W.K., and Gerdemann, S.J., 2006, Chemistry of aqueous mineral
1251   carbonation for carbon sequestration and explanation of experimental results: Environ.
1252   Progress, v. 25, p. 161-166.
1253   Chizmeshya, A.V.G., McKelvy, M.J., Squires, K., Carpenter, R.W., and Béarat, H., 2007, DOE
1254   Final Report 924162: A novel approach to mineral carbonation: Enhancing carbonation while
1255   avoiding mineral pretreatment process cost 29 pages plus appendices: Tempe, AZ, Arizona
1256   State University.
1257   Cipolli, F., Gambardella, B., Marini, L., Ottonello, G., and Zuccolini, M.V., 2004, Geochemistry
1258   of high-pH waters from serpentinites of the Gruppo di Voltri (Genova, Italy) and reaction
1259   path modeling of CO2 sequestration in serpentinite aquifers: Applied Geochem., v. 19, p.
1260   787-802.

1261 Clark, I.D., and Fontes, J.C., 1990, Paleoclimatic reconstruction in northern Oman based on
1262   carbonates from hyperalkaline groundwaters: Quaternary Res., v. 33, p. 320-336.
1263 Clark, I.D., Fontes, J.C., and Fritz, P., 1992, Stable Isotope disequilibria in travertine from high
1264   pH waters: Laboratory investigations and field observations from Oman: Geochim.
1265   Cosmochim. Acta, v. 56, p. 2041-2050.
1266 Cox, M.E., Launay, J., and Paris, J.-P., 1982, Geochemistry of low temperature geothermal
1267   systems in New Caledonia: Proc. Pacific Geothermal Conference, University of Aukland,
1268   New Zealand, Part 2, p. 453-459.
1269 Delacour, A., Früh-Green, G.L., Bernasconi, S.M., Schaeffer, P., and Kelley, D.S., 2008, Carbon
1270   geochemistry of serpentinites in the Lost City hydrothermal system (30°N, MAR): Geochim.
1271   Cosmochim. Acta, v. 72, p. 3681-3702.
1272 Dewandel, B., Lachassagne, P., Boudier, F., Al-Hattali, S., Ladouche, B., Pinault, J.-L., and Al-
1273   Suleimani, Z., 2005, A conceptual hydrogeological model of ophiolite hard-rock aquifers in
1274   Oman based on a multiscale and a multidisciplinary approach: Hydrogeology J., v. 13, p.
1275   708-726.
1276 Dias, A.S., and Barriga, F., 2006, Mineralogy and geochemistry of hydrothermal sediments from
1277   the serpentinite-hosted Saldanha hydrothermal field (36 degrees 34 ' N; 33 degrees 26 ' W) at
1278   MAR: Marine Geology, v. 225, p. 157-175.
1279 Dietzel, M., Usdowski, E., Hoefs, J., 1992, Chemical and $13C/12C$- and $18O/16O$-isotope
1280   evolution of alkaline drainage waters and the precipitation of calcite. Appl. Geochem. v. 7, p.
1281   177–184.
1282 Dorbath, L., Cuenot, N., Genter, A., and Frogneux, M., 2009, Seismic response of the fractured
1283   and faulted granite of Soultz-sous-Forets (France) to 5 km deep massive water injections:
1284   Geophys. J. Int., v. 177, p. 653-675.
1285 Douville, E., Charlou, J.L., Oelkers, E.H., Bienvenu, P., Colon, C.F.J., Donval, J.P., Fouquet, Y.,
1286   Prieur, D., and Appriou, P., 2002, The rainbow vent fluids (36 degrees 14 ' N, MAR): the
1287   influence of ultramafic rocks and phase separation on trace metal content in Mid-Atlantic
1288   Ridge hydrothermal fluids: Chemical Geology, v. 184, p. 37-48.
1289 Driesner, T., 1993, Aspects of Petrographic, Structural and Stable Isotope Geochemical Evolution
1290   of Ophicarbonate Breccias from Ocean-Floor to Subduction and Uplift - an Example from
1291   Chatillon, Middle Aosta Valley, Italian Alps: Schweizerische Mineralogische Und
1292   Petrographische Mitteilungen, v. 73, p. 69-84.
1293 Ece, O.I., Matsubaya, O., and Coban, F., 2005, Genesis of hydrothermal stockwork-type
1294   magnesite deposits associated with ophiolite complexes in the Kutahya-Eskisehir region,
1295   Turkey: Neues Jahrbuch Fur Mineralogie-Abhandlungen, v. 181, p. 191-205.
1296 Eickmann, B., Bach, W., and Peckmann, J., 2009a, Authigenesis of Carbonate Minerals in
1297   Modern and Devonian Ocean-Floor Hard Rocks: Journal of Geology, v. 117, p. 307-323.
1298 —, 2009b, Authigenesis of carbonate minerals in modern and Devonian ocean-floor hard rocks: J.
1299   Geol., v. 117, p. 307-323.
1300 Eickmann, B., Bach, W., Rosner, M., and Peckmann, J., 2009c, Geochemical constraints on the
1301   modes of carbonate precipitation in peridotites from the Logatchev Hydrothermal Vent Field
1302   and Gakkel Ridge: Chemical Geology, v. 268, p. 97-106.
1303 Emmanuel, S., and Berkowitz, B., 2006, Suppression and stimulation of seafloor hydrothermal
1304   convection by exothermic mineral hydration: Earth Planet. Sci. Lett., v. 243, p. 657-668.
1305 Evans, B.W., 2004, The serpentinite multisystem revisited: Chrysotile is metastable: Int. Geol.
1306   Rev., v. 46, p. 479-506.
1307 —, 2008, Control of the products of serpentinization by the Fe2+Mg-1 exchange potential of
1308   olivine and orthopyroxene: J. Petrol., v. 49, p. 1873-1887.
1309 Evans, C.A., and Baltuck, M., 1988, Low-temperature alteration of peridotite, Hole 637A, in
1310   Boillot, G., Winterer, E.L., and al., e., eds., Proceedings of the Ocean Drilling Program,
1311   Scientific Results 103: College Station, TX, ODP, p. 235-239.

1312 Fallick, A.E., Ilich, M., and Russell, M.J., 1991, A Stable Isotope Study of the Magnesite
1313   Deposits Associated with the Alpine-Type Ultramafic Rocks of Yugoslavia: Economic
1314   Geology and the Bulletin of the Society of Economic Geologists, v. 86, p. 847-861.
1315 Ferry, J.M., 1995, Fluid-Flow During Contact-Metamorphism of Ophicarbonate Rocks in the
1316   Bergell-Aureole, Val-Malenco, Italian Alps: Journal of Petrology, v. 36, p. 1039-1053.
1317 Fisher, A.T., 1998, Permeability within basaltic oceanic crust: Rev. Geophys., v. 36, p. 143-182.
1318 Fisher, A.T., and Becker, K., 2000, Channelized fluid flow in oceanic crust reconciles heat-flow
1319   and permeability data: Nature, v. 403, p. 71-74.
1320 Fisher, A.T., Becker, K., and Davis, E.E., 1997, The permeability of young oceanic crust east of
1321   Juan de Fuca Ridge determined using borehole thermal measurements: Geophys. Res. Lett.,
1322   v. 24, p. 1311-1314.
1323 Fisher, R.T., and Engel, C.G., 1969, Ultramafic and basaltic rocks dredged from the nearshore
1324   flank of the Tonga trench: GSA Bull., v. 80, p. 1373-1378.
1325 Fleitmann, D., Burns, S.J., Mangini, A., Mudelsee, M., Kramers, J., Villa, I., Neff, U., Al-
1326   Subbary, A.A., Buettner, A., Hippler, D., and Matter, A., 2007, Holocene ITCZ and Indian
1327   monsoon dynamics recorded in stalagmites from Oman and Yemen (Socotra): Quat. Sci.
1328   Reviews, v. 26, p. 170-188.
1329 Fleitmann, D., Burns, S.J., Mudelsee, M., Neff, U., Kramers, J., Mangini, A., and Matter, A.,
1330   2003, Holocene forcing of the Indian monsoon recorded in a stalagmite from southern Oman:
1331   Science, v. 300, p. 1737-1739.
1332 Fletcher, R.C., Buss, H.L., and Brantley, S.L., 2006, A spheroidal weathering model coupling
1333   porewater chemistry to soil thickness during steady-state denudation: Earth Planet. Sci. Lett.,
1334   v. 244, p. 444-457.
1335 Folk, R.L., and McBride, E.F., 1976, Possible Pedogenic Origin of Ligurian Ophicalcite -
1336   Mesozoic Calichified Serpentinite: Geology, v. 4, p. 327-332.
1337 Foustoukos, D.I., Savov, I.P., and Janecky, D.R., 2008, Chemical and isotopic constraints on
1338   water/rock interactions at the Lost City hydrothermal field, 30 degrees N Mid-Atlantic Ridge:
1339   Geochimica Et Cosmochimica Acta, v. 72, p. 5457-5474.
1340 Foustoukos, D.I., and Seyfried, W.E., 2007, Fluid phase separation processes in submarine
1341   hydrothermal systems, in Liebscher, A., and Heinrich, C.A., eds., Fluid-Fluid Interactions,
1342   Volume 65: Reviews in Mineralogy & Geochemistry, p. 213-239.
1343 Frost, B.R., and Beard, J.S., 2007, On silica activity and serpentinization: J. Petrol., v. 48, p.
1344   1351-1368.
1345 Frost, B.R., Beard, J.S., McCaig, A., and Condliffe, E., 2008, The formation of micro-rodingites
1346   from IODP hole U1309D: Key to understanding the process of serpentinization: J. Petrol., v.
1347   49, p. 1579-1588.
1348 Früh-Green, G., Weissert, H., and Bernoulli, D., 1990, A multiple fluid history recorded in Alpine
1349   ophiolites: J. Geol. Sco. London, v. 147, p. 959-970.
1350 Früh-Green, G.L., Kelley, D.S., Bernasconi, S.M., Karson, J.A., Ludwig, K.A., Butterfield, D.A.,
1351   Boschi, C., and Proskurowski, G., 2003, 30,000 years of hydrothermal activity at the Lost
1352   City vent field: Science, v. 301, p. 495-498.
1353 Fryer, P., 1992, Mud volcanoes of the Marianas: Scientific American, v. 266, p. 46-52.
1354 Fuchs, M., and Buerkert, A., 2008, A 20 ka sediment record from the Hajar Mountain range in N-
1355   Oman, and its implication for detecting arid-humid periods on the southeastern Arabian
1356   Peninsula: Earth Planet. Sci. Lett., v. 265, p. 546-558.
1357 Fyfe, W.S., 1974, Heats of chemical reactions and submarine heat production: Geophys. J. Roy.
1358   Astr. Soc., v. 37, p. 213-215.
1359 Gallant, R.M., and Von Damm, K.L., 2006, Geochemical controls on hydrothermal fluids from
1360   the Kairei and Edmond Vent Fields, 23 degrees-25 degrees S, Central Indian Ridge:
1361   Geochemistry Geophysics Geosystems, v. 7.

1362 Gebruk, A.V., Chevaldonne, P., Shank, T., Lutz, R.A., and Vrijenhoek, R.C., 2000, Deep-sea
1363   hydrothermal vent communities of the Logatchev area (14 degrees 45 ' N, Mid-Atlantic
1364   Ridge): diverse biotopes and high biomass: Journal of the Marine Biological Association of
1365   the United Kingdom, v. 80, p. 383-393.
1366 Gerbert-Gaillard, L., 2002, Caracterisation geochimique des peridotites de l'ophiolite d'Oman:
1367   Processus magmatiques aux limites lithosphere/asthenosphere [PhD thesis]: Montpellier,
1368   Université de Montpellier II.
1369 Gerdemann, S.J., O'Connor, W.K., Dahlin, D.C., Penner, L.R., and Rush, H., 2007, Ex situ
1370   aqueous mineral carbonation: Environ. Sci. Technol., v. 41, p. 2587-2593.
1371 German, C.R., Klinkhammer, G.P., and Rudnicki, M.D., 1996, The Rainbow hydrothermal
1372   plume, 36 degrees 15'N, MAR: Geophysical Research Letters, v. 23, p. 2979-2982.
1373 German, C.R., Thurnherr, A.M., Knoery, J., Charlou, J.L., Jean-Baptiste, P., and Edmonds, H.N.,
1374   2010, Heat, volume and chemical fluxes from submarine venting: A synthesis of results from
1375   the Rainbow hydrothermal field, 36°N MAR: Deep Sea Res. I, v. 57, p. 518-527.
1376 Genter, A., Goerke, X., Graff, J.-J., Cuenot, N., Krall, G., Schindler, M., and Ravier, G., 2010,
1377   Current status of the EGS Soultz geothermal project (France): Proc. World Geothermal Conf.,
1378   Bali, Indonesia, 25-29 April 2010, p. 1-6.
1379 Giammar, D.E., Bruant, R.G.J., and Peters, C.A., 2005, Forsterite dissolution and magnesite
1380   precipitation at conditions relevant for deep saline aquifer storage and sequestration of carbon
1381   dioxide: Chemical Geology, v. 217, p. 257-276.
1382 Gibson, I.L., Beslier, M.-O., Cornen, G., Milliken, K.L., and Seifert, K.E., 1996, Major- and
1383   trace-element seawater alteration profiles in serpentinite formed during the development of
1384   the Iberia Margin, Site 897: Proc. Ocean Drilling Program, Sci. Res., v. 149, p. 519-527.
1385 Gislason, S.R., and Oelkers, E.H., 2003, Mechanism, rates and consequences of basaltic glass
1386   dissolution: II. An experimental study of the dissolution rates of basaltic glass as a function of
1387   pH and temperature: Geochim. Cosmochim. Acta, v. 67, p. 3817-3832.
1388 Goldberg, D., and Slagle, A.L., 2009, A global assessment of deep-sea basalt sites for carbon
1389   sequestration: Energy Procedia, v. submitted.
1390 Goldberg, D.S., Takahashi, T., and Slagle, A.L., 2008, Carbon dioxide sequestration in deep-sea
1391   basalt: Proc. Nat. Acad. Sci. USA, v. 105, p. 9920-9925.
1392 Green, M., and Taube, H., 1963, Isotopic fractionation in the OH - H2O exchange reaction: J.
1393   Phys. Chem., v. 67, p. 1565-1566.
1394 Haggerty, J.A., 1991, Evidence from fluid seeps atop serpentine seamounts in the Mariana
1395   Forearc: Clues for emplacement of the seamounts and their relationship to forearc tectonics:
1396   Marine Geology, v. 102, p. 293-309.
1397 Halls, C., and Zhao, R., 1995, Listvenite and related rocks: Perspectives on terminology and
1398   mineralogy with reference to an occurrence at Cregganbaun, Co. Mayo, Republic of Ireland:
1399   Mineral. Deposita, v. 30, p. 303-313.
1400 Hammer, O., Jamtveit, B., Benning, L.G., and Dysthe, D.K., 2005, Evolution of fluid chemistry
1401   during travertine formation in the Troll thermal springs, Svalbard, Norway: Geofluids, v. 5, p.
1402   140-150.
1403 Hänchen, M., Prigiobbe, V., Baciocchi, R., and Mazzotti, M., 2008, Precipitation in the Mg-
1404   carbonate system: Effects of temperature and CO2 pressure: Chem. Eng. Sci., v. 63, p. 1012-
1405   1028.
1406 Hänchen, M., Prigiobbe, V., Storti, G., Seward, T.M., and Mazzotti, M., 2006, Dissolution
1407   kinetics of fosteritic olivine at 90–150°C including effects of the presence of CO2: Geochim.
1408   Cosmochim. Acta, v. 70, p. 4403-4416.
1409 Hanghøj, K., Kelemen, P.B., Hassler, D., and Godard, M., 2010, Composition and genesis of
1410   depleted mantle peridotites from the Wadi Tayin massif, Oman ophiolite: Major and trace
1411   element geochemistry, and Os isotope and PGE systematics: J. Petrol., v. 51, p. 206-227.

Hansen, L.D., Dipple, G.M., Gordon, T.M., and Kellett, D.A., 2005, Carbonated serpentinite (listwanite) at Atlin, British Columbia: A geological analogue to carbon dioxide sequestration: Can. Mineral., v. 43, p. 225-239.

Ito, H., 2003, Inferred role of natural fractures, veins, and breccias in development of the artificial geothermal reservoir at the Ogachi Hot Dry Rock site, Japan: J. Geophys. Res., v. 108, p. 2426, doi:10.1029/2001JB001671.

Iyer, K., Jamtveit, B., Mathiesen, J., Malthe-Sorenssen, A., and Feder, J., 2008, Reaction-assisted hierarchical fracturing during serpentinization: Earth Planet. Sci. Lett., v. 267, p. 503-516.

Jamtveit, B., Hammer, Ø., Andersson, C., Dysthe, D.K., Heldmann, J., and Fogel, M.L., 2006, Travertines from the Troll thermal springs, Svalbard: Norwegian J. Geol., v. 86, p. 387-395.

Jamtveit, B., Malthe-Sorenssen, A., and Kostenko, O., 2008, Reaction enhanced permeability during retrogressive metamorphism: Earth Planet. Sci. Lett., v. 267, p. 620-627.

Jarvis, K., Carpenter, R.W., Windman, T., Kim, Y., Nunez, R., and Alawneh, F., 2009, Reaction mechanisms for enchancing mineral sequestration of CO2: Environ. Sci. Technol., v. in press.

Jedrysek, M.O., and Sachanbinski, M., 1994, Stable-isotope and trace-element studies of vein ophicarbonates at Gogolow-Jordanow serpentinite massif (Poland): A contribution to the origin of ophiaragonite and ophimagnesite: Geochem. J., v. 28, p. 341-350.

Kelemen, P.B., Kikawa, E., and Miller, J., 2004, Igneous crystallization and localized deformation > 15 km beneath the Mid-Atlantic Ridge, 14-16 N: Geochimica Et Cosmochimica Acta, v. 68, p. A690-A690.

Kelemen, P.B., and Matter, J.M., 2008, In situ carbonation of peridotite for CO2 storage: Proc. Nat. Acad. Sci. USA, v. 105, p. 17,295-17,300.

Kelley, D.S., Karson, J.A., Blackman, D.K., Fruh-Green, G.L., Butterfield, D.A., Lilley, M.D., Olson, E.J., Schrenk, M.O., Roe, K.K., Lebon, G.T., and Rivizzigno, P., 2001, An off-axis hydrothermal vent field near the Mid-Atlantic Ridge at 30 degrees N: Nature, v. 412, p. 145-149.

Kelley, D.S., Karson, J.A., Fruh-Green, G.L., Yoerger, D.R., Shank, T.M., Butterfield, D.A., Hayes, J.M., Schrenk, M.O., Olson, E.J., Proskurowski, G., Jakuba, M., Bradley, A., Larson, B., Ludwig, K., Glickson, D., Buckman, K., Bradley, A.S., Brazelton, W.J., Roe, K., Elend, M.J., Delacour, A., Bernasconi, S.M., Lilley, M.D., Baross, J.A., Summons, R.T., and Sylva, S.P., 2005, A serpentinite-hosted ecosystem: The Lost City hydrothermal field: Science, v. 307, p. 1428-1434.

Klein, F., Bach, W., Jons, N., McCollom, T., Moskowitz, B., and Berquo, T., 2009, Iron partitioning and hydrogen generation during serpentinization of abyssal peridotites from 15 degrees N on the Mid-Atlantic Ridge: Geochimica Et Cosmochimica Acta, v. 73, p. 6868-6893.

Klein, F., and Bach, W.G., 2009, FeNiCoOS Phase Relations in PeridotiteSeawater Interactions: Journal of Petrology, v. 50, p. 37-59.

Konn, C., Charlou, J.L., Donval, J.P., Holm, N.G., Dehairs, F., and Bouillon, S., 2009, Hydrocarbons and oxidized organic compounds in hydrothermal fluids from Rainbow and Lost City ultramafic-hosted vents: Chemical Geology, v. 258, p. 299-314.

Kosednar-Legenstein, B., Dietzel, M., Leis, A., Stingl, K., 2008, Stable carbon and oxygen isotope investigation in historical lime mortar and plaster: Results from field and experimental study, App. Geochem., v. 23, p. 2425-2437.

Krevor, S.C., 2008, Developments in mineral carbon dioxide sequestration [PhD thesis]: New York, Columbia University.

Krevor, S.C., Graves, C.R., Van Gosen, B.S., and McCafferty, A.E., 2009, Mapping the mineral resource base for mineral carbon-dioxide sequestration in the conterminous United States: U.S. Geological Survey Digital Data Series 414, 14 p., 1 plate. [Only available at URL http://pubs.usgs.gov/ds/414].

1462   Kumagai, H., Nakamura, K., Toki, T., Morishita, T., Okino, K., Ishibashi, J.I., Tsunogai, U.,
1463   Kawagucci, S., Gamo, T., Shibuya, T., Sawaguchi, T., Neo, N., Joshima, M., Sato, T., and
1464   Takai, K., 2008, Geological background of the Kairei and Edmond hydrothermal fields along
1465   the Central Indian Ridge: Implications of their vent fluids' distinct chemistry: Geofluids, v. 8,
1466   p. 239-251.
1467   Lang, S.Q., Butterfield, D.A., Schulte, M.D., Kelley, D.S., and Lilley, M.D., 2010, Elevated
1468   concentrations of formate, acetate and dissolved organic carbon found at the Lost City
1469   hydrothermal field: Geochim. Cosmochim. Acta, v. 74, p. 941-952.
1470   Launay, J., and Fontes, J.-C., 1985, Les sources thermales de Prony (Nouvelle-Calédonie) et leurs
1471   précipités chimiques: Exemple de formation de brucite primaire: Géologie de la France, p.
1472   83-100.
1473   Leake, B.E., Tanner, P.W.G., and Senior, A., 1975, Composition and Origin of Connemara
1474   Dolomitic Marbles and Ophicalcites, Ireland: Journal of Petrology, v. 16, p. 237-257.
1475   Lein, A.Y., Bogdanova, O.Y., Bogdanov, Y.A., and Magazina, L.I., 2007, Mineralogical and
1476   geochemical features of authigenic carbonates on seepings and hydrothermal fields (By the
1477   examples of the Black Sea reefs and the mounds of the Lost City field): Oceanology, v. 47, p.
1478   537-553.
1479   Lemoine, M., 1980, Serpentinites, Gabbros and Ophicalcites in the Piemont-Ligurian Domain of
1480   the Western Alps - Possible Indicators of Oceanic Fracture-Zones and of Associated
1481   Serpentinite Protrusions in the Jurassic-Cretaceous Tethys: Archives Des Sciences, v. 33, p.
1482   103-115.
1483   Léveillé, R.J., Longstaffe, F.J., and Fyfe, W.S., 2007, An isotopic and geochemical study of
1484   carbonate-clay mineralization in basaltic caves: Abiotic versus microbial processes:
1485   Geobiology, v. 5, p. 235-249.
1486   Liu, Z., Li, H., You, C., Wan, N., and Sun, H., 2006, Thickness and stable isotopic characteristics
1487   of modern seasonal climate-controlled sub-annual travertine laminas in a travertine-
1488   depositing stream at Baishuitai, SW China: Implications for paleoclimate reconstruction:
1489   Environ. Geol., v. 51, p. 257-265.
1490   Ludwig, K.A., Kelley, D.S., Butterfield, D.A., Nelson, B.K., and Früh-Green, G., 2006,
1491   Formation and evolution of carbonate chimneys at the Lost City hydrothermal field:
1492   Geochim. Cosmochim. Acta, v. 70, p. 3625-3645.
1493   Lugli, S., Morteani, G., and Blamart, D., 2002, Petrographic, REE, fluid inclusion and stable
1494   isotope study of magnesite from the Upper Triassic Burano evaporites (Secchia Valley,
1495   northern Apennines): Contributions from sedimentary, hydrothermal and metasomatic
1496   sources: Mineral. Deposita, v. 37, p. 480-494.
1497   Madu, B.E., Nesbitt, B.E., and Muehlenbachs, K., 1990, A mesothermal gold-stibnite-quartz vein
1498   occurrence in the Canadian Cordillera: Econ. Geol., v. 85, p. 1260-1268.
1499   Manning, C.E., and Ingebritsen, E., 1999, Permeability of the continental crust: implications of
1500   geothermal data and metamorphic systems: Rev. Geophys., v. 37, p. 127-150.
1501   Matter, J.M., 2001, Geochemical evolution and hydrodynamics of groundwaters in the alluvial
1502   aquifer of the Dakhiliya Area, Sultanate of Oman, ETH-Zurich.
1503   Matter, J.M., and Kelemen, P.B., 2009, Permanent CO_2 storage and mineral carbonation in
1504   geologic reservoirs: Nature Geoscience, v. 2, p. 837-841.
1505   McCollom, T., 2007, Geochemical constraints on sources of metabolic energy for
1506   chemolithoautotrophy in ultramafic-hosted deep-sea hydrothermal systems: Astrobiology, v.
1507   7, p. 933-950.
1508   Mccollom, T.M., and Bach, W., 2009, Thermodynamic constraints on hydrogen generation
1509   during serpentinization of ultramafic rocks: Geochim. Cosmochim. Acta, v. 73, p. 856-875.
1510   McConnaughey, T., 1989a, 13C and 18O isotopic disequilibrium in biological carbonates: I.
1511   Patterns: Geochim. Cosmochim. Acta, v. 53, p. 151-162.

1512 —, 1989b, 13C and 18O isotopic disequilibrium in biological carbonates: II. In vitro simulation
1513   of kinetic isotope effects: Geochim. Cosmochim. Acta, v. 53, p. 163-171.
1514 McGrail, B.P., Schaef, H.T., Ho, A.M., Chien, Y.-J., Dooley, J.J., and Davidson, C.L., 2006,
1515   Potential for carbon dioxide sequestration in flood basalts: J. Geophys. Res., v. 111, p.
1516   B12201, doi: 10.1029/2005JB004169.
1517 McKelvy, M.J., Chizmeshya, A.V.G., Diefenbacher, J., Bearat, H., and Wolf, G., 2004,
1518   Exploration of the role of heat activation in enhancing serpentine carbon sequestration
1519   reactions: Environ. Sci. Technol., v. 38, p. 6897-6903.
1520 Melchert, B., Devey, C.W., German, C.R., Lackschewitz, K.S., Seifert, R., Walter, M., Mertens,
1521   C., Yoerger, D.R., Baker, E.T., Paulick, H., and Nakamura, K., 2008, First evidence for high-
1522   temperature off-axis venting of deep crustal/mantle heat: The Nibelungen hydrothermal field,
1523   southern Mid-Atlantic Ridge: Earth and Planetary Science Letters, v. 275, p. 61-69.
1524 Milliken, K.L., and Morgan, J.K., 1996, Chemical evidence for near-seafloor precipitation of
1525   calcite in serpentinites (Site 897) and serpentinite breccias (Site 899), Iberia abyssal plain, in
1526   Whitmarsh, R.B., Sawyer, D.S., Klaus, A., and Masson, D.G., eds., Proceedings of the Ocean
1527   Drilling Program, Scientific Results 149: College Station, TX, ODP, p. 553-558.
1528 Morrill, P.L., Johnson, O.J., Cotton, J., Eigenbrode, J.L., and Nealson, K.H., 2009, Microbial
1529   hydrocarbon gases in ultrabasic reducing waters at a continental site of active serpentinization
1530   in N. California: Geochim. Cosmochim. Acta, v. submitted.
1531 Mottl, M.J., Komor, S.C., Fryer, P., and Moyer, C.L., 2003, Deep-slab fluids fuel extremophilic
1532   Archaea on a Mariana forearc serpentinite mud volcano: Ocean Drilling Program Leg 195: G-
1533   cubed, v. 4, p. doi:10.1029/2003GC000588.
1534 Mottl, M.J., Wheat, G., Fryer, P., Gharib, J., and Martin, J.B., 2004, Chemistry of springs across
1535   the Mariana forearc shows progressive devolatilization of the subducting plate: Geochim.
1536   Cosmochim. Acta, v. 68, p. 4915-4933.
1537 Müntener, O., and Manatschal, G., 2006, High degrees of melt extraction recorded by spinel
1538   harzburgite of the Newfoundland margin: The role of inheritance and consequences for the
1539   evolution of the southern North Atlantic: Earth Planet. Sci. Lett., v. 252, p. 437-452.
1540 Naldrett, A.J., 1966, Talc-carbonate alteration of some serpentinized ultramafic rocks south of
1541   Timmins, Ontario: J. Petrol., v. 7, p. 489-499.
1542 Nasir, S., Al Sayigh, A.R., Al Harthy, A., Al-Khirbash, S., Al-Jaaidi, O., Musllam, A., Al-
1543   Mishwat, A., and Al-Bu'saidi, S., 2007, Mineralogical and geochemical characterization of
1544   listwaenite from the Semail ophiolite, Oman: Chemie Der Erde, v. 67, p. 213-228.
1545 Neal, C., and Shand, P., 2002, Spring and surface water quality of the Cyprus ophiolites: Hydrol.
1546   Earth Sys. Sci., v. 6, p. 797-817.
1547 Neal, C., and Stanger, G., 1983, Hydrogen generation from mantle source rocks in Oman: Earth
1548   Planet. Sci. Lett., v. 66, p. 315-320.
1549 —, 1984, Calcium and magnesium-hydroxide precipitation from alkaline groundwaters in Oman,
1550   and their significance to the process of serpentinization: Min. Mag., v. 48, p. 237-241.
1551 —, 1985, Past and present serpentinization of ultramafic rocks: An example from the Semail
1552   ophiolite nappe of northern Oman, in Drewer, J.I., ed., The Chemistry of Weathering:
1553   Holland, D. Reidel Publishing Company, p. 249-275.
1554 O'Connor, W.K., Dahlin, D.C., Nilsen, D.N., Gerdemann, S.J., Rush, G.E., Penner, L.R., Walters,
1555   R.P., and Turner, P.C., 2003, Continuing studies on direct aqueous mineral carbonation for
1556   CO2 sequestration, presented at 27th International Technical Conference on Coal Utilization
1557   and Fuel Systems, Clear Water, Florida, March 4-7, 2002: DOE/ARC-02-003, v. 13 pp.
1558 O'Connor, W.K., Dahlin, D.C., Rush, G.E., Gerdemann, S.J., and Nilsen, D.N., 2004, Final
1559   report: Aqueous mineral carbonation, DOE/ARC-TR-04-002: Albany, OR, Office of Process
1560   Development, Albany Research Center, Office of Fossil Energy, US DOE, p. 21 pages plus
1561   appendices.

1562   O'Neil, J.R., and Barnes, I., 1971, C13 and O18 compositions in some fresh-water carbonates
1563   associated with ultramafic rocks and serpentinites, western United-States: Geochim.
1564   Cosmochim. Acta, v. 35, p. 687-&.
1565   Olsen, A.A., 2007, Forsterite dissolution kinetics: Applications and implications for chemical
1566   weathering [PhD thesis]: Blacksburg VA, USA, Virginia Polytechnic Institute.
1567   Olsen, A.A., and Rimstidt, J.D., 2008, Oxalate-promoted forsterite dissolution at low pH:
1568   Geochim. Cosmochim. Acta, v. 72, p. 1758-1766.
1569   Palandri, J.L., and Kharaka, Y.K., 2004, A compilation of rate parameters of water-mineral
1570   interaction kinetics for application to geochemical modeling: US Geological Survey Open
1571   File Report, v. 2004-1068, p. 1-64.
1572   Phillips, W.S., Rutledge, J.T., House, L.S., and Fehler, M.C., 2002, Induced microearthquake
1573   patterns in hydrocarbon and geothermal reservoirs: Six case studies Pure Appl. Geophys., v.
1574   159, p. 345-369.
1575   Pollard, D.D., and Aydin, A., 1988, Progress in understanding jointing over the past century:
1576   GSA Bull., v. 100, p. 1181-1204.
1577   Poupeau, G., Saddiqi, O., Michard, A., Goffé, B., and Oberhänsli, R., 1998, Late thermal
1578   evolution of the Oman Mountains subophiolitic windows: Apatite fission-track
1579   thermochronology: Geology, v. 26, p. 1139-1142.
1580   Power, I.M., Wilson, S.A., Thom, J.M., Dipple, G.M., and Southam, G., 2007, Biologically
1581   induced mineralization of dypingite by cyanobacteria from an alkaline wetland near Atlin,
1582   British Columbia, Canada: Geochem. Transactions, v. 8, p. doi:10.1186/1467-4866-8-13.
1583   Pozzorini, D., and Früh-Green, G.L., 1996, Stable isotope systematics of the Ventina
1584   Ophicarbonate Zone, Bergell contact aureole: Schweiz. Min. Pet. Mitt., v. 76, p. 549-564.
1585   Prigiobbe, V., Costa, G., Baciocchi, R., Hänchen, M., and Mazzotti, M., 2009, The effect of CO2
1586   and salinity on olivine dissolution kinetics at 120°C: Chem. Eng. Sci., v. 64, p. 3510-3515.
1587   Proskurowski, G., Lilley, M.D., Kelley, D.S., and Olson, E.J., 2006, Low temperature volatile
1588   production at the Lost City Hydrothermal Field, evidence from a hydrogen stable isotope
1589   geothermometer: Chemical Geology, v. 229, p. 331-343.
1590   Proskurowski, G., Lilley, M.D., Seewald, J.S., Frueh-Green, G., Olson, E.J., Lupton, J.E., Sylva,
1591   S.P., and Kelley, D.S., 2008, Abiogenic hydrocarbon production at Lost City hydrothermal
1592   field: Science, v. 319, p. 604-607.
1593   Ray, D., Banerjee, R., Iyer, S.D., and Mukhopadhyay, S., 2008, A New Report of Serpentinites
1594   from Northern Central Indian Ridge (at 6 degrees S) - An Implication for Hydrothermal
1595   Activity: Acta Geologica Sinica-English Edition, v. 82, p. 1213-1222.
1596   —, 2009, Evidences for seawater-rock hydrothermal interaction in the serpentinites from
1597   Northern Central Indian Ridge: Current Science, v. 97, p. 1239-1243.
1598   Renforth, P., Manning, D. A. C., Lopez-Capel, E., 2009, Carbonate precipitation in artificial soils
1599   as a sink for atmospheric carbon dioxide. Appl. Geochem., v. 24, p. 1757–1764.
1600   Resing, J.A., Lupton, J.E., Feely, R.A., and Lilley, M.D., 2004, CO2 and 3He in hydrothermal
1601   plumes: Implications for mid-ocean ridge CO2 flux: Earth Planet. Sci. Lett., v. 226, p. 449-
1602   464.
1603   Ribeiro Da Costa, I., Barriga, F.J.A.S., and Taylor, R.N., 2008, Late seafloor carbonate
1604   precipitation in serpentinites from the Rainbow and Saldanha sites (Mid-Atlantic Ridge): Eur.
1605   J. Mineral., v. 20, p. 173-181.
1606   Robinson, P.T., Malpas, J., Zhou, M.F., Ash, C., Yang, J.S., and Bai, W.J., 2005, Geochemistry
1607   and origin of listwanites in the Sartohay and Luobnsa ophiolites, China: Int. Geol. Rev., v.
1608   47, p. 177-202.
1609   Rouleau, A., and Gale, J.E., 1985, Statistical characterization of the fracture system in the Stripa
1610   granite, Sweden: Int. J. Rock Mech. Min. Sci. & Geomech. Abstr., v. 22, p. 352-367.

1611 Rudge, J.F., Kelemen, P.B., and Spiegelman, M., 2010, A simple model of reaction induced
1612   cracking applied to serpentinization and carbonation of peridotite: Earth Planet. Sci. Lett., v.
1613   291, p. 215-227.
1614 Saal, A.E., Hauri, E.H., Langmuir, C.H., and Perfit, M.R., 2006, Vapour undersaturation in
1615   primitive mid-ocean ridge basalt and the volatile content of the Earth's upper mantle: Nature,
1616   v. 419, p. 451-455.
1617 Saldi, G.D., Jordan, G., Schott, J., and Oelkers, E.H., 2009, Magnesite growth rates as a function
1618   of temperature and saturation state: Geochim. Cosmochim. Acta, v. 73, p. 5646-5657.
1619 Schaef, H.T., and McGrail, B.P., 2008, Dissolution of Columbia River Basalt under mildly acidic
1620   conditions as a function of temperature: Experimental results relevant to the geological
1621   sequestration of carbon dioxide: Applied Geochem., v. 24, p. 980-987.
1622 Schandl, E.S., and Wicks, F.J., 1991, Carbonate and associated alteration of ultramafic and
1623   rhyolitic rocks at the Hemingway Property, Kidd Creek Volcanic Complex, Timmins,
1624   Ontario: Econ. Geol., v. 88, p. 1615-1635.
1625 Schmidt, K., Koschinsky, A., Garbe-Schonberg, D., de Carvalho, L.M., and Seifert, R., 2007,
1626   Geochemistry of hydrothermal fluids from the ultramafic-hosted Logatchev hydrothermal
1627   field, 15 degrees N on the Mid-Atlantic Ridge: Temporal and spatial investigation: Chemical
1628   Geology, v. 242, p. 1-21.
1629 Schramm, B., Devey, C., Gillis, K.M., and Lackschewitz, K., 2005, Quantitative assessment of
1630   chemical and mineralogical changes due to progressive low-temperature alteration of East
1631   Pacific Rise basalts from 0 to 9 Ma: Chem. Geol., v. 218, p. 281-313.
1632 Schuiling, R.D., 1964, Serpentization as a possible cause of high heat-flow values in and near the
1633   oceanic ridges: Nature, v. 201, p. 807-808.
1634 Seyfried, W.E., Foustoukos, D.I., and Fu, Q., 2007, Redox evolution and mass transfer during
1635   serpentinization: An experimental and theoretical study at 200 C, 500 bar with implications
1636   for ultramafic-hosted hydrothermal systems at Mid-Ocean Ridges: Geochim. Cosmochim.
1637   Acta, v. 71, p. 3872-3886.
1638 Shaw, A.M., Behn, M.D., Humphris, S.E., Sohn, R.A., and Gregg, P.M., 2010, Deep pooling of
1639   low degree melts and volatile fluxes at the 85°E segment of the Gakkel Ridge: Evidence from
1640   olivine-hosted melt inclusions and glasses: Earth Planet. Sci. Lett., v. 289, p. 311-322.
1641 Shervais, J.W., Kolesar, P., and Andreasen, K., 2005, A field and chemical study of
1642   serpentinization, Stonyford, California: Chemical flux and mass balance: Int. Geol. Rev., v.
1643   47, p. 1-23.
1644 Silantyev, S., Mironenko, M., and Novoselov, A., 2009a, Hydrothermal systems in peridotites of
1645   slow-spreading mid-oceanic ridges. Modeling phase transitions and material balance:
1646   Downwelling limb of a hydrothermal circulation cell: Petrology, v. 17, p. 138-157.
1647 Silantyev, S.A., Mironenko, M.V., and Novoselov, A.A., 2009b, Hydrothermal systems hosted in
1648   peridotites at slow-spreading ridges. Modeling phase transformations and material balance:
1649   Upwelling limb of the hydrothermal cell: Petrology, v. 17, p. 523-536.
1650 Smith, J.R., Giegengack, R., and Schwarcz, H.P., 2004, Constraints on Pleistocene pluvial
1651   climates through stable-isotope analysis of fossil-spring tufas and associated gastropods,
1652   Kharga Oasis, Egypt: Palaeogeog. Palaeoclimat. Palaeoecol., v. 206, p. 157-175.
1653 Spiridonov, E.M., 1991, Listvenites and zodites: Int. Geol. Rev., v. 33, p. 397-407.
1654 Stanger, G., 1985, Silicified serpentinite in the Semail nappe of Oman: Lithos, v. 18, p. 13-22.
1655 Sudarikov, S.M., and Roumiantsev, A.B., 2000, Structure of hydrothermal plumes at the
1656   Logatchev vent field, 14 degrees 45 ' N, Mid-Atlantic Ridge: evidence from geochemical and
1657   geophysical data: Journal of Volcanology and Geothermal Research, v. 101, p. 245-252.
1658 Sun, H., and Liu, Z., 2010, Wet-dry seasonal and spatial variations in the d13C and d18O values
1659   of the modern endogenic travertine at Baishuitai, Yunnan, SW China and their paleoclimatic
1660   and paleoenvironmental implications: Geochim. Cosmochim. Acta, v. 74, p. 1016-1029.

1661 Surour, A.A., and Arafa, E.H., 1997, Ophicarbonates: Calichified serpentinites from Gebel
1662   Mohagara, Wadi Ghadir area, Eastern Desert, Egypt: Journal of African Earth Sciences, v.
1663   24, p. 315-324.
1664 Talarico, F., Kleinschmidt, G., and Henjes-Kunst, F., 1999, First report of an ophiolitic complex
1665   in the northern Shackleton Range, Antarctica: Terra Antartica, v. 6, p. 293-316.
1666 Trommsdorff, V., Evans, B., and Pfeifer, H.R., 1980, Ophicarbonate rocks: Metamorphic
1667   reactions and possible origin: Archives des Sciences Genève, v. 33, p. 3610364.
1668 Trommsdorff, V., and Evans, B.W., 1977, Antigorite-ophicarbonates: Contact metamorphism in
1669   Valmalenco, Italy: Contrib. Mineral. Petrol., v. 62, p. 301-312.
1670 Tsikouras, B., Karipi, S., Grammatikopoulos, T.A., and Hatzipanagiotou, K., 2006, Listwaenite
1671   evolution in the ophiolite melange of Iti Mountain (continental central Greece): Eur. J.
1672   Mineral., v. 18, p. 243-255.
1673 Tucholke, B., Sibuet, J.-C., and Klaus, A., 2004, Proceedings of the Ocean Drilling Programm,
1674   Initial reports, vol. 210, Online at http://www-odp.amu.edu/publications/210_IR/210ir.htm:
1675   College Station TX, Ocean Drilling Program.
1676 Ucurum, A., 2000, Listwaenites in Turkey: Perspectives on formation and precious metal
1677   concentration with reference to occurrences in East-Central Anatolia: Ofioliti, v. 25, p. 15-29.
1678 Van Strydonck, M.J.Y., Dupas, M., Keppens, E., Isotopic fractionation of oxygen and carbon
1679   isotopes in mortar under natural environmental conditions, Radiocarbon, v. 31, p. 610-618.
1680 Weissert, H., and Bernoulli, D., 1984, Oxygen Isotope Composition of Calcite in Alpine
1681   Ophicarbonates - a Hydrothermal or Alpine Metamorphic Signal: Eclogae Geologicae
1682   Helvetiae, v. 77, p. 29-43.
1683 Weyhenmeyer, C.E., 2000, Origin and evolution of groundwater in the alluvial aquifer of the
1684   eastern Batinah coastal plain, Sultanate of Oman: A hydrogeochemical approach: Bern,
1685   Switzerland, Universität Bern.
1686 Weyhenmeyer, C.E., Burns, S.J., Waber, H.N., Aeschbach-Hertig, W., Kipfer, R., Loosli, H.H.,
1687   and Matter, A., 2000, Cool glacial temperatures and changes in moisture source recorded in
1688   Oman groundwaters: Science, v. 287, p. 842-845.
1689 Wilde, A., Simpson, L., and Hanna, S., 2002, Preliminary study of Cenozoic alteration and
1690   platinum deposition in the Oman ophiolite: J. Virtual Explorer, v. 6, p. 7-13.
1691 Wilson, S.A., Barker, S.L.L., Dipple, G.M., and Atudorei, 2010, Isotopic disequilibrium during
1692   uptake of atmospheric CO2 into mine process waters: Implications for CO2 sequestration,
1693   Env. Sci. Tech., v. 44, p. 9522-9529.
1694 Wilson, S.A., Dipple, G.M., Power, I.M., Thom, J.M., Anderson, R.G., Raudsepp, M., Gabites,
1695   J.E., and Southam, G., 2009, Carbon dioxide fixation within mine wastes of ultramafic-hosted
1696   ore deposits: Examples from the Clinton Creek and Cassiar Chrysotile deposits, Canada:
1697   Econ. Geol., v. 104, p. 95-112.
1698 Wilson, S.A., Raudsepp, M., and Dipple, G.M., 2006, Verifying and quantifying carbon fixation
1699   in minerals from serpentine-rich mine tailings using the Rietveld method with X-ray powder
1700   diffraction data: Am. Min., v. 91, p. 1331–1341.
1701 Wu, Y.-S., Zhang, K., and Liu, H.-H., 2006, Estimating large-scale fracture permeability of
1702   unsaturated rock using barometric pressure data: Vadose Zone Journal, v. 5, p. 1129-1142.

Table 1: Parameters for estimating uptake of CO2 via natural peridotite carbonation in the ophiolite massifs of northern Oman.							
calculating volume of carbonate in travertine and veins in peridotite	**length**	**width**	**thickness**	**factor**	**product**	**units**	**notes**
exposed volume of one travertine terrace	1000	200	1		2.00E+05	m^3	from mapping
plus travertine extending beneath alluvium: (ratio of alluvium/exposed+1)*exposed				1	4.00E+05	m^3	from observation of continuation beneath alluvium, e.g. in wells
plus veins immediately below travertine terraces/travertine, 10 m thick with 5% veins = total volume of one partially exposed travertine			10	0.05	6.00E+05	m^3	from observation that veins just beneath travertines are (a) calcite and (b) more abundant than elsewhere (~ 5%)
# travertines including associated veins & extensions under alluvium				45	2.70E+07	m^3	from fact that we've done reconnaissance mapping of about 1/3 ophiolite with 15 terraces known in that area
plus completely buried travertine (completely buried/partiall exposed+1)*partially exposed = **total travertine volume**				1	5.40E+07	m^3	probably an underestimate of amount of buried travertine in alluvial material
volume of peridotite hosted, magnesite & dolomite veins distant from travertines (ratio of veins/travertine*travertine volume)				14	**8.10E+08**	m^3	factor from ("max" HCO3 in Mg-HCO3 waters - low HCO3 in Ca-OH waters)/(max Ca in Ca-OH waters - avg Ca in surface waters), see Table 2
total carbonate volume in Oman peridotite					8.64E+08	m^3	
checking for consistency with observation of ~ 1% veins in roadcuts far from travertine							
area perid	4E+05	15,000			5.25E+09	m^2	30% of ophiolite area is peridotite
thickness carbonate veined peridotite			15		7.88E+10	m^3	thickness based on erosion rate of 0.0003 m/yr * 50,000 year 14C age of oldest veins
% veins in carbonated perid*total volume of veined peridotite = **volume of peridotite hosted veins distant from travertine**				0.01	**7.88E+08**	m^3	1% Mg-rich veins based on reconnaissance measurements in road cuts far from travertine
converting volume of carbonate to mass CO2		**density**	**mass fraction CO2**				
volume & density to mass CO2 in travertine using calcite		2700	0.44		6.42E+07	tons CO2	
volume & density to mass CO2 in veins using magnesite		3000	0.52		1.26E+09	tons CO2	
calculating "present day", steady state CO2 uptake flux using average 14C ages		**average 14C age veins, years**	**average 14C age travertine, years**				
flux using average vein age and magnesite mass for veins, average travertine age and calcite mass for travertine		26,000	20,000		5.18E+04	tons CO2/yr	

	mg/L	mg carbonate precipitated per liter of water	magnesite veins/calcite in travertine
Table 2: Parameters for estimating the relative mass of sub-surface veins in peridotite, versus surficial travertine deposits associated with alkaline springs in peridotite catchments. Data sources: Liguria (Cipolli et al., 2004) and L. Marini, pers. comm., 2008. California (Barnes et al., 1967; Barnes and O'Neil, 1969). Oman (Dewandel et al., 2005; Matter, 2001; Neal and Stanger, 1985).			
Liguria			
Ca concentration in alkaline spring waters to form calcite	61.9	154.58	
HCO3 in Mg-HCO3 ground waters to form magnesite	543	750.32	4.85
California			
Ca concentration in alkaline spring waters to form calcite	53	132.35	
HCO3 in Mg-HCO3 ground waters to form magnesite	1353	1869.59	14.12
Oman			
Ca concentration in alkaline spring waters to form calcite	58.5	146.13	
HCO3 in Mg-HCO3 ground waters to form magnesite	462.5	639.10	4.37

Table 3

sample	location	description	mineral proportions, %						lat °N	lon °E	elev, m
			cct	mgs	dol	serp	qtz	kaol			
OM07-08	**village of Jill**	**erosional remnant above level of travertine terrace**	**94.3**			**5.7**			**22.8634**	**57.5150**	**483**
OM07-09	village of Jill	2 meters below 08 on currently active travertine							22.8634	57.5150	482
OM07-10	village of Jill	globular carbonate sitting on top of travertine							22.8634	57.5150	482
OM07-11B	village of Jill	three different stalactites one meter below 09							22.863	57.51475	481
OM07-12	**village of Jill**	**carbonate veins in serpentine, 1 m below stalactites**	**98.4**			**1.6**			**22.863**	**57.51476**	**481**
OM07-13	**village of Jill**	**between 11 and 12**	**82.1**			**17.9**			**22.8630**	**57.5148**	**482**
OM07-14	village of Jill	very base of outcrop area in wadi	63.3		11.8	16.3	4.4	4.3	22.8627	57.5149	478
OM07-16	"Duck outcrop"	top of erosional remnant	60.1		16.4	22.5		1.0	22.8146	57.8381	~ 480
OM07-18	"Duck outcrop"	travertine forming now	88.3		9.7	0.4	1.6		22.8146	57.8381	~ 480
OM07-25	settlement of Tuf	travertine in wadi (?)							23.105	57.957	~ 900
OM07-34A	**village of Falaij**	**old travertine, 1.5 m above current spring level**	**91.4**		**2.9**	**5.7**			**22.8461**	**58.0562**	**551**
OM07-34C	village of Falaij	flakes of currently forming travertine	96.4		2.1	0.5		1.0	22.8461	58.0562	551
OM07-01	mtns between Muttrah & Muscat	carbonate vein on fault							23.616	58.574	~ 115
OM07-02	mtns between Muttrah & Muscat	carbonate vein on fault							23.616	58.574	~ 115
OM07-03	Wadi Bani Karous/Al Abyad	carbonate vein on fault							23.3902	57.6592	307
OM07-04	Wadi Bani Karous/Al Abyad	alteration associated with carbonate veins							23.43	57.66816	269
OM07-05	Sohar to Muqbah highway	carbonate vein in serpentine			45.2	47.9			23.9756	56.5020	472
OM07-07	**Sohar to Muqbah highway**	**massive carb vein in serpentine ≤ 10 cm thick**		**94.1**	**5.9**				**23.9756**	**56.5020**	**472**
OM07-17	"Duck outcrop"	carbonate vein in serpentine	31.9		43.3	23.7		1.0	22.8146	57.8381	~ 480
OM07-26	settlement of Tuf	botryoidal carbonate weathering from veins							23.105	57.957	~ 900
OM07-27	settlement of Tuf	massive carbonate in wadi assoc w big (≤ 1 m) veins	7.8		72.6	17.0		2.6	23.1081	57.9579	917
OM07-28C	settlement of Tuf	altered peridotite in wadi, tabular body ~ 2 m wide							23.0994	57.9525	883
OM07-30A	settlement of Tuf	travertine or dipslope vein in gully below Tuf	19.3		66.9	11.3		2.5	23.0994	57.9525	883
OM07-30B	settlement of Tuf	dark grey blocks within dipslope vein or travertine	91.4			7.4		1.2	23.0994	57.9525	883
OM07-32	village of Falaij	carbonate veins in serpentinized perid nr 34							22.8461	58.0562	551
OM07-34B	village of Falaij	small carbonate vein in perid below travertine deposits							22.8461	58.0562	551
OM07-39	**Wadi Lufti**	**50 cm carbonate vein in wadi wall**		**86.6**	**10.0**	**3.5**			**23.2483**	**58.3099**	**600**
OM07-52	Wadi Nassif	serp & carb veins 5 cm thick in perid							22.908	58.374	~ 710
OM07-53	Wadi Nassif	carb vein in dunite, low angle dip							22.908	58.374	~ 710
OM07-54	pass betw W Khafifah & W Dima	carbonate coating/veins on joints			49.4	45.1		5.5	22.9359	58.4262	748
OM07-56	pass betw W Khafifah & W Dima	coarse, gree serpentine vein 1 cm wide							22.9359	58.4262	748
OM07-57	pass betw W Khafifah & W Dima	mixed serpentine and carbonate, cm scale veins							22.9359	58.4262	748
OM07-58	pass betw W Khafifah & W Dima	perid with mm scale carbonate on joints							22.9407	58.4418	915
OM07-59	Wadi Dhuli	4 mm carbonate chips in serpentine, several photos							22.9841	58.6331	414
OM07-60	near center of the universe	sub-horizontal vein grading into carbonated dunite			21.5	60.6	17.9		22.9391	58.6681	497
OM07-61A	**Batin camp**	**erosional remnant of massive, low angle vein**		**80.8**	**19.3**				**22.9256**	**58.6711**	**522**
OM07-61B	Batin camp	different textural types near 61A							22.9256	58.6711	522
OM07-61C	Batin camp	different textural types near 61A			33.4	61.9	4.7		22.9256	58.6711	522
	*: Vein sample immediately below, and continuous with, overlying travertine										

Table 3

sample	fraction modern carbon (avg when N=2)	Fm Error (if N=2, larger of the two values for analytical precision)	14C age (avg when N=2) years	Age Error (if N=2, larger of the two values for analytical precision) years	N	stdev when N=2 years	trav?	from NOSAMS during 14C analyses δ13C VPDB per mil	from NOSAMS during 14C analyses, stdev δ13 VPDB (n=2) per mil	measured by Al Gagnon at WHOI, n=1, δ13C VPDB per mil	measured by Al Gagnon at WHOI, n=1, δ18O VPDB per mil
OM07-08	**0.008**	**0.0003**	**38950**	**310**	**2**	**2051**	**trav**	**-15.84**	**0.13**		
OM07-09	0.0369	0.0005	26500	120			trav	-16.51			
OM07-10	0.746	0.004	2350	40			trav	-27.21			
OM07-11B	0.7535	0.0027	2270	30			trav	-22.80			
OM07-12	**0.0277**	**0.0005**	**28800**	**150**			**trav***	**-12.30**			
OM07-13	**0.0163**	**0.0003**	**33100**	**140**			**trav**	**-9.91**			
OM07-14	0.6328	0.0023	3670	30			trav	-3.36			
OM07-16	0.0105	0.0003	36600	240			trav	-12.44		-10.81	-2.78
OM07-18	0.8159	0.0027	1630	25			trav	-17.19			
OM07-25							trav				
OM07-34A	**0.10545**	**0.0011**	**18450**	**90**	**2**	**3465**	**trav**	**-12.43**	**1.71**	**-14.44**	**-6.90**
OM07-34C	1.1296	0.0043	0				trav	-25.55			
OM07-01	0.0494	0.0006	24200	100			vein	-5.56			
OM07-02	0.0251	0.0008	29600	250			vein	-10.14			
OM07-03	0.0063	0.0004	40700	460			vein	-7.47			
OM07-04	0.0113	0.0004	36000	280			vein	2.50			
OM07-05										-5.49	2.53
OM07-07	**0.01265**	**0.0004**	**36950**	**360**	**2**	**7990**	**vein**	**-9.64**	**0.12**	**-7.80**	**2.57**
OM07-17	0.4901	0.002	5730	35			vein	-0.12			
OM07-26	0.0404	0.0006	25800	130			vein	-7.78			
OM07-27	0.0071	0.0003	40500	340	2	5091	vein	-5.87	0.58	-5.08	0.78
OM07-28C							vein				
OM07-30A	0.0118	0.0003	35600	220			vein?	-7.43			
OM07-30B	0.0845	0.0008	19850	75			vein?	0.36			
OM07-32	0.3836	0.0018	7700	35			vein	-7.39			
OM07-34B	0.4521	0.0019	6380	35			vein	-6.30			
OM07-39	**0.0191**	**0.0003**	**31800**	**140**			**vein**	**-8.39**		**-3.79**	**0.87**
OM07-52	0.4146	0.0029	7070	55			vein	-7.34			
OM07-53	0.0056	0.0002	41700	340			vein	-8.10			
OM07-54	0.0086	0.0003	38200	300			vein	-2.78		-1.58	4.81
OM07-56	0.0358	0.0008	26700	170			vein	-4.83			
OM07-57	0.0052	0.0002	42200	350			vein	-7.35			
OM07-58	0.2606	0.0014	10800	40			vein	-4.34			
OM07-59	0.184	0.0013	13775	70	2	3465	vein	0.73	1.22	0.62	1.68
OM07-60	0.0142	0.0004	34500	340	2	3536	vein	-9.84	2.93	-8.47	1.72
OM07-61A	**0.0275**	**0.0004**	**28900**	**110**			**vein**	**-8.06**	**0.42**	**-2.61**	**6.15**
OM07-61B	0.1526	0.0012	15100	65			vein	-0.88			
OM07-61C	0.1123	0.001	17550	75			vein	-2.12			

Table 3

sample	measured by Rindy Osterman & Bill Curry at WHOI, δ13C VPDB per mil	measured by Rindy Osterman & Bill Curry at WHOI, δ13C std dev per mil	measured by Rindy Osterman & Bill Curry at WHOI, δ18O VPDB per mil	measured by Rindy Osterman & Bill Curry at WHOI, δ18O SMOW per mil	measured by Rindy Osterman & Bill Curry at WHOI, δ18O std dev per mil	O & C N	mag-nesite corrected δ18O SMOW per mil	avg for all δ13C data per mil	stdev for all δ13C data per mil	all N	avg for all δ18C VPDB data per mil	avg for all δ18O SMOW data per mil	stdev for all δ18C data per mil	all N	mag-nesite corrected δ18O SMOW per mil	$^{87}Sr/^{86}Sr$
OM07-08	**-15.63**	**0.01**	**-7.00**	**23.70**	**0.03**	**1**		**-15.77**	**0.15**	**3**	**-7.00**	**23.70**	**0.03**	**1**		
OM07-09	-15.31	0.01	-7.17	23.53	0.07	1		-15.91	0.85	2	-7.17	23.53	0.07	1		
OM07-10	-27.09	0.02	-13.19	17.32	0.03	1		-27.15	0.08	2	-13.19	17.32	0.03	1		
OM07-11B	-23.47	0.02	-14.04	16.44	0.02	1		-23.13	0.47	2	-14.04	16.44	0.02	1		
OM07-12	**-12.54**	**0.03**	**-5.23**	**25.53**	**0.03**	**1**		**-12.42**	**0.17**	**2**	**-5.23**	**25.53**	**0.03**	**1**		0.707660
OM07-13	**-7.28**	**0.39**	**-5.80**	**24.94**	**0.12**	**2**		**-8.16**	**1.54**	**3**	**-5.80**	**24.94**	**0.12**	**2**		
OM07-14	-6.54	0.06	-2.70	28.13	0.10	2		-5.48	1.84	3	-2.70	28.13	0.10	2		0.708090
OM07-16								-11.62	1.15	2	-2.78	28.05		1		
OM07-18	-19.47	0.02	-10.77	19.81	0.03	1		-18.33	1.61	2	-10.77	19.81	0.03	1		0.708461
OM07-25	-3.26	0.02	-6.73	23.98	0.03	1		-3.26	0.02	1	-6.73	23.98	0.03	1		
OM07-34A	**-14.70**	**0.02**	**-8.07**	**22.60**	**0.03**	**1**		**-13.50**	**1.59**	**4**	**-7.48**	**23.20**	**0.83**	**1**		0.708475
OM07-34C	-25.86	0.11	-14.97	15.49	0.15	2		-25.76	0.20	3	-14.97	15.49	0.15	2		
OM07-01	-2.29	2.95	2.42	33.41	1.25	3		-3.11	2.92	4	2.42	33.41	1.25	3		
OM07-02	-1.45	0.15	3.49	34.52	0.73	2		-4.35	5.02	3	3.49	34.52	0.73	2		
OM07-03	-5.86	0.28	2.07	33.06	0.64	3		-6.26	0.84	4	2.07	33.06	0.64	3		
OM07-04	-0.53	0.03	-10.12	20.49	0.02	1		0.98	2.14	2	-10.12	20.49	0.02	1		
OM07-05								-5.49		1	2.53	33.53		1		0.708682
OM07-07	**-3.86**	**0.04**	**6.88**	**38.02**	**0.01**	**2**	**36.64**	**-6.29**	**2.90**	**4**	**5.44**	**36.53**	**2.49**	**3**	**35.15**	
OM07-17	-0.83	0.16	1.67	32.64	0.35	2		-0.60	0.43	3	1.67	32.64	0.35	2		0.708473
OM07-26	-1.96	0.06	-0.91	29.98	1.01	1		-4.87	4.11	2	-0.91	29.98	1.01	1		
OM07-27	-4.11	0.01	1.16	32.11	0.02	1		-5.23	0.90	4	0.97	31.92	0.27	2		0.708489
OM07-28C	0.33	0.01	5.70	36.79	0.02	1		0.33	0.01	1	5.70	36.79	0.02	1		
OM07-30A	-5.84	0.34	0.78	31.72	0.22	2		-6.37	0.95	3	0.78	31.72	0.22	2		
OM07-30B	-0.21	0.14	-9.74	20.88	0.57	2		-0.02	0.34	3	-9.74	20.88	0.57	2		0.708539
OM07-32	-4.40	0.60	3.52	34.55	0.42	2		-4.94	0.78	4	3.52	34.55	0.42	2		
OM07-34B	-6.35	0.13	-3.25	27.57	0.37	2		-6.33	0.10	3	-3.25	27.57	0.37	2		
OM07-39							**30.43**	**-6.09**	**3.25**	**2**	**0.87**	**31.81**		**1**	**30.43**	
OM07-52	-6.95	5.86	-0.67	30.22	4.32	2		-7.08	4.15	3	-0.67	30.22	4.32	2		
OM07-53	-7.91	0.55	0.82	31.77	0.53	2		-7.97	0.41	3	0.82	31.77	0.53	2		
OM07-54								-2.18	0.85	2	4.81	35.88		1		0.708575
OM07-56	-4.88	0.18	4.61	35.67	0.26	3		-4.87	0.15	3	4.61	35.67	0.26	3		
OM07-57	-6.67	0.42	2.96	33.97	0.09	2		-6.90	0.49	3	2.96	33.97	0.09	2		
OM07-58	-3.83	0.02	-2.59	28.25	0.04	1		-4.08	0.36	2	-2.59	28.25	0.04	1		
OM07-59	-0.15	0.04	4.03	35.07	0.27	2		0.29	0.87	4	3.25	34.27	1.37	3		0.708589
OM07-60								-9.38	2.22	3	1.72	32.69		1		0.708494
OM07-61A	**-1.35**	**0.07**	**6.84**	**37.97**	**0.32**	**2**	**36.59**	**-4.70**	**3.88**	**4**	**6.61**	**37.73**	**0.46**	**3**	**36.35**	
OM07-61B	-0.86	1.35	4.09	35.14	2.75	2		-0.86	0.96	3	4.09	35.14	2.75	2		
OM07-61C	-2.10	0.19	9.78	41.01	0.09	2		-2.11	0.14	3	9.78	41.01	0.09	2		0.708565

Table 3, notes

All sample analyses reported here were done at the Woods Hole Oceanographic Institution, except for XRF measurements of major element composition used in calculating mineral proportions.

Samples were washed in dilute HCl and broken into 5mm-sized fragments, after which some were ground to powder in an agate mill.
For other samples, fragments were acid washed a second time before being powdered for analysis. Please see Kelemen & Matter, 2008, for preparation information for each sample.

Proportion of minerals was determined using a combination of X-Ray Flourescence analyses for major element composition (Washington State University, analytical information at http://www.sees.wsu.edu/Geolab/equipment/xrf.html) and X-Ray Diffraction (at Woods Hole Oceanographic Institution, by Margaret Sulanowska) using standard procedure on powders, with data analaysis using Mac-Diff software. Proportions were determined by Lisa Streit using least squares mass balance of the XRF data, beginning with the mineral identifications from XRD. Minerals included are dolomite (dol), calcite (cct), magnesite (mgs), chrysotile + greenalite (serpentine minerals serp), quartz (qtz), and kaolinite (kaol). Some of these mineral identifications are uncertain, so that other Mg-Ca carbonates such as huntite may be present instead of or in addition to dolomite, calcite, and magnesite, and clays and other hydrous silicates may be present instead of or in addition to kaolinite. In preliminary electron microprobe analyses we have identified carbonates with Ca/Mg intermediate between calcite and dolomite, as reported for some veins and travertines in California (Barnes & O'Neil, Geochim. Cosmochim. Acta, 51, 699–713, 1951) and Oman (Stanger & Neal, Chem. Geol. 112, 247–254, 1994). Hydrous Mg-carbonates (nesquehonite, hydro-magnesite) have not been detected by XRD or electron probe analyses.

Sr isotope analyses: Samples were crushed and ground in an agate mortar, then dissolved in weak HCl. Sr was separated using Bio-Rad AG50W X8 200-400 mesh cation exchange resin using standard column methods. Sr samples were analyzed on a ThermoElctron "Neptune" multi-collector inductively coupled plasma mass spectrometer (MC-ICP-MS) at Woods Hole Oceanographic Institution. Sample measurements were normalized to 86Sr/88Sr = 0.1194 and referenced to a value of 0.710240 for NBS987 standard. The internal precision for Sr isotopic measurements was 8-14 ppm (2 sigma). Repeated measurement of a NBS987 standard yielded precision estimates of 25 ppm (2 sigma).

Oxygen isotope analyses performed by Rindy Ostermann and Bill Curry: Stable oxygen isotopes were analyzed on a Finnigan MAT 253 isotope ratio mass spectrometer coupled to a Kiel III carbonate device at WHOI using standard procedures (Ostermann & Curry 2000, Paleoceanography 15, 353– 360). During the course of this laboratory analysis, the external precision of the laboratory standards was d13C = 0.06% and d18O = 0.09%. Conversion to the Vienna Peedee belemnite (VPDB) scale was completed using comparison to an external standard, NBS19 (d18O = 2.20%). Some samples were not homogenous in oxygen and carbon isotopes, as is evident from relatively poor reproducibility for some. We did not know the carbonate concentration in our samples so the first carousel run had many analyses with greater than 4 expansions. Because there can be unpredictable isotope fractionations for very large carbonate samples, samples were re-run until there was at least one analysis with fewer than 4 expansions from each vial. Data reported here are only for runs with fewer than 4 expansions. Reproducibility (one standard deviation) is reported for data from Ostermann & Curry's lab alone, and for averages including data from NOSAMS, Al Gagnon, and Ostermann & Curry.

Oxygen and carbon isotope analyses performed by Al Gagnon: STILL LACKING ANALYTICAL INFORMATION FOR THESE

14C analyses were performed at the National Ocean Sciences Accelerator Mass Spectrometry Facility in Woods Hole, Massachusetts (NOSAMS). Please see Kelemen & Matter, 2008, Table S1, for analytical information. NOSAMS also determined δ13C VPDB during the course of 14C analyses, and these values are tabulated above. We sent blind duplicates to NOSAMS, and so there are two 14C age determinations and two stable carbon isotope ratios determined by NOSAMS for some samples. For these, tabulated values are the average of two duplicates, and one standard deviation from the average is also tabulated. The differences between duplicate analyses are much larger than the analytical precision, indicating that our sample powders are inhomogeneous in their carbon isotope content.

δ18O relative to SMOW is calculated as 1.03092*δ18O relative to VPDB + 30.92.

"Magnesite-corrected" values are presented in a separate column for three samples containing more than 80 wt% magnesite (rows in bold font, and are the reported values for these three samples minus 1.38 per mil, based on the difference between calcite-phosphoric acid and magnesite-phosphoric acid fractionation at 70°C (Das Sharma et al., Geochim. Cosmochim. Acta 66, 589-593, 2002).

Kelemen et al., Figure S1

Kelemen et al., Figure S2

Kelemen et al., Figure S3
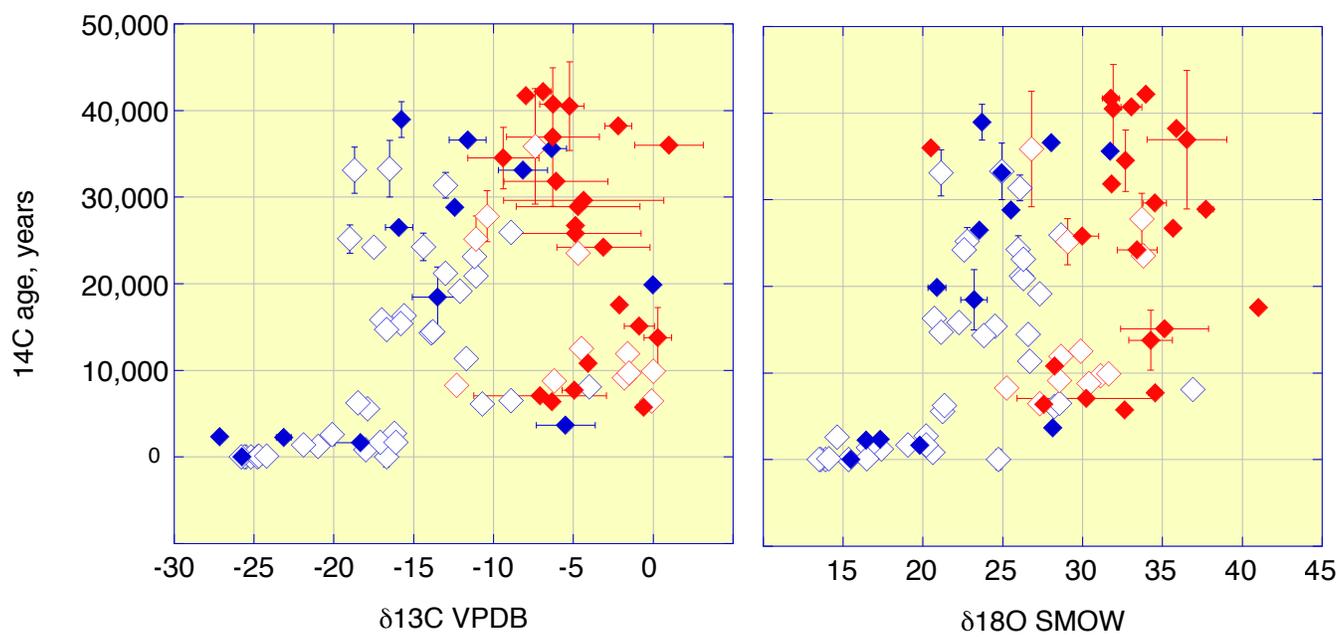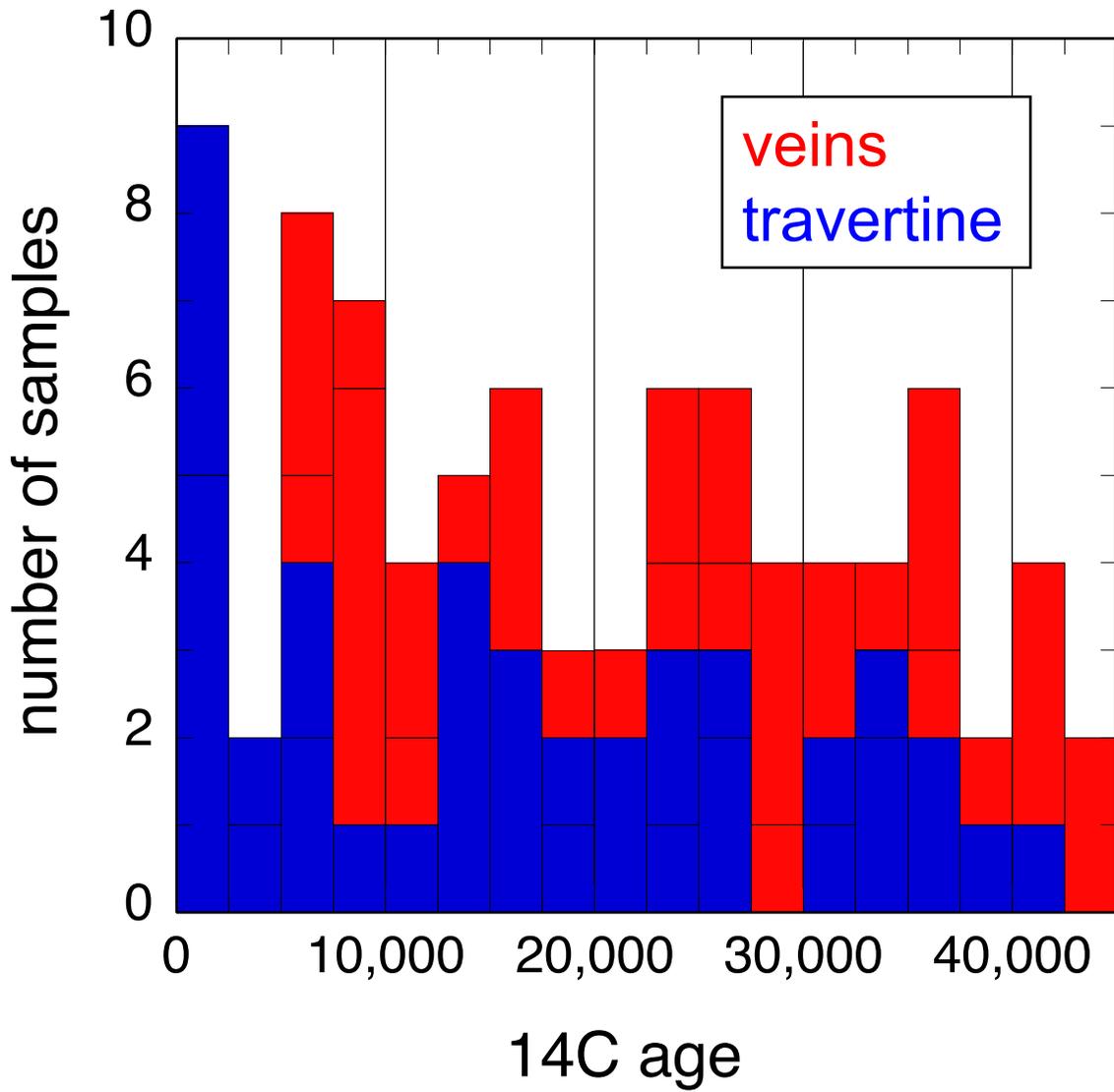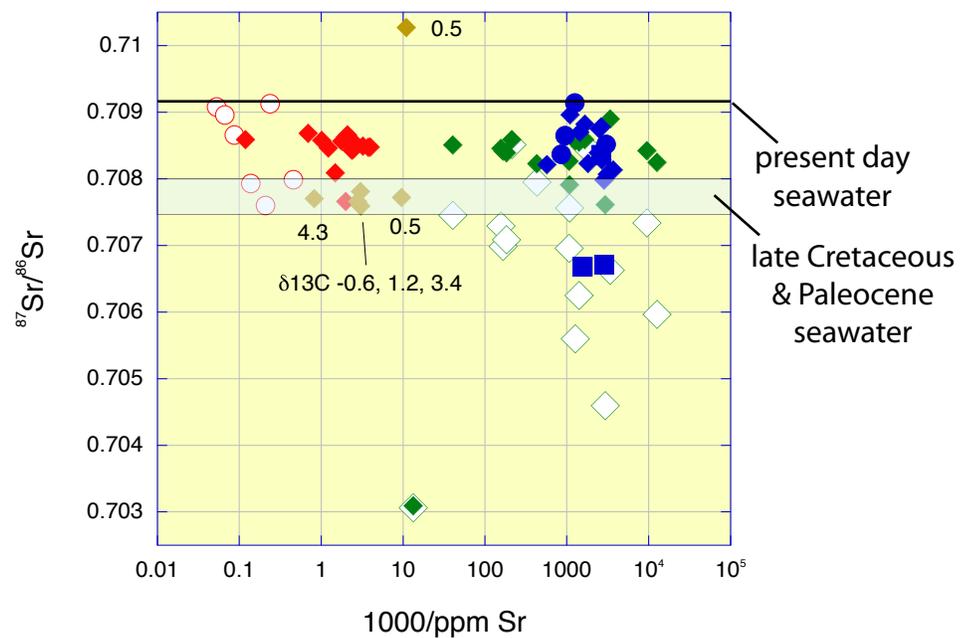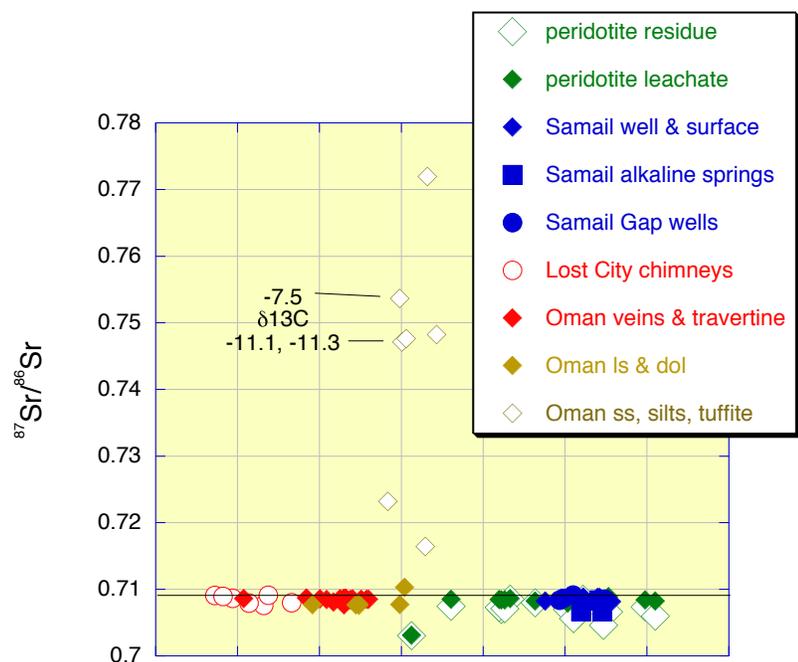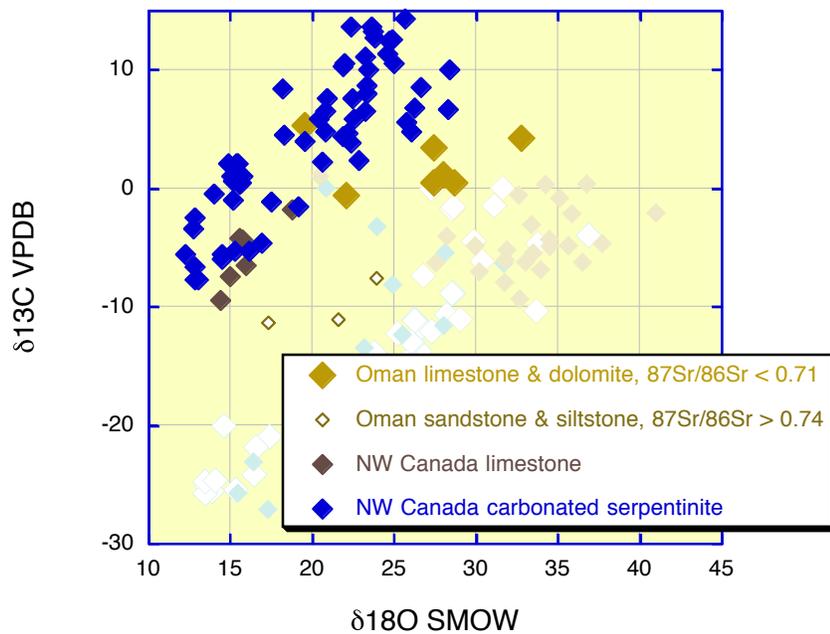
olivine carbonation
O'Connor et al. 2004 data
our fit to data

one hour

$y = 0.00653 \, (time)^{(1/2)}$

$R^2 = 0.990$

mass fraction carbonated

time, seconds